ABSTRACT

Title of dissertation: CONFINED ULTRACOLD BOSONS
                           IN ONE DIMENSIONAL OPTICAL LATTICES

                           Guido Pupillo, Doctor of Philosophy, 2005

Dissertation directed by: Prof. Bei-Lok Hu
                            Department of Physics

                            Dr. Carl J. Williams
                            National Institute of Standards and Technology

This dissertation presents my research covering the field of ultracold atoms loaded in optical lattices. The static and dynamical properties of atoms in combined periodic and parabolic potentials are studied, with a focus on the strongly interacting regimes. Because parabolic magnetic and optical potentials are routinely used to confine atoms, the results of this research are directly relevant to ongoing experimental endeavours in atomic physics.

After a review of the basic theory of atoms in homogeneous periodic potentials, the equilibrium and non-equilibrium properties of non-interacting and interacting atoms in periodic plus parabolic potentials are studied. The problem of the localization of the many-body wavefunction for systems with arbitrary peak onsite density is presented in Chapters 3 and 4. The physics pertaining to the experimental realization of Mott insulator states with one or more atoms per sites in inhomogeneous lattices is elucidated by introducing an intuitive model for strongly interacting bosons in one dimension. This model is then utilized to study the decay of the dipole oscillations of atomic ensembles subject to a small displacement of the parabolic potential. Good agreement is found with results of recent experiments.

Chapters 5 and 6 are dedicated to the characterization of the Mott insulator state with unit filling, which plays a central role in proposed schemes for neutral atom quantum computation. The usefulness of Bragg spectroscopy to probe the excitation spectrum of the Mott state in homogeneous lattices is analyzed in Chapter 5, where the limits of validity of linear response theory in this strongly correlated regime are

delimited. In Chapter 6 the effects of finite temperature on the confined Mott insulator state are studied, and a scheme is devised for possibly estimating the system's temperature, at energies of the order of the inter-particle interaction energy.

Finally, in Chapter 7, a proposal is introduced to utilize the Mott state as a robust register for neutral atom quantum computation. Unwanted residual quantum coherences inherent to the Mott insulator ground state are eliminated by a judicious choice of the trapping potentials and a selective measurement on a molecular photo-associative transition.

CONFINED ULTRACOLD BOSONS IN ONE DIMENSIONAL OPTICAL LATTICES

by

Guido Pupillo

Dissertation submitted to the Faculty of the Graduate School of the
University of Maryland, College Park in partial fulfillment
of the requirements for the degree of
Doctor of Philosophy
2005

Advisory Committee:

Professor Bei-Lok Hu, Chair/Advisor
Dr. Carl J. Williams, Advisor
Dr. Charles W. Clark
Professor Steven L. Rolston
Professor Victor M. Yakovenko
Professor Michael Coplan

ACKNOWLEDGMENTS

TABLE OF CONTENTS

LIST OF TABLES

LIST OF FIGURES

Chapter 1

Introduction

This dissertation describes my research on the static and dynamical properties of atoms confined in combined periodic and quadratic potentials, with a focus on the strongly correlated regimes which are experimentally attainable.

In recent years tremendous progress has been made in coherent control and manipulation of quantum systems in atomic, molecular, and optical physics. In order to improve on precision measurement and noise reduction, a variety of new methods have been developed, including laser cooling of atoms [1], atom interferometry [2], cavity QED [3], and optical lattices [4]. This thesis is concerned with the last of these experimental breakthroughs, recognizing the pivotal role that optical lattice potentials are increasingly playing in the study of strongly correlated systems.

Optical lattices are periodic conservative trapping potentials for atoms, and are created by the interference of two or more traveling laser beams yielding standing laser waves. The laser light induces an AC-Stark shift in the atoms, and acts largely as a conservative periodic potential. Although the motion of atoms in an optical lattice is closely analogous to that of electrons in a solid crystal, optical lattices are very different from natural crystals, in that they are essentially defect-free. Of particular appeal is the possibility of varying their depth and geometry, as well as creating state-dependent potentials that allow for independent trapping of atoms with different spin states.

While the loading of ultracold atoms in the ground motional state of the lattice has been successfully achieved by means of Raman cooling [5], the simple application of this technique allows only for a lattice filling factor which is much less than one. A high phase-space density has been obtained by loading the lattice with ultracold atoms originating from a Bose-Einstein condensate (BEC) [6, 7]. A BEC is the macroscopic occupation of a single-particle wave-function by an ensemble of atoms obeying Bose statistics. Such an occupation occurs below a certain temperature, which corresponds to the temperature at which de Broglie wave-length is of the order of the mean interparticle spacing. The existence of a BEC was first

predicted by Einstein for ideal gases in 1924 [8], and its presence invoked by London to justify superfluidity in liquid ^{4}He in 1938 [9], but a clear experimental realization of a condensate had to wait until 1995, when a BEC was obtained for a dilute gas of alkali atoms trapped by magnetic fields [10]. In this system, about $10^5 - 10^6$ atoms are confined in a relatively small region of space, with densities in the range of 10^{11} to 10^{15} cm^{-3} and temperatures varying between a few tens of nK to about 50 μK. A BEC of alkali atoms can be considered a dilute system, because under typical conditions the quantity $\gamma \sim n^{1/3} a_s$, the so-called *gas parameter*, is at most of order 10^{-2}. Here, γ is proportional to the ratio between the interaction to kinetic energies in three dimensions, a_s is the s-wave scattering length, that parametrizes the collisional properties of the atoms at very low temperatures, and n is the particle density. Because of its diluteness, a BEC in alkali atoms is nearly the opposite of a strongly correlated system. Nevertheless, when BEC atoms are loaded in a lattice the ratio of the interaction to kinetic energies can be easily tuned and made very large by varying the depth of the lattice. In fact, the tunneling of atoms between different sites, that is the kinetic energy, decreases exponentially with increasing lattice depth, while the interaction energy can be shown to slightly increase. A BEC in an optical lattice is therefore an ideal system for studying strongly correlated regimes. This conceptual breakthrough was first suggested in a seminal paper by D. Jaksch and coworkers [11]. In that paper it was shown that the relevant Hamiltonian for the atoms in the lattice is the Bose-Hubbard (BH) Hamiltonian, which is known to display an interaction-induced phase transition at zero temperature between a superfluid and a Mott insulator state [12]. The existence of such a transition has been experimentally confirmed in a remarkable experiment by M. Greiner and coworkers [13], which showed the loss of coherence of a BEC when the lattice depth was tuned above a certain threshold value. The loss of coherence corresponded to the transition from a phase-coherent superfluid to a phase-incoherent Mott insulator, in agreement with the transition expected in the BH model.

Since then, neutral atoms in optical lattices have been used in a series of impressive experiments to explore strongly correlated regimes [14, 15, 16, 17, 18, 19]. These experiments mainly focused on systems with reduced dimensionality, which allow for interaction-induced effects such as "fermionization" of the bosonic wave-function not present in higher dimensions [14, 15, 16]. These systems have become a test-bed for studying fundamental problems like the loss of superfluid current in bosonic systems and localization

of the many-body wave-function [17, 18, 20].

While cross-fertilization between the atomic and the condensed matter communities promises to be very fruitful in the advancement of our knowledge of basic properties of model Hamiltonians of intrinsic interest, another field which has largely benefitted from the advancement of AMO techniques is the field of Quantum Information and Computation. In this respect, the experiments on the superfluid to insulator transition can be seen as an important step towards realizing theoretical ideas for controlled entanglement creation in optical lattices by interactions between neutral atoms [21, 22, 23]. Together with single-particle manipulations, such entanglement operations constitute the basic building block of a quantum computer as proposed by D. DiVincenzo [24]. The first important experimental steps towards realizing multi-particle entangled states have recently been achieved by Mandel and coworkers [25], and experiments are also under way at NIST.

To date, many proposals for neutral atom quantum computation envision the Mott state with an ordered array of two-level atoms as the quantum register.

The overall goal of this thesis is to characterize the many-body states of interacting atoms in realistic periodic plus quadratic potentials. While this study is theoretical, it intentionally ties to ongoing experimental efforts in atomic physics, condensed matter, and quantum information processing.

1.1   Overview of research

Chapter 2 introduces the theory of optical potentials and reviews the basic theory of periodic lattices, single-particle band-structure and the tight-binding approximation valid for deep enough lattices. To treat interacting many-body systems, it is convenient to introduce the Bose-Hubbard Hamiltonian and show how it is derived from the full second-quantized many-body Hamiltonian for bosons in periodic potentials, following Ref. [11]. Chapter 2 concludes with a review of the phase diagram of the BH Hamiltonian, which is characterized by superfluid and Mott insulating phases.

Chapter 3 reports on my thesis work on non-interacting and interacting atoms trapped in an optical

lattice plus a parabolic potential in one dimension with a focus on systems where the on-site particle density is less than or equal to one. This regime has been recently obtained in a remarkable experiment by B. Paredes and coworkers [15], where an array of quasi one dimensional tubes was created by loading a BEC in a deep two-dimensional lattice, which confined the atomic dynamics to the third, or axial, direction. A weaker optical lattice was then superimposed in the axial direction in order to increase the atoms' effective mass, and therefore the ratio $\gamma = U/J$ of the interaction to kinetic energies. The latter measures the degree of correlation of the system, so that for $\gamma \ll 1$ the system is weakly interacting, and at zero temperature most atoms occupy the single-particle wave-function, while for $\gamma \gg 1$, the system is highly correlated and becomes "fermionized", in that repulsive interactions mimic the effects of the Pauli exclusion principle. Thus, the low energy excitation spectrum of a bosonic gas resembles that of a gas of non-interacting fermions.

In Chapter 3 we show that, in the tight-binding approximation, the non-interacting problem is exactly solvable in terms of Mathieu functions. Then, the exact solutions show the existence of two types of behavior, according to whether the energy is dominated by site hopping or parabolic contributions. In the site hopping dominated regime, where the trapping energy is smaller than the lattice band-width, the single-particle eigenmodes are extended around the trap center and closely resemble harmonic oscillator eigenstates. The lattice discretization produces modifications to the harmonic spectrum, which become more and more severe with increasing quantum number. When the parabolic trapping potential is larger than the lattice band-width, eigenstates become almost two-fold degenerate and localized far from the trap center. Localization of the modes is linked to the appearance of non-classical turning points when the quasimomentum reaches the end of the Brillouin zone, and can therefore be associated with Bragg scattering induced by the lattice. This localization effect is interesting in its own, as it occurs in the absence of disorder, and is connected to the so-called "mobility edge" discussed in the context of quasi-periodic potentials [26].

The analytic solutions are used to study the collective oscillations of ideal bosonic and fermionic ensembles induced by small displacements of the parabolic potential. In contrast to the well-known case of the displaced harmonic oscillator, a non-trivial modulation of the center of mass motion occurs due to the

presence of the lattice potential. In particular, an initial decay of the amplitude of oscillations is observed due to the dephasing of modes which are not harmonic in character. Because it occurs without dissipation, we refer to this decay as *effective* damping.

The interacting boson problem is treated by numerical diagonalization of the Bose-Hubbard Hamiltonian. From analysis of the dependence upon lattice depth of the low-energy excitation spectrum of the interacting system, we consider the problems of "fermionization" of a Bose gas, and the superfluid-Mott insulator transition in a trapped system. In this case, numerical DMRG and quantum Monte-Carlo simulations have previously shown the coexistence of superfluid and Mott insulating phases [27, 28, 29]. We state the conditions for fermionization to occur in the lattice plus quadratic potential and show that it takes place for a large range of experimentally accessible parameters. We show in this case that the Mott state is a particular case of a fermionized state with integer filling and explain this using the Bose-Fermi mapping. In fact, when the Fermi energy of the corresponding Fermi system becomes larger than the lattice band-width, single particle states are populated which are trapping-dominated and are therefore localized far from the trap center. Then, the density in the many-body density profile approaches one in a few sites at the trap center with reduced number fluctuations, corresponding to the realization of the Mott insulator.

Chapter 3 concludes with an analysis of the collective dipole dynamics of an interacting bosonic gas obtained by exact numerical calculations. The dynamics is studied for two different scenarios that are experimentally realizable. The first corresponds to experiments in which the trapping potentials are kept fixed and the interatomic scattering length is varied (e.g. by use of a Feshbach resonance). In this situation, parameters are chosen such that there is no Mott insulator at the center of the trap in the large γ limit. It is shown that while for very small γ interactions actually slightly decrease the damping, for $\gamma \gg 1$ the damping of oscillation for the bosonic system exponentially approaches that for ideal fermions. Here the damping is dominated by the dephasing of the different modes during the time evolution. The second scenario corresponds to experiments in which the lattice depth is increased while the frequency of the parabolic potential is kept fixed. These results show a strong inhibition of the transport properties of the system if localized single-particle states are populated as a result of the displacement. If the initial state was a unit filled Mott insulator at the trap center the dynamics is completely overdamped. Remarkably, if after the

trap displacement most atoms occupy localized single-particle modes far from the trap center, the center of mass position of the atomic cloud remains localized far from the trap center, without relaxing towards the bottom of the parabolic potential. This effect has been recently observed by Inguscio and coworkers [20] in an experiment with trapped non-interacting fermions.

Chapter 4 presents a generalization of the Bose-Fermi mapping for bosons in one-dimensional optical lattices to situations where the average number of atoms per site is larger than one. We call this generalization "extended-fermionization" (EF). This work is relevant to many current experiments with ultracold bosons, where the peak on-site density is greater than one [17, 18, 19]. Because the standard fermionization technique utilized in Chapter 3 is not applicable to these cases, the study of these regimes beyond the use of mean-field theory has relied mainly on numerical simulations [27, 28, 29]. The goal of this Chapter is to show that even when the on-site density is larger than one, single-particle solutions can still be used to successfully describe strongly correlated regimes in many situations.

The EF idea is most easily explained for the homogenous case. When the number of atoms equals the number of lattice sites and $\gamma > \gamma_c$, the ground state is a Mott insulator state with one atom per site and reduced fluctuations. Here, γ_c is the critical ratio for the superfluid-Mott insulator phase transition. If some extra atoms are added to the system and $\gamma \gg 2\gamma_c$, the extra atoms are delocalized over the entire lattice, and can be thought of as fermionized bosons with hopping energy $2J$ on top of a Mott insulator core containing one atom per site. The lowest-energy eigenstates and eigenenergies can then be described by means of the standard Bose-Fermi mapping with J replaced by $2J$. This approach is referred to as extended fermionization. The generalization to a Mott state with a generic number of atoms per site is then straightforward. The extension of the EF model to the case in which a parabolic trap is present, although less obvious, proved to be remarkably accurate in reproducing equilibrium and non-equilibrium properties of one-dimensional systems in a large and experimentally relevant parameter regime.

When the parabolic trap is present, atoms tend to pile up at the trap center and, for zero hopping energy, the many-body density profile shows a layered "cake"-like structure. For small enough hopping energy, the layered structure survives and we show that atoms in each layer can still be thought of as being

fermionized in analogy to the homogenous system, if the appropriate hopping energy is considered in each layer. Then, by independently applying fermionization techniques to each horizontal layer, it is possible to obtain expressions for all many-body observables. The success and limitations of our approach are tested by applying it to a system with the same parameters as the ones used in an experiment recently performed at NIST. In the NIST experiment [17] approximately $N_T = 1.4 \times 10^5$ ^{87}Rb atoms were trapped in an array of one-dimensional tubes with $N = 80$ atoms in the central tube. An additional periodic potential was added along the direction of the tubes and its depth was varied during the experiment. Center of mass oscillations were induced by a sudden displacement of the harmonic potential by few lattice sites, and an unexpectedly large damping of oscillations was observed for relatively small lattice depths. Similar results for the damping of the oscillations were also observed in an experiment performed by Esslinger and coworkers [19]. For equilibrium properties, we compare our EF model's predictions for the density profile, the momentum distribution, and the ground-state energy for atoms in the central tube to exact numerical quantum Monte-Carlo simulations, performed by using the Worm Algorithm [30], and find very good agreement in the deep-lattice limit. The model's prediction for the non-equilibrium dipole oscillations are directly compared to the experimental results, and good agreement is found. In particular, the experimentally observed over-damping of the dipolar motion corresponds to the formation of a Mott insulator state in the lowest layer in the EF model, that is, to a large population of localized single-particle states in the lowest layer. We notice that in Chapter 3 it was shown that the same phenomenon is responsible for the damping of the oscillations in systems with at most one atom per site.

Chapters 5 and 6 are dedicated to characterizing the Mott insulator state. The Mott state is not only intrinsically interesting as an example of a strongly correlated state, but in recent years has received increased attention because of its possible use in schemes for quantum information processing for neutral-atom quantum computation. To use the Mott state for initializing a quantum register requires that the Mott state be realized with near perfect fidelity. To date, a key piece of evidence for the realization of the Mott state has been the loss of global phase coherence of the matter wave-function when the lattice depth is increased beyond a critical value [13]. Unfortunately, this is not a clear-cut signature of the super-

fluid/insulator transition. In fact, the loss of coherence could arise from many sources, such as quantum or thermal depletion of the condensate during the loading process.

In Chapter 5 we propose to use Bragg spectroscopy as a method for probing the excitation spectrum in the Mott insulator phase in homogeneous lattices, and therefore for fully characterizing the Mott insulator state. Bragg spectroscopy is a well known high-precision experimental technique, which has already been used to coherently split a BEC into two momentum components [31], to measure the excitation spectrum in the superfluid regime [32], and even to measure the light-shifted energy levels of an atom in an optical lattice [33]. Its use has been only recently suggested as a means to characterize the localized state of a BEC in an optical lattice [34, 35]. The typical Bragg spectroscopic procedure is to gently scatter atoms with a moving optical grating. We propose that a Bragg potential be generated independent of and much weaker than the optical lattice potential. This allows us to treat the scattering process with linear response theory. Generating the Bragg potential independently of the lattice potential also provides for considerable flexibility in the range of momentum and frequency values that can be obtained. In contrast to earlier experiments that used momentum as the response observable, here we choose to examine the imparted energy. In trapped systems this allows long excitation duration that facilitates more precise spectral resolution. The use of energy spectroscopy has been recently illustrated in the experiment by Esslinger *et al.* [19].

For atoms confined in a homogeneous lattice deep in the Mott regime, the lowest-energy excitations are particle-hole excitations, whose energy is of the order of the interaction energy. Treating the hopping energy J as a first-order perturbation, an expression is found for the eigenenergies and eigenfunctions of these excitations, which is strictly valid when many atoms occupy each site of the lattice. The accuracy of the solution for the interesting case of one atom per site is checked by comparing the analytical results with exact diagonalizations of the BH Hamiltonian. We show that, deep in the Mott regime, Bragg peaks are centered around the characteristic Mott gap and are contained in an interval whose width is proportional to the hopping energy J. Most importantly, we discuss in detail the limit of validity of linear response, finding that the correlated nature of the Mott state makes reaching the linear regime rather difficult. In fact, linear response requires that the total excited state population at the conclusion of the Bragg perturbation be small compared to unity. In turn, this implies that the maximum energy transfer possible is of the order of the

interaction energy itself. For comparison, in the superfluid regime the only requirement is that at the end of the perturbation the amount of excited atoms be small compared to the condensate population.

On the other hand, we show that, contrary to the superfluid case, Bragg spectroscopy in the Mott regime is sensitive to temperature. In particular, low-frequency peaks are observed in the Bragg response for temperatures of the order of the interaction energy. These thermally activated peaks are at frequencies equal to the energy difference between two different particle-hole excitations. Because current experimental techniques for estimating temperature do not provide any information on the scale of the interaction energy, temperature dependence may turn out to be experimentally useful. Current experimental techniques rely on the analysis of the atomic interference pattern after a certain time of flight after the release of the atoms from the trapping potentials. The precision in the temperature measurements is of the order of the level spacing to the second band, which is typically an order of magnitude larger than the interaction energy.

Chapter 6 reports on our study of temperature effects on a realistic Mott insulator state in the presence of a parabolic potential. As mentioned above, the problem of temperature determination in the Mott state is crucial for the practical implementation of lattice-based quantum computation schemes. In fact, finite temperature can introduce errors in the register, such as empty or doubly occupied sites, and therefore a decrease in overall gate fidelity. This must be corrected at the cost of overheads in computational resources and gate times.

In this work we devise a scheme for estimating temperatures of order of the interaction energy for a Mott state in a parabolic potential. The scheme is based on molecular photo-association of atomic pairs, and because it is largely insensitive to the total number of atoms in the system, it should be suited for calibrating experimental set-ups.

In Chapter 6 we begin by showing that the density of atomic pairs, which is proportional to the probability of atomic pair detection in an experiment, depends both on the mixing of particle-hole excitations at zero temperature, and on finite-temperature population of high energy states. In particular, by comparing our theory with exact numerical Monte-Carlo simulations, we show that the finite-temperature pair-density distribution has a well defined Gaussian profile, whose width depends solely on the temperature and the

known trap geometry. We therefore propose to use a position-dependent measurement of the atomic pair density, in order to directly infer a bound for the system's temperature. As a measurement, we propose to utilize photoassociation of the atomic pair by means of an external laser beam, which is in resonance between two atoms in a trap and an excited molecular state. Ionization of the molecule, and detection of the ion would provide for an efficient measurement of the pair's presence. Although this proposed experiment is admittedly difficult, due to the problem of focusing the photoassociative laser on a region of the size of the lattice wave-length, if realized it would provide for a bound on the system's temperature, at temperatures of order of the interaction energy.

Finally, Chapter 7 reports on our proposal to create a register for neutral atom quantum computation. Several proposals indicated the Mott state as a candidate for the quantum register [21, 36]. In these proposals, each site of the lattice is exactly filled by one particle, and the qubit is stored in internal states of the atom. Unfortunately, the Mott state corresponds to the state with exactly one atom per site only in the limit of zero particle hopping. For any realistic finite hopping energy, the ground state of the BH Hamiltonian has residual mixing of particle-hole pairs which inevitably degrades the fidelity of the register, defined as the population in the unit-filled state. The same effect is also likely to be caused by finite temperature, as the analysis of Chapter 6 suggests. The presence of unoccupied sites in the lattice at zero or finite temperature also introduces unwanted errors in the register initialization.

Our study shows that it is possible to provide a robust register for quantum computation even from an imperfect Mott state. Our proposed scheme is comprised of two parts. First we show that the spatial inhomogeneity created by the quadratic magnetic potential can be used to isolate a subspace in the center which is impervious to hole hopping. The problem of the presence of unoccupied sites in the register is then naturally solved by defining the register in this physical subspace. Then, components of the many-body wave-function with more than one atom per well can be projected out by selective measurement on a molecular photo-associative transition. Maintaining the molecular coupling induces a quantum Zeno effect that can sustain a commensurately filled register for the duration of a quantum computation. Finally, by means of numerical diagonalizations of the BH Hamiltonian, we provide evidence that our proposal is

robust against the effects of moderate finite temperatures.

Chapter	Publications included in the dissertation	
3	A.M. Rey, G. Pupillo, C.W. Clark, and C.J. Williams, *Ultracold atoms confined in an optical lattice plus parabolic potential: a closed-form approach*, Submitted for publication in Phys. Rev. A, cond-mat/0503477 (2005).	
4	G. Pupillo, A.M. Rey, C.W. Clark, and C.J. Williams, *Pseudo-fermionization of 1-D bosons in optical lattices*, Submitted for publication in Phys. Rev. Lett., cond-mat/0505325 (2005).	
5	A.M. Rey, P.B. Blakie, G. Pupillo, C.J. Williams, C.W. Clark *Bragg Spectroscopy of ultracold atoms loaded in an optical lattice*, Accepted for publication in Phys. Rev. A, cond-mat/0406552 (2004).	
6	G. Pupillo, C.J. Williams, N.V. Prokof'ev, *Accurate and robust temperature measurement for ultracold atoms in deep optical lattices*, Submitted for publication in Phys. Rev. A, cond-mat/0407075 (2004).	
7	G. Pupillo, A.M. Rey, G.K. Brennen, C.J. Williams, C.W. Clark, *Scalable quantum computation in systems with Bose-Hubbard dynamics*, Journal of Modern Optics **51**, 2395 (2004). G.K. Brennen, G. Pupillo, A.M. Rey, C.W. Clark, C.J. Williams, *Scalable register initialization for quantum computing in an optical lattice*, Journal of Physics B **38**, 1687 (2005).	
	Publications not included in the dissertation	
	G. Pupillo, E. Tiesinga, C. J. Williams, *Effects of Inhomogeneity on the Spectrum of the Mott-Insulator State*, Phys. Rev. A **68**, 063604 (2003).	
	J. Gea-Banacloche, A.M. Rey, G. Pupillo, C.J. Williams, C.W. Clark, *Role of quantum fluctuations in the dissipative dynamics of a 1D Bose gas in an optical lattice*, Submitted for publication in Phys. Rev. A, cond-mat/0410677 (2004).	

Table 1.1: List of chapters in this dissertation, and corresponding submitted and published papers.

Chapter 2

A review of optical lattices and of atoms in periodic potentials

In this Chapter we review the basic theory of ultracold atoms in homogeneous optical lattices, where optical lattices are periodic potentials created by standing waves of interfering laser light. After reviewing the basic theory of optical potentials, in Sect.2.2 we analyze the energy spectrum of a single-particle in the optical lattice and the tight-binding approximation to the single-particle Hamiltonian valid for deep enough lattices. In order to treat interacting many-body systems, in Sect. 2.3 we introduce the Bose-Hubbard Hamiltonian and show how the latter is derived from the full second-quantized many-body Hamiltonian for bosons in periodic potentials. The phase diagram of the BH Hamiltonian, which is characterized by superfluid and Mott insulating phases, is reviewed.

2.1 Optical potentials

The kinematic processes pertaining to an atom interacting with a traveling wave comprise stimulated absorption of a photon followed by stimulated emission, and stimulated absorption followed by spontaneous emission. The first process corresponds to the conservative part of the atom-photon interaction and causes a shift in the atomic energy levels, due to the interaction between the light field and the induced dipole moment of the atom. This shift is known as *light* shift, or *ac-Stark* shift. The second process, that is stimulated absorption followed by spontaneous emission, can induce a dissipative force on the atom, because the momentum transferred back to the atom upon re-emission is on the average zero, while the photon is always absorbed from the laser's direction. In fact, by using a laser detuned below atomic resonance this process is routinely used to cool atoms.

In the following, we review the theory of optical lattice potentials. For the sake of simplicity, we focus on the case of a single two-level atom interacting with a classical monochromatic field, and we derive the light shift for the atomic levels, neglecting spontaneous emission. At the end of this Section, we show that our choice to neglect dissipative effects is in fact justified if the laser light is tuned far enough from the

atomic resonance.

In the dipole approximation valid for light wavelengths much larger than the atomic dimensions, the Hamiltonian of a two-level atom interacting with a classical electric field $\mathbf{E}(\mathbf{x}, t) = E_o(\mathbf{x}) \cos(\omega t - \phi) \mathbf{e}_L$ is

$$
\begin{aligned}
H &= \frac{\hbar\omega_o}{2} \left(|e\rangle\langle e| - |g\rangle\langle g| \right) - \hbar\Omega(\mathbf{x}) \left(|e\rangle\langle g| + |g\rangle\langle e| \right) \cos(\omega t - \phi) \\
&= \frac{\hbar\omega_o}{2}\sigma_z - \hbar\Omega(\mathbf{x}) \cos(\omega t - \phi)\sigma_x,
\end{aligned} \tag{2.1}
$$

where the bare atomic states $|g\rangle$ and $|e\rangle$ are separated in energy by $\hbar\omega_o$, $\Omega(\mathbf{x}) = E_o(\mathbf{x})\langle e|\mathbf{e}_L\cdot\mathbf{d}|g\rangle$ is the so-called Rabi frequency, $E_o(\mathbf{x})$ is the amplitude of the electric field, $\mathbf{e}_L$ is the electric field's polarization, ω is the frequency of the laser light, ϕ is a phase, $\mathbf{d}$ is the electric dipole of the atom, and $\sigma_z \equiv (\sigma^+\sigma^- - \sigma^-\sigma^+)$ and $\sigma_x \equiv (\sigma^+ + \sigma^-)$ are Pauli matrices, with

$$
\sigma^+ \equiv |e\rangle\langle g| = \begin{pmatrix} 0 & 1 \\ 0 & 0 \end{pmatrix}, \qquad \sigma^- \equiv |g\rangle\langle e| = \begin{pmatrix} 0 & 0 \\ 1 & 0 \end{pmatrix}.
$$

Expanding Eq.(2.1) yields

$$
H = \frac{\hbar\omega_o}{2}\sigma_z - \frac{\hbar\Omega(\mathbf{x})}{2} \left(e^{-i(\omega t - \phi)}\sigma_+ + e^{i(\omega t - \phi)}\sigma_- + e^{+i(\omega t - \phi)}\sigma_+ + e^{-i(\omega t - \phi)}\sigma_- \right). \tag{2.2}
$$

The first two terms inside the brackets describe processes where the atom rises from $|g\rangle$ to $|e\rangle$ by absorbing a photon, and falls from $|e\rangle$ to $|g\rangle$ by emitting a photon, respectively. The last two terms inside the brackets describe processes where the atom rises from $|g\rangle$ to $|e\rangle$ by emitting a photon, and falls from $|e\rangle$ to $|g\rangle$ by absorbing a photon, respectively. In order to remove the time dependence from Eq.(2.2), it is useful to choose a coordinate frame co-rotating with the laser. This is accomplished by the unitary transformation $|\tilde{\psi}\rangle = U^{-1}(t)|\psi\rangle$, where $U(t) = e^{-i\frac{\omega}{2}t\sigma_z}$. This gives

$$
\begin{aligned}
i\hbar\frac{d}{dt}|\tilde{\psi}\rangle &= U^{-1}(t)\left(i\hbar\frac{d}{dt}|\psi\rangle\right) + i\hbar\left(\frac{d}{dt}U^{-1}(t)\right)|\psi\rangle \\
&= U^{-1}(t)HU(t)|\tilde{\psi}\rangle - \frac{\hbar\omega}{2}\sigma_z|\tilde{\psi}\rangle.
\end{aligned} \tag{2.3}
$$

14

Because $U^{-1}(t)\sigma_z U(t) = \sigma_z$ and $U^{-1}(t)\sigma_{\pm}U(t) = e^{\pm i\omega t}\sigma_{\pm}$, in the new coordinate frame Eq.(2.2) reads

$$H = -\frac{\hbar\Delta}{2}\sigma_z - \frac{\hbar\Omega(\mathbf{x})}{2}\left(e^{i\phi}\sigma_+ + e^{-i\phi}\sigma_- + e^{-i\phi}e^{2i\omega t}\sigma_+ + e^{i\phi}e^{-2i\omega t}\sigma_-\right), \tag{2.4}$$

where $\Delta \equiv \omega - \omega_o$ is the *detuning* from atomic resonance. For times much longer than $1/\omega$ and provided $\Omega \ll \omega_o$, the net time average effect of the last two terms of Eq.(2.4) is approximately zero, and such processes can be therefore neglected. In this approximation, known as the Rotating Wave Approximation, Eq.(2.4) reduces to

$$H \approx -\frac{\hbar\Delta}{2}\sigma_z - \frac{\hbar\Omega(\mathbf{x})}{2}\left(e^{i\phi}\sigma_+ + e^{-i\phi}\sigma_-\right) = -\frac{\hbar\Delta}{2}\sigma_z - \frac{\hbar\Omega(\mathbf{x})}{2}\left[\cos(\phi)\sigma_x - \sin(\phi)\sigma_y\right]. \tag{2.5}$$

In the rotating frame the new Hamiltonian is therefore $H = \mathbf{\Omega}_{eff} \cdot \sigma$, with $\mathbf{\Omega}_{eff} = \tilde{\Omega}\mathbf{e}_n$ and $\mathbf{e}_n$ a unit vector along the direction n. The energy eigenvalues of this Hamiltonian are readily given by $E = \pm\sqrt{(\hbar\Delta/2)^2 + (\hbar\Omega/2)^2}$. In the limit of large detuning, $\Delta \ll \Omega$, where the excited state population $s = \Omega^2/(2\Delta^2)$ is negligible, the energy shift becomes

$$E \simeq \pm\frac{\hbar\Delta}{2}\left[1 + \frac{1}{2}\left(\frac{\Omega(\mathbf{x})}{\Delta}\right)^2\right] \tag{2.6}$$

The last term in the square brackets is the so-called light shift, or *ac-Stark* shift. This is the shift to the energies of the bare atomic levels due to the interaction with the light field. For a red detuning, $\Delta < 0$, the minima of the potential are found at points where the intensity is maximum. For a blue detuning, $\Delta > 0$, the points of highest intensity correspond to maxima of the potential, and atoms are therefore attracted to the points of lowest intensity.

The ac-Stark shift corresponds to the conservative part of the interaction between the atom and the light field. The non-conservative part is due to spontaneous emission to the electromagnetic field. This process can be taken into account by introducing a term proportional to the atom's spontaneous emission rate Γ in Eq.(2.1), $-i\Gamma/2|e\rangle\langle e|$. In the limit of small population of the excited state $s = 2\Omega^2/(4\Delta^2 + \Gamma^2)$, the effective scattering rate is $\Gamma' = s\Gamma$ which leads to the following expression for the non-conservative part of the potential in the limit $\Delta \gg \Gamma$:

$$\frac{\hbar\Omega(\mathbf{x})^2\Gamma}{8\Delta^2}.$$ (2.7)

The fact that the conservative part of the potential depends on the detuning as $\sim 1/\Delta$ (Eq.(2.6)) while the non-conservative part depends on Δ as $\sim 1/\Delta^2$ shows that the choice of a sufficiently large detuning can make the optical potential largely conservative.

2.1.1 Periodic lattices

Optical lattices are created by the superposition of two or more laser beams. In particular, a one dimensional optical lattice is realized by the superposition of two laser beams counter-propagating in the x-direction with amplitude $E_\pm(x) = E_o exp(\pm ikx)$, wave-vector k and wavelength $\lambda = 2\pi/k$. This lasers' configuration produces an optical potential $V_{Latt}(x) = V_o \cos^2(kx) = \frac{\Omega^2}{\Delta}\cos^2(kx)$, whose depth is determined by the beams' intensity. Such potential varies periodically in space with periodicity $a = \lambda/2$, where a is the lattice spacing. The addition of pairs of beams in the orthogonal directions gives rise to two and three dimensional lattices. The depth and geometry of the lattices can be easily varied by modifying the intensity of the lasers and the angles between the beams, respectively [37]. Even the position of the lattice minima can be varied by changing the laser polarizations. This flexibility together with the defect-free nature of the optical potentials make the optical lattices almost perfect crystals.

2.2 Non interacting atoms in the optical lattice

2.2.1 Bloch functions and Wannier functions

Solutions of the Schrödinger equation for a particle of mass m in a lattice potential

$$H_o\phi = -\frac{\hbar^2}{2m}\frac{\partial^2\phi}{\partial x^2} + V_o\cos^2\left(\frac{\pi}{a}x\right)\phi$$ (2.8)

are Bloch functions $\phi_q^{(n)}(x) = exp(iqx)u_q^{(n)}(x)$, with q the lattice quasi-momentum and n the band index. The quasi-momentum q is restricted to the first *Brillouin* zone, or $-\pi/a < q < \pi/a$, and the function

$u_q^{(n)}(x)$ is periodic with period a. An atom in the periodic lattice therefore behaves like a plane-wave, whose amplitude modulates with the period of the lattice.
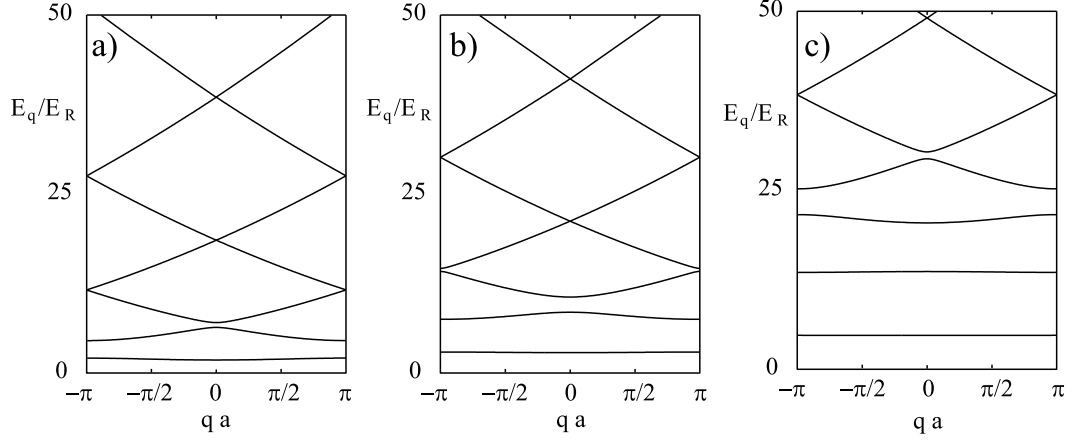
Figure 2.1: Band structure of an optical lattice of the form $V_o(x) = V_o cos^2(kx)$. Panels a), b), and c) correspond to lattice depths $V_o/E_R = 5, 10,$ and 25, respectively. (From Ref. [38])

Figure 2.1 shows the energy of a single particle in a periodic potential as a function of q, for different values of the optical lattice depth V_o. Here, $E_R = \hbar^2 k^2/2m$ is the photon recoil energy, where $k = 2\pi/\lambda$ is the wave-vector. For $V_o/E_R > 0$ a gap is formed between the lowest two bands. For larger V_o/E_R ratios, this gap becomes larger than the width of the two bands, and gaps between higher bands are also formed. For deep enough lattices, the gap between successive bands is approximately proportional to the oscillation frequency ω_{Latt} of a particle trapped at the potential minimum of a lattice site. Because the lattice potential is well approximated by a parabolic potential around the minimum, the frequency of oscillation is roughly $\omega_{Latt} = \sqrt{4V_o E_R}/\hbar$.

For deep enough lattices, the amplitude of the single-particle wave-function is largely localized around the minima of the lattice potential. In this case, a convenient choice of basis for describing the particle's dynamics is constituted by the so-called *Wannier* states, $w_n(x)$. For a proper choice of the phases of the functions $\phi_q^{(n)}(x)$, the Wannier states are defined as

$$w_n(x - x_j) = \frac{1}{\sqrt{M}} \sum_q e^{-iqx_j} \phi_q^{(n)}(x). \qquad (2.9)$$

17

where x_j is the position of the jth minimum of the lattice potential, and M is the total number of lattice sites. When the bands are not degenerate, Wannier states are localized at single lattice sites, and the wave-function $w_n(x)$ tends to one of the nth excited state of a harmonic oscillator.

2.2.2   Single-band tight-binding approximation

In the following we focus on the case where atoms are loaded onto the lowest vibrational level of each lattice site only, *e.g.* $n = 0$. In this case the wave-function $\phi(x)$ of a particle in the lattice potential can be expanded in terms of lowest-band Wannier states

$$\phi(x) = \sum_j z_j w_0(x - ja), \tag{2.10}$$

where $w_0(x - ja)$ is the first-band Wannier function centered at lattice site j, and $\{z_j\}$ are complex ampli-tudes. For a deep enough lattice, tunneling to next nearest neighbors can be ignored. This approximation known as the tight binding approximation yields the following equations for the amplitudes $\{z_j\}$:

$$E z_j = -J \left(z_{j+1} + z_{j-1} \right), \tag{2.11}$$

with

$$J = - \int dx w_0^*(x) H_o w_0(x - a) dx. \tag{2.12}$$

where J is the tunneling matrix element between nearest neighboring lattice sites. In Eq.(2.11) the overall energy shift $\varepsilon_o = \int dx w_0^*(x) H_o w_0(x) dx$ has been set to zero. The dispersion relation is here given by $E_q = -2J \cos(qa)$, and the band width is therefore equal to $4J$.

2.3 Interacting bosons in the optical lattice

2.3.1 The Bose-Hubbard Hamiltonian

When inter-particle interactions are taken into account, it is convenient to treat the many-body system in a second quantized formalism. Then, the relevant Hamiltonian for interacting bosons in optical lattices in the tight-binding limit is the so-called *Bose-Hubbard* (*BH*) Hamiltonian [11, 12]. In the absence of external potentials, the latter is comprised of particle-hopping and inter-particle interaction terms. In the following we derive the BH Hamiltonian from the full many-body Hamiltonian including local two-particle interactions and external confining potentials, and summarize the basic properties of its zero-temperature phase diagram, which shows both superfluid and insulating phases. In particular, the BH model predicts the existence of a quantum phase transition from a superfluid to a Mott insulator due to the competition of particle-hopping and inter-particle interaction energies, at commensurate fillings of the lattice. Since its experimental realization in inhomogeneous lattices [13], this quantum phase transition has become a paradigm for the study of strongly interacting systems.

Derivation of the BH Hamiltonian

The Hamiltonian for interacting atoms in an optical lattice in three dimensions is

$$H = \int d^3x \hat{\phi}^\dagger(\mathbf{x}) \left(-\frac{\hbar^2}{2m}\frac{\partial^2}{\partial \mathbf{x}^2} + V_{Latt}(\mathbf{x}) + V_T(\mathbf{x}) \right) \hat{\phi}(\mathbf{x}) + \frac{1}{2} \int d^3x d^3y \hat{\phi}^\dagger(\mathbf{x}) \hat{\phi}^\dagger(\mathbf{y}) V_{int}(\mathbf{x}-\mathbf{y}) \hat{\phi}(\mathbf{x}) \hat{\phi}(\mathbf{y}),$$

(2.13)

where $\hat{\phi}(\mathbf{x})$ is the bosonic field operator, $V_{Latt}(\mathbf{x})$ is the sinusoidal lattice potential, $V_T(\mathbf{x})$ is an external potential which varies slowly with respect to the lattice spacing (e.g., a magnetic parabolic potential), and $V_{int}(\mathbf{x}-\mathbf{y})$ is a two-body short-range interaction potential. Because the thermal de-Broglie wave-length of ultracold atoms is much larger than the s-wave scattering length a_s, only s-wave scattering with a relative wave vector bewteen the two particles k much larger than the inverse of the scattering length, $1/a_s \ll k$, is important in interatomic collisions. Then, the full two-body interaction potential can be substituted by a delta-function potential, whose strength is proportional to a_s [42]

$$V_{int}(\mathbf{x} - \mathbf{y}) \sim \frac{4\pi a_s \hbar^2}{m} \delta(\mathbf{x} - \mathbf{y}). \tag{2.14}$$

The last term of Eq.(2.13) then reads

$$\frac{2\pi a_s \hbar^2}{m} \int d^3x \hat{\phi}^\dagger(\mathbf{x}) \hat{\phi}^\dagger(\mathbf{x}) \hat{\phi}(\mathbf{x}) \hat{\phi}(\mathbf{x}) \tag{2.15}$$

Analogous to Eq. (2.10), if the lattice is loaded such that only the lowest vibrational level of each lattice site is occupied, the field operator can be expanded in terms of lowest-band Wannier states only [11]

$$\hat{\phi}(\mathbf{x}) = \sum_{\mathbf{j}} \hat{a}_{\mathbf{j}} w_0(\mathbf{x} - \mathbf{x_j}), \tag{2.16}$$

where $\hat{a}_{\mathbf{j}}$ is the bosonic annihilation operator of a particle at site $\mathbf{j} = (j_x, j_y, j_z)$. Substitution of this expansion into Eq. (2.13) yields the Bose-Hubbard Hamiltonian [11]

$$H_{BH} = -\sum_{\langle \mathbf{j}, \mathbf{l} \rangle} J(\mathbf{j}) \hat{a}_{\mathbf{j}}^\dagger \hat{a}_{\mathbf{l}} + \sum_{\mathbf{j}} \left[\frac{U}{2} \hat{n}_{\mathbf{j}} (\hat{n}_{\mathbf{j}} - 1) + \epsilon_{\mathbf{j}} \hat{n}_{\mathbf{j}} \right]. \tag{2.17}$$

Here $J(\mathbf{j}) = -\int d^3x w_0^*(\mathbf{x} - \mathbf{x_j}) \left(-\frac{\hbar^2}{2m} \frac{\partial^2}{\partial \mathbf{x}^2} + V_{Latt}(\mathbf{x}) \right) w_0(\mathbf{x} - \mathbf{x_l})$ is the hopping energy at site $\mathbf{j}$, analogous to Eq. (2.12), $\langle \mathbf{j}, \mathbf{l} \rangle$ restricts the sum to nearest-neighbors, and U is the on-site interaction energy given by $U = \frac{4\pi a_s \hbar^2}{m} \int d^3x |w_0(\mathbf{x})|^4$. The quantity U is the energy cost for having two atoms at the same lattice site. The energy $\epsilon_{\mathbf{j}} = V_T(\mathbf{x_j})$ is due to the discretization of the external potential. In the remainder of this thesis, V_T is an external magnetic parabolic potential.

The quantities J and U are both dependent on the depth $V_{Latt}(\mathbf{x})$ of the optical lattice in each of the three directions $\alpha \equiv \{\hat{x}, \hat{y}, \hat{z}\}$. In fact, a deepening of the lattices exponentially suppresses the tunneling between neighboring sites, while the tighter confinement of atoms in the lattice wells increases the repulsive energy U. The tunneling rate J_α in the direction α decreases with $V_{Latt}(\alpha)$ for sinusoidal lattices as

$$J_\alpha = A \left(\frac{V_{Latt}(\alpha)}{E_R} \right)^B \exp \left(-C \sqrt{\frac{V_{Latt}(\alpha)}{E_R}} \right) E_R, \tag{2.18}$$

where the numerically obtained constants are $A = 1.397$, $B = 1.051$, and $C = 2.121$. The interaction

energy depends on the depth of the lattices as

$$U = \frac{2a_s\hbar}{\sqrt{2\pi}E_R} \left(\frac{\omega_{Latt}^x \omega_{Latt}^y \omega_{Latt}^z}{a_x a_y a_z} \right)^{\frac{1}{3}} \tag{2.19}$$

where $\omega_{Latt}^\alpha = \sqrt{4E_R V_{Latt}(\alpha)}/\hbar$ and $a_\alpha = \sqrt{\hbar/(m\omega_{Latt}^\alpha)}$. In the remainder of this thesis we will be concerned with one-dimensional optical lattices. In current experiments, one-dimensional lattices are obtained by tightly confining in two directions atoms loaded in three-dimensional lattices. Then, the interaction energy increases with the lattice depth $V_o \equiv V_{Latt}(x)$ in the longitudinal direction $\hat{x}$ as

$$U = \beta E_R \left(\frac{V_o}{E_R} \right)^{1/4}, \tag{2.20}$$

where $\beta = 4\sqrt{2\pi}(a_s/\lambda)(V_\perp/E_R)^{1/2}$, and $V_\perp$ is the depth of the lattice in the transverse directions $\hat{y}$ and $\hat{z}$ [71, 72].

We will be interested in systems with an additional continuous parabolic magnetic potentials that can be modeled as the discrete potential

$$\epsilon_j = \Omega j^2, \tag{2.21}$$

where $\Omega = ma^2 \omega_T^2/2$, with ω_T the frequency of the magnetic trap.

2.3.2 Phase diagram of the BH Hamiltonian

The physics of ultracold atoms in an optical lattice in the absence of external potentials is fully characterized by the average particle density $n = N/M$ and by the ratio $\gamma = U/J$ between the onsite interaction energy U and the hopping energy J. In fact, according to the values of n and γ, the system can be in either one of the two following phases: a so-called "superfluid" phase, where single-particle wave-functions are delocalized on a region which is of the order of the lattice size, and an insulator phase, known as "Mott" phase, where single-particle wave-functions are localized at single lattice sites.

Superfluid phase

The onset of superfluidity is a consequence of the competition between the kinetic energy, which tries to delocalize the particles, and the interactions, which try to localize the particles and make the number fluctuations small. The superfluid phase occurs both when n is an integer and γ is small, which corresponds to the limit where the kinetic energy dominates over the interaction energy, and when the mean particle density n is non-integer, independent of the ratio γ.

The nature of the superfluid phase is best understood in the limit of small interactions, in dimensions larger than one. When the kinetic energy dominates over the repulsion of two particles sitting in the same lattice site, nearly all atoms occupy the same single-particle state. This single-particle state corresponds to the eigenstate of the single-particle density matrix $\rho_{ij} = \langle a_i^\dagger a_j \rangle$ with the largest eigenvalue, and for very small interaction energies is very close to the Bloch wave-function with quasi-momentum $q = 0$ of the lowest Bloch band. The macroscopic occupation of one eigenstate of ρ_{ij} for small interactions corresponds to the realization of a *Bose-Einstein condensate* (BEC). Because this state is delocalized over the whole lattice, and has a well defined phase difference between the various sites, the system shows long-range off-diagonal coherence, meaning that the value of ρ_{ij} is independent of the distance between the sites i and j, $\rho_{ij} = N/M$. Particle number fluctuations $\Delta n_i = (\langle \hat{n}_i^2 \rangle - \langle \hat{n}_i \rangle^2)^{1/2}$ are large, and scale as $\Delta n_i = \sqrt{N/M}$. The energy spectrum in the superfluid regime is gapless. This is clear in the limit of zero interactions, where the lowest energy excitations are Bloch waves with quasi-momentum q. Then, the energy of the first excited state scales like J/M^2, which tends to zero for large M.

The presence of BEC at zero temperature should be regarded as a signal of and not as a necessary condition for superfluidity. In fact, the exact relation between BEC and superfluidity is still a subject of active research [45, 46]. A simple example of the fact that BEC is not necessary for superfluidity is a one-dimensional system of strongly interacting bosons. For large enough interactions, the energy spectrum of strongly interacting bosons maps to that of non-interacting fermions, the correspondence being exact in the limit of infinitely large interactions. This is the so-called *Tonks-Girardeau* (TG) limit [47]. In the TG

limit the largest eigenvalue of the single-particle density matrix is of order $\sqrt{N}$, and there is no BEC [39]. Nevertheless, the system is a superfluid, with the superfluid fraction ρ_s being equal to $\rho_s = \frac{\sin(\pi N/M)}{\pi N/M}$ [1] [40].

Mott insulating regime

When the interaction energy is much larger than the kinetic energy, $\gamma \gg 1$, particles minimize their energy by avoiding each other. When the average particle density n is an integer and equal to one, the energy is minimized when particles are localized each in a different site. In the limit of infinitely strong interactions, or, equivalently of zero kinetic energy J, the ground state $|\psi_g\rangle$ is then exactly the Fock state with one atom per site, $|\psi_g\rangle = |T\rangle \equiv \prod_i a_i^\dagger |0\rangle$, where $|0\rangle$ represents the vacuum. This state has exactly zero interaction energy, $\sum_j \langle T|U(\hat{n}_j^2 - \hat{n}_j)/2|T\rangle = 0$. The lowest lying excitations, known as particle-hole excitations, are obtained by removing a particle from a site and putting it on top of an atom sitting in another site. The energy required for this is U, independent of the lattice size, and therefore the system is characterized by a finite gap U which is large compared to the small excitation energies of the superfluid limit.

For finite small J, perturbation theory readily shows that the ground state is a superposition of the Fock state with one atom per site $|T\rangle$ and Fock-states $|S\rangle = 1/\sqrt{4N} \sum_{j=1}^N (a_{j+1}^\dagger a_j + a_j^\dagger a_{j+1})|T\rangle$ with zero particles in one site and an extra particle in one of the nearest neighboring sites. This state is the so-called Mott state

$$|\psi_g\rangle = \alpha \left(|T\rangle + 2\sqrt{N} J/U |S\rangle \right), \qquad (2.22)$$

where the normalization constant is $\alpha = \left(1 + 4N(J/U)^2\right)^{-1/2}$. The energy of the Mott state is approximately $E_g = -4NJ^2/U$.

---

[1]This finite value of ρ_s is obtained by imposing a phase variation to the wave-function, and measuring the response of the system to the perturbation. The difference in energy before and after the perturbation is proportional to the superfluid fraction [43, 44].
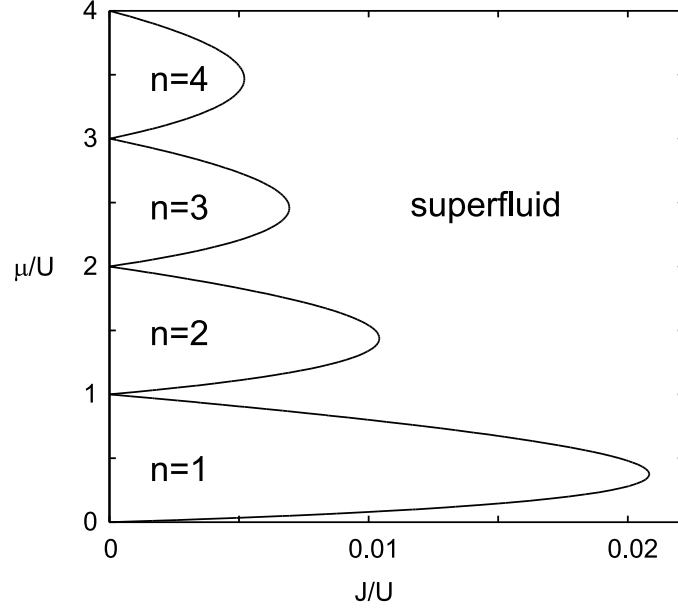
Figure 2.2: Zero-temperature phase-diagram for the BH Hamiltonian in the $\mu - J$ plane in three dimensions, in the absence of external confinement, $\Omega = 0$. The lobe-like structures are Mott insulator phases with average number of atoms n per site.

Phase diagram

The phase diagram of the system in the absence of external potentials, ($\Omega = 0$), is given in the grand canonical ensemble, where the mean particle number is fixed by a particle reservoir of chemical potential μ [12, 48]. The BH Hamiltonian reads

$$H_{BH} = \sum_j \left[-J(\hat{a}_j^\dagger \hat{a}_{j+1} + \hat{a}_{j+1}^\dagger \hat{a}_j) + \frac{U}{2}\hat{n}_j(\hat{n}_j - 1) - \mu \hat{n} \right]. \tag{2.23}$$

Figure 2.2 shows the phase diagram in the $\mu - J$ plane in three dimensions. The corresponding phase diagram in one dimension shows the same qualitative features. In agreement with our previous discussion, the phase diagram shows the presence of a large region of parameters where the system is superfluid, and lobe-like structures where the mean particle density is integer. These lobes correspond to the Mott insulating regions, where particle fluctuations, and therefore the compressibility $\partial n/\partial \mu$, vanish. For any point within the Mott phase, the energy gap for the creation of an extra particle (hole) is the distance in the μ direction to the upper (lower) phase boundary. Thus, the energy gap to number-conserving particle-hole excitations in the Mott phase is here represented by the width in μ of the lobe, for any fixed value of J. At $J = 0$ this
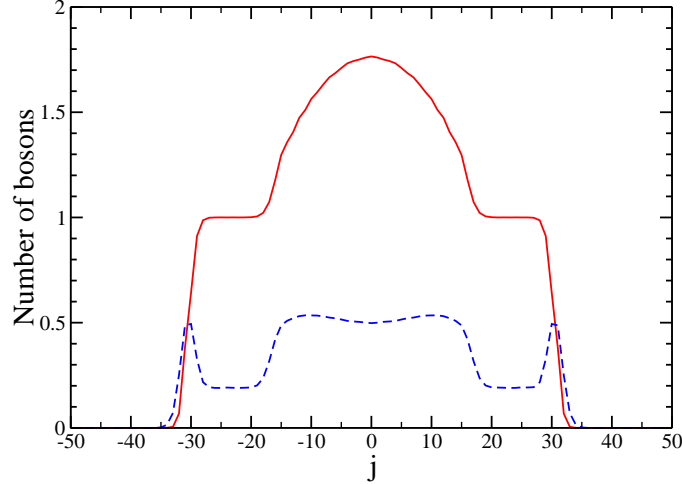
Figure 2.3: On-site density, continuous(red) line, and number fluctuations, dashed(blue) line, as a function of the site index j, in one dimension. Here, $N = 80$, $\Omega/J \approx 0.02$, and $U/J \approx 15$. The regions of integer and non-integer density correspond to the Mott insulating and superfluid phases, respectively. The site $j = 0$ corresponds to the center of the parabolic potential.

gap is exactly U. Because the kinetic energies of the extra particle and the hole increase with increasing J, the width in μ of the Mott phase decreases, determining the lobe-like structure.

The transition from a Mott insulating phase to the superfluid phase occurs either as the density moves away from a commensurate (integer) value, or as the hopping energy is increased at fixed commensurate density. This last transition occurs only at the tip of each Mott lobe, while the transition at a generic point of the insulator/superfluid phase boundary is of the density-type. In Ref. [12] it is shown that these phase transitions actually belong to two distinct universality classes. For the density-transition at a generic point of the insulator/superfluid phase boundary, the parameter measuring the distance from the transition point can be defined as $\mu - \mu_c$, where μ_c is the chemical potential at the transition point. Then, the compressibility diverges near the transition as $\partial n/\partial \mu \sim (\mu - \mu_c)^{-\zeta}$, with $\zeta > 0$. Here, $\mu - \mu_c$ and $\partial n/\partial \mu$ are the analogs of the reduced temperature $T - T_c$ and the specific heat for finite temperature transitions, respectively. For the special case of the constant-density transition at the tip of the Mott lobes, the parameter measuring the distance from the transition point is $(J/U) - (J/U)_c = \gamma - \gamma_c$, with $\gamma_c \approx 4$ for the Mott phase with unit particle density in one dimension [48]. Here, differentiation with respect to $(J/U) - (J/U)_c$ becomes inequivalent to differentiation with respect to the chemical potential.

When the external parabolic potential is present, $\Omega > 0$, the density profile of the bosonic ensemble

is determined by an interplay of Ω, N, J, and U. Different from the homogeneous case, it has been found numerically [11, 27, 28, 49] and investigated analytically [50] that Mott insulating and superfluid phases can actually coexist for $\Omega > 0$. Figure 2.3 shows an example of the coexistence of superfluid and insulating phases, for $N = 80$ particles, $\Omega/J \approx 0.02$, $U/J \approx 15$, in one dimension. These results have been obtained by utilizing a Quantum Monte-Carlo code, Worm Algorithm [30], with a temperature $T = 0.01\,J/k_B$, where k_B is the Boltzmann constant. In the figure, the continuous(red) and the dashed(blue) lines are the on-site density and number fluctuations as a function of the lattice position j, respectively. Here, $j = 0$ corresponds to the bottom of the parabolic potential. The density profile decreases from a peak density of about $n_j = 1.7$ at $j = 0$ to a value of one for $20 \leq |j| \leq 30$, and then to zero. Here, the regions of non-integer density correspond to superfluid phases, while the integer-valued plateaux correspond to a Mott insulator with unit filling. This interpretation is confirmed by the behavior of the number fluctuations. In fact, fluctuations are large where the density is non-integer, and drop to a small constant value when the density becomes integer. This value is $\approx 2\sqrt{2}J/U$, and is due to the mixing of particle-hole excitations in the Mott insulator at zero temperature, in analogy to the homogeneous system [51]. Qualitatively, the coexistence of superfluid and insulating phases for Ω small enough can be understood on the basis of the phase diagram of the homogeneous system, by defining a local chemical potential $\mu_j = \mu - \Omega j^2$. Then, for any choice of U, J, and N, the density at site j is fixed by the value of μ_j, according to the diagram of Fig. 2.2. Because of the coexistence of compressible and incompressible phases, in Ref. [28] it was shown that the formation of the Mott region is actually not a true quantum critical phenomenon in the confined case as it is in the unconfined case. In Chapters 3 and 4 we explain microscopically how the Mott insulating regions are created in the parabolically confined systems of current experimental interest.

Chapter 3

Ultracold atoms confined in an optical lattice plus parabolic potential: a closed-form approach

We discuss interacting and non-interacting one dimensional atomic systems trapped in an optical lattice plus a parabolic potential. We show that, in the tight-binding approximation, the non-interacting problem is exactly solvable in terms of Mathieu functions. We use the analytic solutions to study the collective oscillations of ideal bosonic and fermionic ensembles induced by small displacements of the parabolic potential. We treat the interacting boson problem by numerical diagonalization of the Bose-Hubbard Hamiltonian. From analysis of the dependence upon lattice depth of the low-energy excitation spectrum of the interacting system, we consider the problems of "fermionization" of a Bose gas, and the superfluid-Mott insulator transition. The spectrum of the noninteracting system turns out to provide a useful guide to understanding the collective oscillations of the interacting system, throughout a large and experimentally relevant parameter regime.

3.1   Introduction

In recent experiments [14, 15, 16, 18, 19], quasi-one dimensional systems have been realized by tight confinement of gases in two dimensions. Due to the enhanced importance of quantum correlations as dimensionality is reduced, such systems exhibit physical phenomena not present in higher dimensions, such as "fermionization" of a Bose gas.

The degree of correlation is measured by the ratio of the interaction energy to the kinetic energy, γ. For $\gamma \ll 1$ the system is weakly interacting, and at zero temperature most atoms are Bose-condensed. In this limit quantum correlations are negligible and the dynamics is governed by the mean-field Gross-Pitaevski equation. For $\gamma \gg 1$, the system is highly correlated and becomes fermionized, in that repulsive interactions mimic the effects of the Pauli exclusion principle. In this "Tonks-Girardeau" regime, [41, 47], the low energy excitation spectrum of a bosonic gas resembles that of a gas of non-interacting fermions.

27

To date, one dimensional systems have been obtained by loading a Bose-Einstein condensate into a two-dimensional optical lattice which is deep enough to restrict the dynamics to one dimension. This procedure creates an array of independent 1D tubes. In most experiments, a weak quadratic potential is superimposed upon the lattice, in order to confine the atoms during the loading proccess. The combined presence of the periodic and quadratic potentials substantially modifies the dynamics of the trapped atoms compared to the cases when only one of the two potentials is present, as shown both experimentally and theoretically [20, 49, 52, 53, 54, 55].

In this chapter we study both ideal and interacting bosonic systems in such potentials. In contrast to previous studies of ideal systems, which used numerical[53] or approximate solutions [20, 49, 54, 55], here we show that the single-particle problem is exactly solvable in terms of Mathieu functions[56, 57, 58]. We use analytic solutions to fully characterize the energy spectrum and eigenfunctions in the various regimes of the trapping potentials and to provide analytic expressions for the oscillations of the center of mass of both ideal bosons and fermions that are induced by small displacements of the parabolic trap. These expressions for the dipolar motion may be tested in experiments.

We further analyze the low-energy spectrum of interacting bosons by means of exact diagonalizations of the Bose-Hubbard Hamiltonian, and identify the conditions required for fermionization to occur. Moreover, we show that specific changes in the spectrum of the fermionized system can be used to describe the characteristics of a Mott insulator state with unit filling at the trap center.

Center-of-mass oscillations are also studied in the weakly interacting and fermionized regimes by comparing exact numerical solutions for the interacting system to solutions for ideal bosons and fermions, respectively. Because fermionization occurs over a large range of trap parameters, knowledge of the properties of the single-particle solutions turns out to provide useful insights in the understanding of the complex many-body dynamics. In addition, we numerically analyze the distribution of frequencies pertaining the modes excited during the collective dynamics, for different values of γ. This helps us gain qualitative insight in the dynamics even in the intermediate regime where interaction and kinetic energies are comparable and no mapping to ideal gases is possible.

The presentation of the results is organized as follows: In Sec. 3.2.1 we discuss the analytic solutions that describe the single-particle physics. These show the existence of two types of behavior, according to whether the energy is dominated by site hopping or parabolic contributions. Different asymptotic expansions of the eigenfunctions and eigenvalues apply to these two regimes, and can be effectively combined to describe the full spectrum.

In Sec. 3.3, we then apply the analytic solutions and asymptotic expansions to the description of the collective dynamics of non-interacting ensembles of bosons and fermions subject to a sudden displacement of the parabolic trap. In contrast to the well-known case of the displaced harmonic oscillator, a non-trivial modulation of the center of mass motion occurs due to the presence of the lattice potential. We derive explicit expressions for the initial decay of the amplitude of the oscillation, to which we refer as *effective* damping.

In Sec. 3.4.1, the low-energy spectrum of interacting bosons is studied as a function of the lattice depth. In particular, we follow the evolution of the spectrum from ideal bosonic to ideal fermionic as the lattice deepens, by means of numerical diagonalization of the Hamiltonian for a moderate number of atoms and wells. We specify the necessary conditions for the formation of a Mott state at the center of the trap, and use the Fermi-Bose mapping to link its appearance and the reduction of number fluctuations to the population of high-energy localized states at the Fermi level.

Section 3.5 is dedicated to the study of the collective dipole dynamics of an interacting bosonic gas by numerical calculations of the exact quantal dynamics. The dynamics is studied for two different scenarios that are experimentally realizable. The first corresponds to experiments in which the trapping potentials are kept fixed and the interatomic scattering length is varied (e.g. by use of a Feshbach resonance), Sec. 3.5.1 B1. Here, parameters have been chosen such that no Mott insulator at the center of the trap is formed in the large γ limit. The second scenario corresponds to experiments in which the lattice depth is increased while the frequency of the parabolic potential is kept fixed, Sec. 3.5.2. In this case a unit filled Mott insulator is formed at the trap center and the inhibition of the transport properties of the system is observed as the lattice deepens.

3.2 Single particle problem

3.2.1 Tight binding solution

The dynamics of a single atom in a one dimensional optical lattice plus a parabolic potential is described by the Schrödinger equation

$$i\hbar\frac{\partial \Phi}{\partial t} = -\frac{\hbar^2}{2m}\frac{\partial^2 \Phi}{\partial x^2} + V_o \sin^2\left(\frac{\pi}{a}x\right)\Phi + \frac{m\omega_T^2}{2}x^2\Phi, \qquad (3.1)$$

where $\Phi(x)$ is the atomic wave function, ω_T is the trapping frequency of the external quadratic potential, V_o is the optical lattice depth which is determined by the intensity of the laser beams, $a = \lambda/2$ is the lattice spacing, λ is the wavelength of the lasers and m is the atomic mass.

As shown in Sect. 2.3.1, if the atom is loaded into the lowest vibrational state of each lattice well and the dynamics induced by external perturbations does not generate interband transitions, the wave function $\Phi(x)$ can be expanded in terms of first-band Wannier functions only [59, 60]

$$\Phi(x,t) = \sum_j z_j(t)w_0(x - ja), \qquad (3.2)$$

where $w_0(x - ja)$ is the first-band Wannier function centered at lattice site j, t is time, and $\{z_j(t)\}$ are complex amplitudes. Numerical comparisons show that for a lattice depth $V_o \gtrsim 2E_R$ tunneling to next-to-nearest-neighbors sites is almost one order of magnitude smaller than tunneling to nearest-neighboring sites and therefore the former can be neglected [61]. Here $E_R = h^2/(2m\lambda^2)$ is the photon recoil energy, a useful energy unit for atoms in optical lattices. The approximation of considering nearest-neighbor tunneling only is known as the tight binding approximation, and yields the following equations of motion for the amplitudes $\{z_j(t)\}$:

$$i\hbar\frac{\partial z_j}{\partial t} = -J\left(z_{j+1} + z_{j-1}\right) + \Omega j^2 z_j, \qquad (3.3)$$

with

$$\Omega = \frac{1}{2}ma^2\omega_T^2, \tag{3.4}$$

$$J = -\int dx w_0^*(x) H_o w_0(x-a) dx, \tag{3.5}$$

$$H_o = -\frac{\hbar^2}{2m}\frac{\partial^2}{\partial x^2} + V_o \sin^2\left(\frac{\pi}{a}x\right) \tag{3.6}$$

where J is the tunneling matrix element between nearest neighboring lattice sites. In Eq.(3.3) the overall energy shift ε_o given by

$$\varepsilon_o = \int dx w_0^*(x) H_o w_0(x) dx, \tag{3.7}$$

has been set to zero.

We notice that because we restrict our discussion to the lowest band only, our results are valid for states whose wave function does not extend beyond the site $j_{max} = \sqrt{\hbar\nu/\Omega}$ where $\hbar\nu$ is the energy difference between the first and the second bands. For lattices deep enough that the orbitals at the bottom of each well can be approximated by those of an harmonic oscillator, $\hbar\nu$ is given by $\hbar\nu = \sqrt{4V_o E_R}$. In the following we provide specific examples for the range of applicability of our theory.

3.2.2 Stationary solutions

The stationary solutions of Eq.(3.3) are of the form $z_j^{(n)}(t) = f_j^{(n)} e^{-iE_n t/\hbar}$, with E_n and $f_j^{(n)}$ the nth eigenenergy and eigenstate, respectively. Substitution into Eq.(3.3) yields

$$E_n f_j^{(n)} = -J\left(f_{j+1}^{(n)} + f_{j-1}^{(n)}\right) + \Omega j^2 f_j^{(n)} \tag{3.8}$$

Equation (3.8) is formally equivalent to the recursion relation satisfied by the Fourier coefficients of the periodic Mathieu functions with period π. Therefore the eigenvalue problem can be exactly solved by identifying the amplitudes $f_j^{(n)}$ and eigenenergies E_n with the Fourier coefficients and characteristic values of such functions, respectively [56]. In terms of Mathieu parameters the symmetric and antisymmetric solutions are

$$f_j^{(n=2r)} \quad = \quad \frac{1}{\pi} \int_0^{2\pi} ce_{2r}\left(x, -q\right) \cos(2jx) dx, \tag{3.9}$$

$$f_j^{(n=2r+1)} \quad = \quad \frac{1}{\pi} \int_0^{2\pi} se_{2r}\left(x, -q\right) \sin(2jx) dx, \tag{3.10}$$

$$E_{n=2r} \quad = \quad \frac{\Omega}{4} a_{2r}\left(q\right) \qquad E_{n=2r+1} = \frac{\Omega}{4} b_{2r}\left(q\right), \tag{3.11}$$

with $r = 0, 1, 2...$ and $ce_{2r}(x, q)$ and $se_{2r}(x, q)$ the even and odd period π solutions of the Mathieu equation with parameter $q = \frac{4J}{\Omega}$ and characteristic parameter $a_{2r}(q)$ and $b_{2r}(q)$ respectively: $\frac{d^2 ce_{2r}}{dx^2} + (a_{2r}(q) - 2q\cos(2x)) ce_{2r} = 0$ and $\frac{d^2 se_{2r}}{dx^2} + (b_{2r}(q) - 2q\cos(2x)) se_{2r} = 0$.

Solutions of the single particle problem are entirely determined by the parameter $q = \frac{4J}{\Omega}$, which is proportional to the ratio of the nearest-neighbor hopping energy J to the energy cost Ω for moving a particle from the central site to its nearest-neighbor. The eigenvalues and eigenstates of the system are in general complicated functions of q. However, asymptotic expansions exist in the literature which can help unveil the underlying physics for different values of q. Most of the asymptotic expansions have been available for almost 50 years due to the work of Meixner and Schäfke [57]. In the remainder of this section we introduce such asymptotic expansions and use them to describe the physics of the system in the tunneling dominated regime where $q > 1$, which we call *high q* regime, and the $q < 1$, or *low q* regime.

High q regime ($4J \gtrsim \Omega$)

Most experiments have been developed in the parameter regime where $q \gg 1$. For example for ^{87}Rb atoms trapped in a lattice with $\lambda = 810$ nm, a value of $q \geq 10$ is obtained for a lattice depth of 2 E_R if $\omega_T < 2\pi \times 538$ Hz and for a lattice of 50 E_R if $\omega_T < 2\pi \times 7.5$ Hz. Here E_R is the photon recoil energy $E_R = h^2/(2m\lambda^2)$, corresponding to a frequency $E_R/h = 3.47$ kHz. Throughout this chapter, in our examples we use atoms with the mass of ^{87}Rb.

In the high q limit the periodic plus harmonic potential possesses two different classes of eigenstates depending on their energy. In fact, as we will show, eigenmodes can be classified as low or high-energy

depending on the quantum number n being smaller or larger than $2\|\sqrt{q/2}\|$, respectively, where $\|x\|$ denotes the closest integer to x. Physically, this classification depends on which one of the two energy scales in the system, the tunneling or the trapping energy, is dominant. To the energy classification corresponds a classification based on localization of the modes in the potentials. In particular, the low-energy (LE) modes are extended around the trap center and high-energy (HE) modes are localized on the sides of the potential. The existence of localized and extended states has been tested experimentally [20, 52] and studied theoretically [49, 53, 54, 55]. Here we show how the asymptotic expansions of the Mathieu solutions can be used to characterize them quantitatively.

Low-energy modes ($n \ll \sqrt{q}$) in the high q regime

In the LE regime the average hopping energy J is larger than Ω. In this regime the eigenmodes have been shown to be approximately harmonic oscillator eigenstates [49, 53, 54, 55]. Asymptotic expansions valid to describe LE eigenmodes in the high q limit have been studied in detail in Ref. [58], where the eigenstates are described in terms of generalized Hermite polynomials. Here we simply outline the basic results and refer the interested reader to [58] and references therein for further details.

The asymptotic expansions for the eigenmodes can be written as

$$f_j^{(n=2r)} \approx A_n \exp\left(-\xi^2\left(\frac{1}{2} + \frac{(3+2n)}{16\sqrt{q}}\right) + \frac{\xi^4}{48\sqrt{q}}\right)$$
$$\cdot \sum_{k=0}^{r} h_k^{(r)} \xi^{2k}\left(1 + \frac{(3k - k^2 + 10kr)}{24\sqrt{q}}\right) \tag{3.12}$$

$$f_j^{(n=2r+1)} \approx A_n \exp\left(-\xi^2\left(\frac{1}{2} + \frac{(3+2n)}{16\sqrt{q}}\right) + \frac{\xi^4}{48\sqrt{q}}\right)$$
$$\cdot \sum_{k=0}^{r} \tilde{h}_k^{(r)} \xi^{2k+1}\left(1 + \frac{(7k - k^2 + 10kr)}{24\sqrt{q}}\right) \tag{3.13}$$

with $\xi = j\sqrt[4]{\frac{4}{q}}$, $h_k^{(r)} = \frac{(-1)^{r+k} 2^{2k} 2r!}{(2k)!(r-k)!}$, $\tilde{h}_k^{(r)} = \frac{(-1)^{r+k} 2^{2k+1} (2r+1)!}{(2k+1)!(r-k)!}$ and A_n a normalization constant. Notice that the coefficients $h_k^{(r)}$ and $\tilde{h}_k^{(r)}$ are related to the Hermite polynomial $H_n(x)$ by the relations $H_{2r}(x) = \sum_{k=0}^{r} h_k^{(r)} x^{2k}$ and $H_{2r+1}(x) = \sum_{k=0}^{r} \tilde{h}_k^{(r)} x^{2k+1}$.

The eigenenergies are approximately given by

$$E_n^{low} \approx \frac{\Omega}{4} \left\{ -2q + 4\sqrt{q}(n + \frac{1}{2}) - \frac{(2n+1)^2 + 1}{8} - \frac{((2n+1)^3 + 3(2n+1))}{2^7\sqrt{q}} + O\left(\frac{1}{q}\right) \right\} \quad (3.14)$$

If one neglects corrections of order $1/\sqrt{q}$ and higher in Eqs. (3.12) and (3.13) and keeps only the first two terms in Eq. (3.14), the expressions for the eigenmodes and eigenenergies reduce to

$$E_n = -\Omega q/2 + \Omega\sqrt{q}(n + \frac{1}{2}) \quad (3.15)$$

$$f_j^{(n)} \approx \sqrt{\frac{\sqrt{2}}{2^n n! \sqrt[4]{q\pi^2}}} \exp\left(-\frac{\xi^2}{2}\right) H_n(\xi). \quad (3.16)$$

The above expressions correspond to the eigenvalues and eigenenergies (shifted by $-\Omega q/2$) of a harmonic oscillator with an effective trapping frequency ω^* and an effective mass m^*. The effective frequency and mass are given by

$$\hbar\omega^* = \Omega\sqrt{q} = \hbar\omega_T\sqrt{\frac{m}{m^*}}, \quad (3.17)$$

$$m^* = \frac{\hbar^2}{2Ja^2}, \quad (3.18)$$

The harmonic oscillator character of the lowest energy modes in the combined lattice plus harmonic potential is consistent with the fact that near the bottom of the Bloch band the dispersion relation has the usual free particle form with m replaced by m^*. It is important to emphasize that the expressions for the effective mass and frequency Eqs. (3.17) and (3.18) are only valid in the tight-binding approximation.

Higher order terms introduce corrections to these harmonic oscillator expressions, that become more and more important as the quantum number n increases. These corrections come from the discrete character of the tight-binding equation. They can be calculated by replacing $f_j^{(n)}$ with $f^{(n)}(\xi)$ and taking the continuous limit of the hopping term proportional to J in Eq.(3.8). This procedure yields:

$$\left(-\frac{1}{2}\frac{\partial^2}{\partial\xi^2} - \frac{1}{12a_{ho}^2}\frac{\partial^4}{\partial\xi^4} + \cdots + \frac{1}{2}\xi^2 \right) f^{(n)} = \widetilde{E}_n f^{(n)} \quad (3.19)$$

where $\xi = j\sqrt[4]{\frac{4}{q}} \equiv \frac{j}{a_{ho}}$, $a_{ho} = \sqrt{\frac{\hbar}{m^*\omega^*}} = (q/4)^{1/4}$ is a characteristic length of the system in lattice units, which can be understood as an effective harmonic oscillator length, and $\widetilde{E}_n = (E_n + 2J)/(\hbar\omega^*)$. To zeroth order in $1/\sqrt{q}$, $(a_{ho} \to \infty)$, the differential equation (3.19) reduces to the harmonic oscillator Schrödinger

equation. Higher order corrections given in Eqs.(3.12), (3.13) and (3.14), can be calculated by treating the higher order derivatives in Eq.(3.19) as a perturbation.

High-energy modes ($n \gg \sqrt{q}$) in the high q regime

High energy modes are close to position eigenstates since for these states the kinetic energy required for an atom to hop from one site to the next becomes insufficient to overcome the potential energy cost [53, 54, 55, 49]. By using asymptotic expansions of the characteristic Mathieu values and functions, we obtain the following expressions for the spectrum and eigenmodes

$$E_{n=2r}^{high} \approx E_{n=2r-1}^{high} \approx \frac{\Omega}{4} \left((2r)^2 + \frac{q^2}{2((2r)^2 - 1)} + \frac{q^4 \left(7 + 5 (2r)^2 \right)}{32 \left((2r)^2 - 1 \right)^3 \left((2r)^2 - 4 \right)} + \ldots \right) \quad (3.20)$$

$$f_j^{(high)\, n=2r} \approx f_j^{(high)\, n=2r-1} \approx A_n \left\{ \delta_{j,r} - \frac{q}{4} \left(\frac{\delta_{j,r-1}}{2r - 1} - \frac{\delta_{j,1+r}}{1 + 2r} \right) + \right.$$
$$\left. \frac{q^2}{32} \left(\frac{\delta_{j,r-2}}{(2r - 2)(2r - 1)} - \frac{2(1 + 4r^2)\delta_{j,r}}{(2r - 1)^2(1 + 2r)^2} + \frac{\delta_{j,2+r}}{(1 + 2r)(2 + 2r)} \right) \right\} \pm \{ j \to -j \} \quad (3.21)$$

with A_n normalization constants. We note that the asymptotic expansions Eqs.(3.20) and (3.21) for the HE-modes in the high q regime are identical to the asymptotic expansions for the modes in the low q regime reported below. While the latter are well known in literature, to our knowledge they have never been used to describe the high q regime. We actually found that as long as $n \gg \sqrt{q}$ these asymptotic expansions reproduce reasonably well the exact results, even for very large q. An example of this is given in Figs. 3.1 and 3.2, which are discussed at the end of this section.

The high energy eigenstates are almost two-fold degenerate with energy spacing mostly determined by Ω. In Ref. [55] the authors show that the localization of these modes can be understood by means of a simple semiclassical analysis. By utilizing a WKB approximation, the localization of the modes can be linked to the appearance of new turning points in addition to the classical harmonic oscillator ones for energies greater than $2J$. While classical harmonic oscillator turning points are reached at zero quasimomentum, the new turning points appear when the quasimomentum reaches the end of the Brillouin zone and can therefore be associated with Bragg scattering induced by the lattice.

35

Finally, we mentioned above that for any given V_o and ω_T the one band approximation is only valid for those states whose wave function does not extend beyond a maximum $j_{max} = \left(\sqrt{4V_o E_R}/\Omega \right)^{1/2}$. This maximum value can vary widely. For example, for $V_o = 2E_R$ and $\omega_T = 2\pi \times 538$ Hz, j_{max} is approximately 7, and it increases to 75 for $\omega_T = 2\pi \times 50$ Hz. For $V_o = 50E_R$ and $\omega_T = 2\pi \times 7.5$ Hz, j_{max} is approximately 1100.

Intermediate states ($n \sim \sqrt{q}$) in the high q regime

In order to reproduce accurately the energy spectrum in the intermediate regime one may expect that many terms in the asymptotic expansions have to be kept. To estimate the energy range where the spectrum changes character from low to high, we solve for the smallest quantum number n_c whose energy calculated by using the low energy asymptotic expansion is higher than the one evaluated by using the high energy expansion. That is

$$E_{n_c-1}^{low} \geq E_{n_c}^{high}, \tag{3.22}$$

where n_c is required to be even.

Solution of Eq. (3.22) gives

$$n_c \approx 2 \| \sqrt{q/2} \|, \tag{3.23}$$

where $\|x\|$ denotes the closest integer to x.

By comparison with the numerically obtained eigenvalues, we actually find that using Eq. (3.14) for $n < n_c - 1$ and Eq. (3.20) for $n \geq n_c - 1$ is enough to reproduce the entire spectrum quite accurately. Moreover, since at n_c the energy is approximately given by $E_{n_c} \approx 2J$, our analytical findings for the transition between harmonic oscillator-like and localized eigenstates are in agreement with the approximate solutions found in [54, 55] by using a WKB analysis.

In Figs. 3.1 and 3.2 we compare the above asymptotic approximations to exact numerical results for the eigenenergies and eigenfunctions. The parameters used for the plots are those of a system with a lattice depth of $7.4E_R$ and quadratic trap frequency $\omega_T = 2\pi \times 60$Hz. These values correspond to
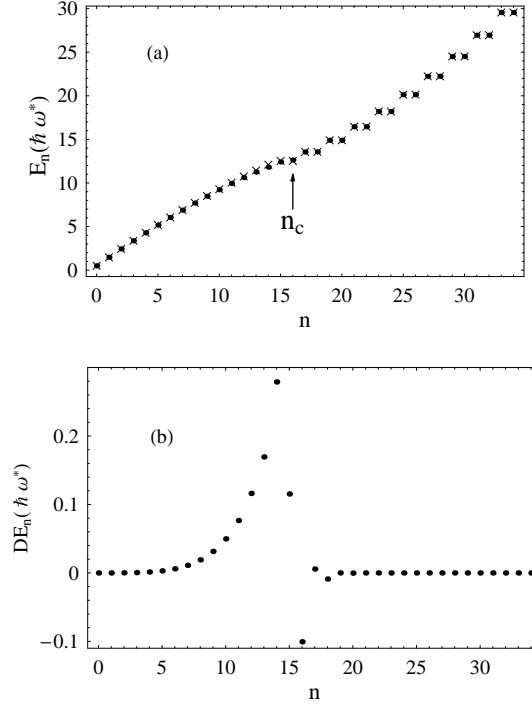
Figure 3.1: Upper panel (a): Spectrum of a particle in combined quadratic and periodic potentials as a function of the quantum number n. The quadratic trap frequency and the depth of the periodic potential are $\omega_T = 2\pi \times 60$ Hz and $V_o = 7.4E_R$, respectively. Points are numerically obtained values, while crosses are asymptotic expansions of the Mathieu characteristic parameters. The arrow indicates the critical value $n_c \approx 2\|\sqrt{q/2}\|$. Lower panel (b): Energy difference between the numerically obtained eigenvalues and the asymptotic expansions.

$J = 0.0357E_R$, $\Omega = 0.0009E_R$ and $q = 157$. Figure 3.1, upper panel, shows the lowest 35 eigenenergies as a function of the quantum number n. The value n_c, which is equal to 16 in this case, is indicated by an arrow. The crosses represent the asymptotic solutions, Eq. (3.14) and (3.20), and the dots the numerically obtained eigenvalues. On the scale of the graph there is no appreciable difference between the two solutions for the entire spectrum. The difference between the the numerically obtained energies and the asymptotic expansions is plotted in the lower panel of Fig. 3.1. In the upper panel of Fig.3.2, asymptotic expressions for the LE eigenvectors $n = 2$(boxes) and $n = 5$(crosses) are compared to the numerically obtained eigenmodes (triangles and dots respectively). The modes clearly exhibit an harmonic oscillator character, and the agreement between the asymptotic and numerical solutions is very good. In the lower panel, the $n = 34$ and $n = 42$ eigenstates belonging to the region $n > n_c$ are depicted. These states are localized far from the trap center. While the overall shape of the modes is well reproduced by the asymptotic solutions,
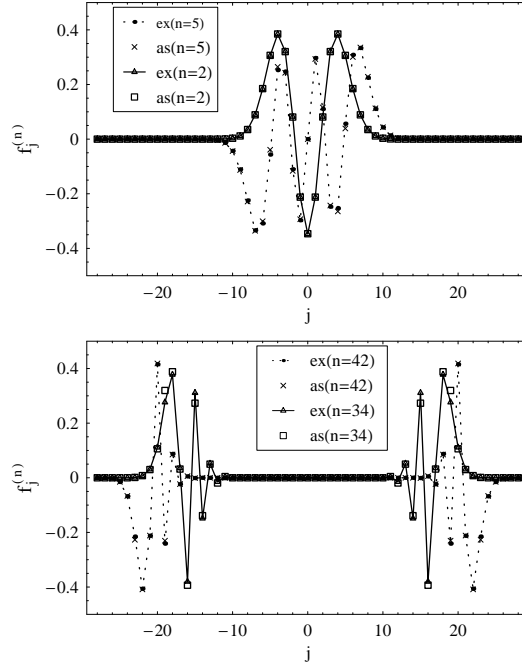
Figure 3.2: Eigenmodes of a particle in a combined quadratic and periodic potentials as a function of the lattice site j. The quadratic trap frequency and the depth of the periodic potential are $\omega_T = 2\pi \times 60$ Hz and $V_o = 7.4 E_R$, respectively. Triangles and dots are numerically obtained values ("ex" in the legend), while boxes and crosses are asymptotic expansions of the Fourier coefficients of the periodic Mathieu functions ("as" in the legend). In the upper panel, triangles and boxes refer to the $n = 2$ mode, while dots and crosses refer to $n = 5$. In the lower panel, triangles and boxes refer to the $n = 34$ mode, while dots and crosses refer to $n = 42$.

for the chosen values of n small differences between the asymptotic (boxes and crosses respectively) and numerical solutions (triangles and dots respectively) can be observed. As expected, the convergence of the asymptotic expansion to the exact solution is better for $n = 42$ than for $n = 34$, as the former has a larger value of n than the latter.

Low q regime ($4J < \Omega$)

This parameter regime is relevant for deep lattices. When $4J < \Omega$ the kinetic energy required for an atom to hop from one site to the next one is insufficient to overcome the trapping energy even at the trap center and all the modes are localized. This is consistent with the previous analysis, because when $4J \lesssim \Omega$, n_c is less than one. The asymptotic expressions that describe this regime are [56]
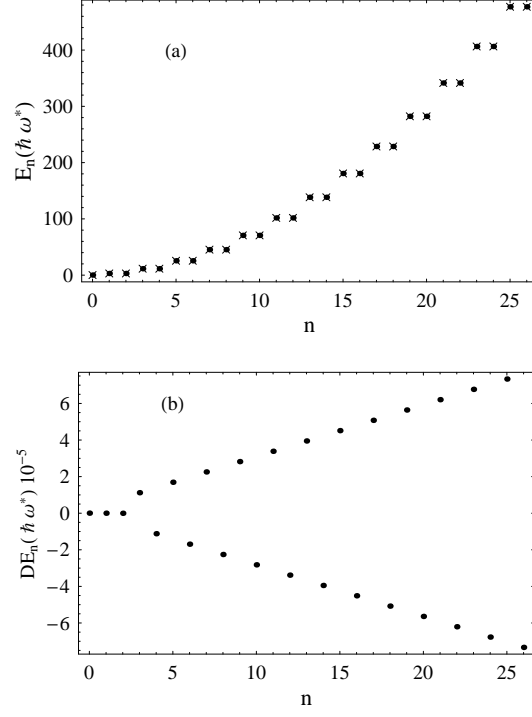
Figure 3.3: Upper panel (a): Spectrum of a particle in combined quadratic and periodic potentials as a function of the quantum number n. The quadratic trap frequency and the depth of the periodic potential are $\omega_T = 2\pi \times 60$ Hz and $V_o = 50.0 E_R$, respectively. Points are numerically obtained values, while crosses are asymptotic expansions of the Mathieu characteristic parameters in the low q limit. Lower panel (b): Energy difference between the numerically obtained eigenvalues and the asymptotic expansions.

$$E_{n=0}^{\mathrm{Low}\,q} \approx \frac{\Omega}{4}\left(-q^2\frac{1}{2} + q^4\frac{7}{128} + \dots\right)$$

$$E_{n=1}^{\mathrm{Low}\,q} \approx \frac{\Omega}{4}\left(4 - q^2\frac{1}{12} + q^4\frac{5}{13824} + \dots\right)$$

$$E_{n=2}^{\mathrm{Low}\,q} \approx \frac{\Omega}{4}\left(4 + q^2\frac{5}{12} - q^4\frac{763}{13824} + \dots\right)$$

$$E_{n=3}^{\mathrm{Low}\,q} \approx \frac{\Omega}{4}\left(16 + q^2\frac{1}{30} - q^4\frac{317}{864000} + \dots\right)$$

$$E_{n=4}^{\mathrm{Low}\,q} \approx \frac{\Omega}{4}\left(16 + q^2\frac{1}{30} + q^4\frac{433}{864000} + \dots\right)$$

$$E_{n\geqslant 5}^{\mathrm{Low}\,q} \approx E_{n\geqslant 5}^{high} \tag{3.24}$$

and

$$f_j^{(\text{Low})\,n=0} \approx A_0 \left\{ \frac{\delta_{j,0}}{\sqrt{8}} + \frac{q}{\sqrt{8}}\delta_{j,1} + \frac{q^2}{32}\frac{\delta_{j,2} - \delta_{j,0}}{\sqrt{2}} \right\} + \{ j \to -j \}$$

$$f_j^{(\text{Low})\,n=1} \approx A_1 \left\{ \delta_{j,1} + \frac{q}{12}\delta_{j,2} + q^2 \left(\frac{\delta_{j,3}}{384} - \frac{\delta_{j,1}}{288} \right) \right\} - \{ j \to -j \}$$

$$f_j^{(\text{Low})\,n=2} \approx A_2 \left\{ \delta_{j,1} + \frac{q}{12}\left(\delta_{j,2} - \frac{3}{2}\delta_{j,0} \right) + q^2 \left(\frac{\delta_{j,3}}{384} - 19\frac{\delta_{j,1}}{288} \right) \right\} + \{ j \to -j \}$$

$$f_j^{(\text{Low})\,n\geq 3} = f_j^{(high)\,n\geq 3} \tag{3.25}$$

with A_n normalization constants. In Fig. 3.3 the above expansions for the energies are compared with the numerically calculated spectrum. Here the lattice is $50E_R$ deep and the external trap frequency is $\omega_T = 2\pi \times 60Hz$. These lead to values of J, Ω and q given by $J = 2.9 \times 10^{-5}E_R$, $\Omega = 0.0009E_R$ and $q = 0.13$. The asymptotic and numerical solutions perfectly agree on the scale of the graph. The energy difference between the numerically obtained eigenvalues and the asymptotic expansions is plotted in Fig. 3.3, lower panel.

3.3 Center of mass evolution of a displaced system

In recent experiments, the transport properties of one dimensional Bose-Einstein condensates loaded in an optical lattice have been studied after a sudden displacement of the quadratic trap [17]. A strong dissipative dynamics was observed even for very small displacements and shallow depths of the optical lattice. This should be contrasted with previous experiments performed with weakly interacting 3D gases where very small damping of the center of mass motion was observed for small trap displacements [62, 63]. Recent theoretical studies have demonstrated that the strongly damped oscillations observed in one dimensional systems reflect the importance of quantum fluctuations as the dimensionality is reduced [64, 65, 66, 67].

In this section we study the dipolar motion of ideal bosonic and fermionic gases trapped in the combined lattice and harmonic potentials. We start by writing an expression for the evolution of the center of mass of an ideal gas with general quantum statistics, and then we use this expression to study the dipole oscillations for bosonic and fermionic systems. The simplicity of the noninteracting treatment allows us to derive analytic equations for the dipole dynamics for both statistics.

Later on, in section 3.4, we show how the knowledge of the bosonic and fermionic ideal gas dy-

namics can be useful in describing the dynamics of the interacting bosonic system for a large range of parameters of the trapping potentials.

3.3.1   Ideal gas dynamics

Consider an ideal gas of N atoms at zero temperature loaded in the ground state of an optical lattice plus a quadratic potential initially displaced from the trap center by δ lattice sites. The initial state of the gas is

$$z_j(t=0) \quad = \quad \frac{1}{N} \sum_n \overline{n}_n f_{j-\delta}^{(n)} \tag{3.26}$$

where $\overline{n}_n$ is the mean occupation number determined by the appropriate quantum statistics, and j is the site index.

The time evolution of the center of mass of the gas is given by

$$\langle x(t) \rangle \quad = \quad \frac{1}{N} \sum_n \overline{n}_n \langle x_n(t) \rangle \tag{3.27}$$

with

$$\langle x_n(t) \rangle \quad = \quad a \sum_{k,l} \left(c_l^{(n)*} c_k^{(n)} e^{-i(E_k - E_l)t/\hbar} \sum_j j f_j^{(k)} f_j^{(l)*} \right)$$
$$c_k^{(n)} \quad = \quad \sum_j f_{j-\delta}^{(n)} f_j^{(k)*}, \tag{3.28}$$

where the quantities $f_j^{(n)}$ and the energies E_n correspond to eigenfunctions and eigenenergies of the undisplaced system. The coefficients $c_k^{(n)}$ are given by the projection of the n excited displaced eigenstate onto the k excited undisplaced one.

Once the E_n and $f_j^{(n)}$ are known, the center of mass evolution can be calculated. In the following we discuss the zero temperature dynamics for the ideal bosonic and fermionic systems.

Bosonic system

At zero temperature the bosons are Bose condensed and $\overline{n}_n = N\delta_{n0}$, where δ_{n0} is the Kronecker delta function. The center of mass motion is then given by

$$
\begin{aligned}
\langle x(t) \rangle &= a \sum_{k,l} \left(c_l^{(0)*} c_k^{(0)} e^{-i(E_k - E_l)t/\hbar} \sum_j j f_j^{(k)} f_j^{(l)*} \right) \\
c_k^{(0)} &= \sum_j f_{j-\delta}^{(0)} f_j^{(k)*}.
\end{aligned}
\tag{3.29}
$$

If the initial displacement of the atomic cloud is small, $2\delta \ll n_c$, and the lattice is not very deep ($q \gg 1$), localized eigenstates are initially not populated. Then, only low-energy states are relevant for the dynamics and the latter can be modeled by utilizing the asymptotic expansions derived in Sec. 3.2.2. To simplify the calculations, we use the harmonic oscillator approximation for the eigenmodes (Eq.(3.16)), and include up to the quadratic corrections in n in the eigenenergies, which corresponds to keep the first three terms of Eq.(3.14). Even though this treatment is not exact, we found that it properly accounts for the period and amplitudes of the center of mass oscillations for small trap displacement. After some algebra it is possible to show that the time evolution of the center of mass is given by

$$
\langle x \rangle = a\delta e^{-\left(\frac{\delta^2}{a_{ho}^2} \sin^2\left(\frac{\Omega t}{8\hbar} \right) \right)} \cos\left(\omega_o^* t - \frac{\delta^2}{2a_{ho}^2} \sin\left(\frac{\Omega t}{4\hbar} \right) \right)
\tag{3.30}
$$

with $\hbar\omega_o^* = \hbar\omega^* - \Omega/4$.

In Fig. 3.4 we plot the average center of mass position in units of the lattice spacing a as a function of time for an ideal bosonic system of atoms with ^{87}Rb mass. The solid line is obtained by numerically solving the tight binding Schrödinger equation, Eq.(3.3), while the dotted line is the analytical solution Eq.(3.30). For the plot we used $V_o = 7.4E_R$, $\omega_T = 2\pi \times 60Hz$ and $\delta = 3$. The time is shown in units of $T_o = 2\pi/\omega^*$, a characteristic time scale. The two solutions exhibit very good agreement for the times shown.

The modulation of the dipole oscillations predicted by Eq.(3.30) can be observed in the plot. At early times, $t \ll \hbar/\Omega$, the amplitude decreases exponentially as $\exp(-\Gamma_o t^2)$, with $\Gamma_o = \left(\frac{\Omega\delta}{8\hbar a_{ho}} \right)^2$, and the frequency is shifted from ω^* by $\frac{\Omega}{4\hbar}\left(1 - \frac{\delta^2}{2a_{ho}^2} \right)$. The initial decay does not correspond to real damping in a dissipative sense, as in a closed system the energy is conserved. The decay is just an initial modulation

and after some time revivals must be observed. Because in the large q limit $\omega_0^* \ll \Omega/\hbar$, the revival time is approximately given by $4h/\Omega$.

It is a general result that the dipole oscillations of a harmonically confined gas in absence of the lattice are undamped. The undamped behavior holds independently of the temperature, quantum statistics and interaction effects (generalized Kohn theorem [68]). Equation (3.30) shows how this result does not apply when the optical lattice is present even for an ideal Bose gas.
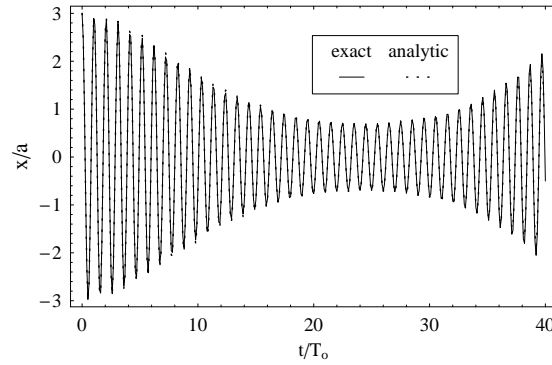
Figure 3.4: Center of mass motion in lattice units as a function of time for an ideal bosonic gas. In the plot, $V_o = 7.4E_R$, $\omega_T = 2\pi \times 60Hz$ and $\delta = 3$. The time has been rescaled by $T_o = 2\pi/\omega^*$. The solid and dotted lines are the numerical and analytical solution Eq. (3.30), respectively.

Recent experimental developments have opened the possibility to create a non-interacting gas for any given strength of the trapping potentials [69, 70]. The techniques use Feshbach resonances for tuning the atomic scattering length to zero. These developments should allow for the experimental observation of the modulation of the dipole oscillations of an ideal gas predicted in this section.

Fermionic system

At zero temperature the Pauli exclusion principle forces fermions to occupy the lowest N eigenmodes, and therefore $\bar{n}_n = 1$ for $0 \leq n \leq N - 1$ and zero elsewhere. The occupation of the first N displaced modes makes the condition of occupying only low-energy eigenstates of the undisplaced potentials more restrictive than in the bosonic case. Nevertheless, if the initial displacement, lattice depth and atom number are chosen such that only LE eigenstates are initially populated, $\sum_{n=n_c-1}^{\infty} |c_n^{(N-1)}|^2 \ll 1$, it is possible to derive simple analytic expressions for the dipole dynamics. This is the focus of the remainder of this

section. Population of localized states considerably complicates the system's dynamics and a numerical

analysis is therefore required. This is postponed to Sec.3.5.2.
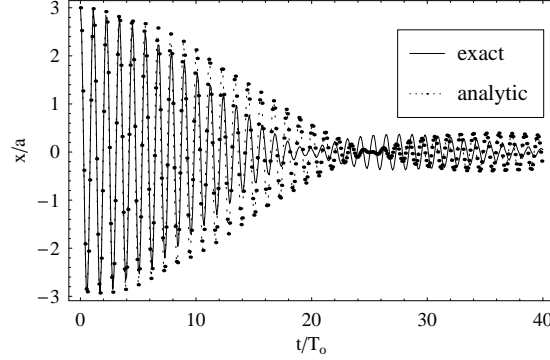
Figure 3.5: Center of mass motion in lattice units as a function of time for $N = 15$ fermions. Here $\omega_T = 2\pi \times 20Hz$ and $V_o = 7.4E_R$ and $\delta = 3$. The time is in units of $T_o = 2\pi/\omega^*$. The solid and dotted lines are the numerical and analytical solution Eq. (3.33), respectively.

When only LE undisplaced eigenstates are occupied, as explained for the bosonic system, to a

good approximation the eigenmodes can be assumed to be the harmonic oscillator eigenstates and only

corrections quadratic in the quantum number n are relevant in Eq.(3.14). After some algebra, the above

approximations yield the following expression for the time evolution of the center of mass:

$$\langle x(t) \rangle = \frac{1}{N} \sum_{n=0}^{N-1} \langle x_n(t) \rangle \tag{3.31}$$

$$\langle x_n(t) \rangle \equiv a\delta \mathrm{Re} \left(\exp\left\{ i\omega_o^* t - \left(\frac{\delta^2(1-\chi(t))}{2a_{ho}^2} \right) \right\} \tilde{x}_n(t) \right) \tag{3.32}$$

$$\tilde{x}_n(t) \equiv \sum_{k=0}^{n-1} \left(\left(\frac{\delta}{a_{ho}} \right)^{2k} \frac{(\chi(t)-1)^{2k}\chi(t)^{n-1-k}((n+1)\chi(t)+k-n)}{(2k)!!(k+1)!} \prod_{s=1}^{k} (n+1-s) \right)$$

$$+ \frac{\left(\frac{\delta}{a_{ho}} \right)^{2n} (1-\chi(t))^{2n}}{(2n)!!} \tag{3.33}$$

where $\chi(t) = \exp^{(-i\Omega t/(4\hbar))}$ and $\hbar\omega_o* = \hbar\omega^* - \Omega/4$.

The parameter $\chi(t)$ takes into account the quadratic corrections to the harmonic oscillator energies.

The corrections are proportional to $\Omega/4$, and due to the presence of the lattice. In the limit $\chi(t) \to 1$,

$\tilde{x}_n(t) \to 1 \; \forall n$ and therefore the amplitude of the dipole oscillations remains constant in time, $\langle x \rangle =$

$a\delta \cos(\omega^* t)$, as predicted by Kohn theorem. The corrections that are quadratic in n cause the modulation
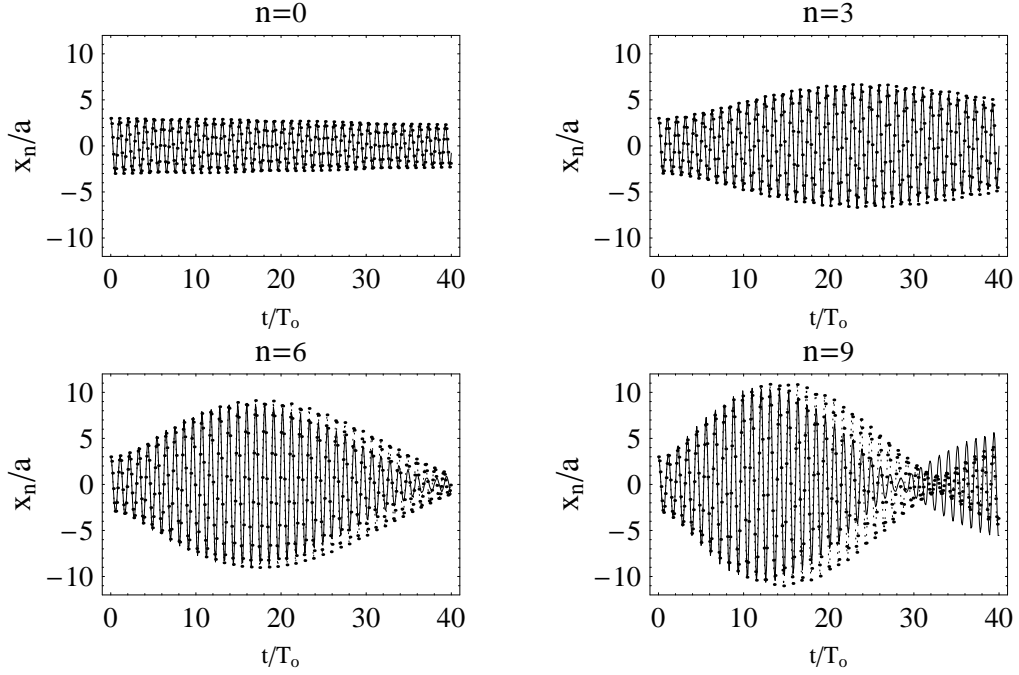
Figure 3.6: Center of mass motion in lattice units as a function of time for some initially occupied modes. The modes are labeled by the quantum number n. As in Fig. 3.5, the parameters are $\omega_T = 2\pi \times 20 Hz$, $V_o = 7.4 E_R$, $N = 15$, $\delta = 3$ and the time is in units of $T_o = 2\pi/\omega^*$. The solid line corresponds to the numerical solution and the dotted line to the solution given by Eq. (3.33). When the center of mass evolution of all the different modes is added, from $n = 0$ to $n = N - 1$ one recovers the total center of mass evolution shown in Fig. 3.5.

of center of mass oscillations.

The modulation is caused not only by the overall envelope generated by the exponential term $\exp\left(-\delta^2(1 - \chi(t))/(2\tilde{a}_{ho}^2)\right)$, which was also present in the bosonic case, but mainly from the interference created by the different evolution of the N average positions $\langle x_n \rangle$ in the sum Eq.(3.31). The latter induces a fast initial decay of the amplitude of the dipole oscillations.

In Fig.3.5 we plot the center of mass motion of the fermionic gas composed of $N = 15$ atoms with the mass of ^{87}Rb. The solid and dotted lines correspond to the numerical and analytic solutions, respectively. Here the depth of the optical lattice is $7.4 E_R$, and $\omega_T = 2\pi \times 20 Hz$. The amplitude of oscillation shows a rapid decay in time. The analytic solution captures the overall qualitative behavior of the numerical curve. Nevertheless, only at short times the agreement is quantitatively good. Population of eigenstates which are not fully harmonic in character is responsible for the disagreement at later times.

This effect is particularly relevant for the evolution of the displaced states with larger quantum number, as explicitly shown in Fig. 3.6 where the time evolution of some displaced modes is plotted. Again, the solid line is the numerical solution and the dotted line is the analytic one. For the lowest energy modes, $n = 0$ and $n = 3$, the agreement between the two curves is almost perfect. For the higher energy modes $n = 6$ and $n = 9$ the analytic solution is underdamped and overestimates the collapse time.

Interestingly, the dynamics of the displaced excited modes exhibits an initial growth of the amplitude. This behavior is a pure quantum mechanical phenomenon due to the constructive interference between the different phases of the undisplaced eigenmodes during the evolution. We explicitly checked for energy conservation during the time evolution. The amplitude increase is captured by the analytic solution and it allowed us to show that the growth happens only when the ratio between the initial displacement δ and a_{ho} is less than one. While such a behavior is not observable in the evolution of a fermionic cloud, as the observable is the center of mass position summed over all initially populated modes $\langle x(t) \rangle$, the experimental observation of growth for an individual mode may be possible if an ideal bosonic gas is initially loaded in a particular excited state, and then suddenly displaced.

As described above, the evolution of LE modes can be handled analytically. On the other hand, when high-energy eigenmodes are populated the dynamics is much more complicated. Nevertheless, there is another simple limiting case that can be solved. This corresponds to the case when the displacement is large enough or the lattice deep enough that the displaced cloud has non-vanishing projection amplitudes only onto high-energy undisplaced modes which can be roughly approximated by position eigenstates, $f_j^{2r,2r-1} \approx (\delta_{j,r} \pm \delta_{-j,r})/\sqrt{2}$. Then, one finds that $\langle x_n \rangle \approx a\delta$ for all n and thus $\langle x \rangle \approx a\delta$. That is, when only high-energy eigenmodes are populated the dynamics is completely overdamped and the cloud tends to remain frozen at the initial displaced position. We show later on in Sec. 3.5.2 where we treat interacting atoms, that in the so-called *Mott* insulator regime most populated modes are actually localized, and this kind of overdamped behavior characterizes the dipole dynamics.

3.4 Many-body system

3.4.1 Spectrum of the BH-Hamiltonian in the presence of an external quadratic potential

In Sec. 2.3.1 it was shown that the Bose-Hubbard (*BH*) Hamiltonian describes the system's dynamics when the lattice is loaded such that only the lowest vibrational level of each lattice site is occupied [11]

$$H_{BH} = \sum_j \left[\Omega j^2 \hat{n}_j - J(\hat{a}_j^\dagger \hat{a}_{j+1} + \hat{a}_{j+1}^\dagger \hat{a}_j) + \frac{U}{2} \hat{n}_j(\hat{n}_j - 1) \right]. \tag{3.34}$$

Here Ω, J and U are defined as in Eqs.(2.21), (2.18) and (2.20), respectively. There it was shown that the tunneling rate decreases for sinusoidal lattices with the axial lattice depth V_o as

$$J = A \left(\frac{V_o}{E_R} \right)^B \exp \left(-C \sqrt{\frac{V_o}{E_R}} \right) E_R, \tag{3.35}$$

where the numerically obtained constants are $A = 1.397$, $B = 1.051$ and $C = 2.121$. The interaction energy increases with V_o as

$$U = \beta E_R \left(\frac{V_o}{E_R} \right)^{1/4}, \tag{3.36}$$

where β is a dimensionless constant proportional to a_s. In current experiments, the one-dimensional lattice is obtained by tightly confining in two directions atoms loaded in a three-dimensional lattice. In this case $\beta = 4\sqrt{2\pi}(a_s/\lambda)(V_\perp/E_R)^{1/2}$, where $V_\perp$ is the depth of the lattice in the transverse directions [71, 72]. The parameter $\gamma = U/J$ therefore increases as a function of the axial lattice depth as

$$\gamma(V_o) = \frac{\beta}{A} \left(\frac{V_o}{E_R} \right)^{1/4 - B} \exp \left(C \sqrt{\frac{V_o}{E_R}} \right). \tag{3.37}$$

In the absence of the external quadratic potential, the bosonic spectrum is fully characterized by the ratio between the interaction and kinetic energies γ and the filling factor N/M, where M is the number of lattice sites [12]. For $\gamma \ll 1$ and any N/M ratio the system is weakly interacting and superfluid. For $\gamma \gg 1$ and $M \geq N$ the system fermionizes to minimize the inter-particle repulsion. In this regime the bosonic energy spectrum mimics the fermionic one, the correspondence being exact in the limit of infinitely strong interactions. In particular, in a lattice model the onset of fermionization is characterized by suppression of multiple particle occupancy of single sites. This implies that fermionization occurs for eigenstates whose energy is lower than the interaction energy U. If $M > N$ there are $M!/(N!(M - N)!)$ fermionized

eigenmodes and the dynamics at energies much lower than U can be accounted for by using these states only. On the other hand, if the lattice is commensurately filled, $N = M$, there is only one fermionized eigenstate, and it corresponds to the ground state. All excited states have at least one multiply occupied site, and therefore excitations are not fermionized. The ground state corresponds to the Mott state with a single particle per site and reduced number fluctuations. The transition from the superfluid to the Mott state is the quantum phase transition studied in Chapter 2.3.2, and the critical point for one-dimensional unit filled lattices is $\gamma_c \simeq 4.65$ [12, 73].

In the presence of the quadratic trap the spectrum is determined by an interplay of U, J, Ω and N. In trapped systems the notion of lattice commensurability becomes meaningless because the size of the wave-function is explicitly determined by these parameters. As a consequence, for any value of N the ground state can be made to be a Mott insulator with one atom per site at the trap center by an appropriate choice of U, J and Ω [51], and the lowest energy modes can always be made to be fermionized in the large U limit. The purpose of this section is to characterize fermionization and localization of the many-body wave-function when both the quadratic and periodic potentials are present, by relating the occurrence of the different regimes to changes in the spectrum at low energies.

We performed exact diagonalizations of the BH-Hamiltonian for $N = 5$ particles and $M = 19$ sites in presence of a quadratic trap of frequency $\omega_T = 2\pi \times 150$ Hz. For the calculations, we chose ^{87}Rb atoms with scattering length $a_s = 5.31$ nm, a lattice constant $a = 405$ nm, and therefore $\Omega \simeq 0.0046 E_R$. We fixed the transverse lattice confinement to $V_\perp \simeq 25.5\ E_r$ and varied the depth of the optical lattice V_o in the parallel direction from $2\ E_R$ to about $17\ E_R$. For these lattice and parabolic potentials, the single-band approximation is always valid because $j_{max} = 25, 43$ for $V_o/E_R = 2$ and 17, respectively, and therefore j_{max} is always larger than $j \approx M/2$. For the given lattice depths, the energies U and J both vary so that their ratio γ increases from 3.3 to about 150. Due to the changes in J, the ratio $q = 4J/\Omega$ characterizing the single-particle solutions decreases from 130 to 4 with increasing V_o. The effective harmonic-oscillator energy spacing $\hbar\omega^*$ decreases approximately from $0.0525\ E_R$ to $0.0092\ E_R$. We used these parameters because they are experimentally attainable and fulfill the condition $U - \Omega((N - 1)/2)^2 > 0$ for the entire
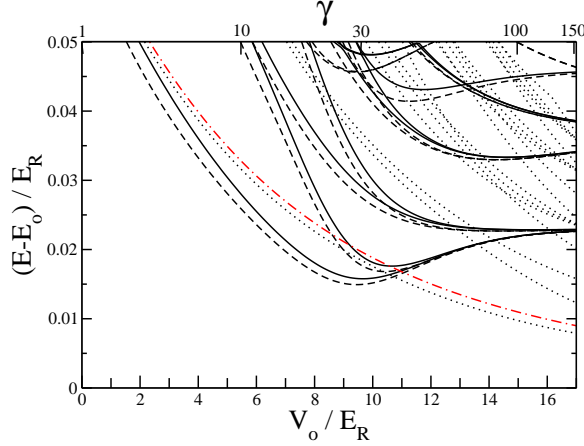
Figure 3.7: Energy spectra as a function of the depth of the axial optical lattice V_o. The continuous, dotted and dashed lines correspond to $N = 5$ interacting bosons, non-interacting bosons and fermions, respectively. The dashed-dotted line corresponds to $\hbar\omega^*$. The horizontal axis on the top of the figure is $\gamma = U/J$, and is only meaningful for interacting bosons. For each energy spectrum, the corresponding ground-state energy E_0 has been subtracted.

range of the trapping potentials. Later on we discuss that, for deep enough lattices, fulfillment of the last inequality ensures the existence of an energy range in which eigenmodes are fermionized.

Figure 3.7 shows the lowest eigenergies of the *BH*-Hamiltonian as a function of V_o. The continuous line is the exact solution for $N = 5$ interacting bosons. The dotted and dashed lines are the exact spectra for 5 non-interacting bosons and fermions, respectively. They have the same mass and are trapped in the same potentials as the interacting bosons. Their spectra are shown for comparison purposes. For each spectrum the energy E_0 of the ground state has been subtracted.

In the absence of the optical lattice, $V_o = 0$, the energy difference $\Delta E_0 = E_1 - E_0$, or *energy spacing*, between the first excited and ground state equals the harmonic oscillator level spacing $\hbar\omega_T$, independent of statistics and interaction strength. Figure 3.7 shows that this is no longer the case in the presence of the lattice.

The dependence of ΔE_0 on statistics is evident in the plot, as the level spacing is different for ideal bosons and fermions. In particular, the energy spacing for bosons is only shifted from $\hbar\omega^* = \sqrt{4\Omega J}$ (dashed-dotted line) by an amount which is almost constant for all lattice depths, while ΔE_0 for fermions clearly deviates from $\hbar\omega^*$, especially for deep lattices. The behavior of ΔE_0 in the two cases can be

49

understood by using the asymptotic solutions of the single-particle problem. For ideal bosons ΔE_0 is equal to the energy difference between the first-excited and ground single-particle eigenenergies. The ratio q used for the plots is such that the critical value n_c of Eq. (3.23) is always larger than 2, and therefore the ground and first-excited eigenenergies are well described by Eq. (3.14). The calculation of the energy difference using this equation yields $\Delta E_0 \approx \hbar \omega^* - \Omega/4$. For fermions, ΔE_0 is equal to the difference between the energies of the $n = N$ and $n = N - 1$ single-particle excited states. For $V_o < 9.6 E_R$, the critical value n_c is larger than N, and therefore the energies of the $n = N$ and $n = N - 1$ single-particle excited states are also well described by Eq. (3.14). Then, ΔE_0 for fermions is smaller than for bosons because lattice corrections are more important for higher quantum numbers, and have all negative sign. On the other hand, for $V_o > 9.6 E_R$, n_c is smaller than $N - 1$ and the energies of the $n = N$ and $n = N - 1$ single-particle excited states are described by Eq. (3.20). The transition of the single-particle eigenmodes at the Fermi level from LE to HE around $V_0 = 9.6 E_R$ is signaled by the minimum of ΔE_0 for fermions. In general, an estimate for the value of J at which the minimum takes place is

$$J \sim \Omega((N-1)/2)^2/2. \tag{3.38}$$

This value is obtained by equating the Fermi energy E_{N-1}, which is of order $\Omega((N-1)/2)^2$ from Eq. (3.20), to E_{n_c}, which is approximately $2J$. The transition of the single-particle eigenmode at the Fermi level from LE to HE is also connected to the formation of a region of particle localization at the trap center in the many-body density profile. As explained in [49], when E_{N-1} is equal to E_{n_c} the on-site density in the central site of the trap approaches 1 with reduced fluctuations. For $V_0 > 9.6 E_R$, Fig. 3.7 shows that ΔE_0 approaches an asymptotic value ΩN, value that can be derived from Eq. (3.20). When the asymptotic value ΩN is reached, most single-particle states below the Fermi level are localized, and this yields a many-body density profile with N unit-filled lattice sites at the trap center.

The dependence of the first excitation energy on interactions can also be seen in Fig. 3.7. In fact, by comparing ΔE_0 for the interacting bosons to the value of ΔE_0 for ideal bosons and fermions, three different regimes can be considered: $1 \lesssim \gamma \lesssim 10$, $10 \lesssim \gamma \lesssim 30$ and $\gamma > 30$. These regimes correspond to the intermediate, fermionized-non-localized and fermionized-Mott regimes, respectively. The weakly

interacting regime $\gamma \lesssim 1$ is only reached for $V_o \ll 2E_R$ for our choice of atoms and trapping potentials. For such lattice depths the tight-binding approximation is not valid, and therefore we do not show the spectra for this regime in Fig. 3.7. In the following we discuss the main features of the different regimes focusing on the connection to the ideal bosonic and fermionic systems.

- For $\gamma \leq 1$ the interacting bosonic system is in the *weakly interacting* regime. In this regime the first excitation energy is almost the same as the ideal bosonic one. Most atoms are Bose-condensed, interaction-induced correlations can be treated as a small perturbation, and the spectrum can be shown to be well reproduced by utilizing Bogoliubov theory [74].

- For $1 < \gamma < 10$, the system is in the *intermediate* regime, where ΔE_0 for interacting bosons deviates from the ideal bosonic energy spacing and approaches the ideal fermionic one. Indeed, Fig.3.7 shows that for $V_0 \lesssim 4E_R$, ΔE_0 for the interacting bosons lies closer to the ideal bosonic energy spacing, while for $V_0 > 4$ it lies closer to the ideal fermionic one. In the presence of the optical lattice γ increases exponentially with V_o, and therefore the intermediate regime occurs for a relatively small range of accessible trapping potentials, here for $1 \lesssim V_o/E_R \lesssim 5.5$.

- For $\gamma \geq 10$ the interacting spectrum approaches the ideal Fermi spectrum and the system is in the *fermionized* regime. The numerical solutions show that the energy difference between the energy spectra of interacting bosons and fermions is of the order of J^2/U and slightly increases for larger frequencies of the quadratic trap.

In general, fermionization in the presence of the external quadratic potential occurs for $N < M$ when the two following inequalities are satisfied

$$\gamma = U/J \gg 1, U > \Omega((N-1)/2)^2. \tag{3.39}$$

While the first inequality is the same as for homogeneous lattices and relates to the building of particle correlations, the second inequality is specific to the trapped case and relates to suppression of double particle occupancy of single sites. If the interaction energy U is larger than the largest trapping energy, which corresponds to trapping an atom at position $(N-1)/2$, it is energetically favorable to have at most one atom per well. The average on-site occupation is therefore less than or equal to one.

The second inequality in Eq. (6.3) poses some limitations on the choice of possible Ω and U for a

51

given number of trapped particles. For our choice of the trapping potentials, this inequality is satisfied for any V_o. Indeed, this is not an unrealistic assumption. In recent experiments with ^{87}Rb atoms, an array of fermionized gases has been created with at most 18 atoms per tube [15]. For such N, the condition $U > \Omega((N-1)/2)^2$ can be fulfilled for many different choices of experimentally feasible trapping potentials.
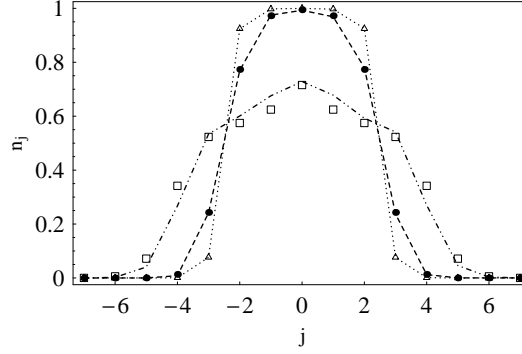
Figure 3.8: Density profiles $n_j \equiv \langle \hat{n}_j \rangle$ as a function of the lattice site j for different lattice depths. The dash-dotted, dashed and dotted lines correspond to interacting bosons, while the boxes, dots and triangles correspond to ideal fermions for $V_o/E_R = 7, 12$ and 15 lattice depths, respectively.
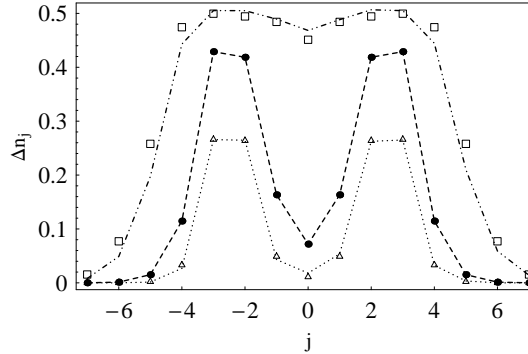
Figure 3.9: Number fluctuations $\Delta n_j \equiv \sqrt{\langle \hat{n}_j^2 \rangle - \langle \hat{n}_j \rangle^2}$ as a function of the lattice site j for different lattice depths. Conventions and parameters are the same as in Fig.3.8

• For $\gamma > 30$ the system enters the fermionized-*Mott* regime. In fact, Fig. 3.7 shows that for $\gamma > 30$ the energy spacing for the interacting bosons (and also for ideal fermions) begins to increase until it reaches an asymptotic value at $\gamma \approx 150$.

The approaching of the asymptotic value signals the formation of a localized many-body state for the interacting bosons, the so-called Mott insulator state, Where atoms occupy each a different site around the trap center, with reduced particle fluctuations. The relevant relation between N, Ω and J for the formation

of an extended core of unit-filled sites at the trap center with fluctuations mainly at the outermost occupied sites is

$$\Omega N \geq J. \tag{3.40}$$

This is explained as ΩN is the energy cost for moving a particle from position $|(N-1)/2|$ to position $|(N+1)/2|$ at the borders of the occupied lattice and it is the lowest excitation energy deep in the Mott state.

Figure 3.7 shows that for $\gamma \approx 150$ the energies of the first four excited states become degenerate. This degeneracy occurs because deep in the Mott regime the energy required to shift all the atoms of one lattice site to the right or left is the same as the energy required for moving an atom from site $\pm(N-1)/2$ to site $\pm(N+1)/2$. For $\gamma \approx 150$, J is approximately Ω, and therefore the tunneling energy is barely sufficient to overcome the potential energy cost Ω for moving a particle from the central site of the trap to one of its neighbors. In the single-particle picture,when $J \approx \Omega$ all the single-particle states below E_{N-1} are localized.

In order to better understand the formation of the Mott insulator, in Figs. 3.8 and 3.9 the on-site particle number $n_j = \langle \hat{n}_j \rangle$ and fluctuations $\Delta n_j = \sqrt{\langle \hat{n}_j^2 \rangle - \langle \hat{n}_j \rangle^2}$ are plotted as a function of the lattice site j, for different lattice depths V_o. The lines and symbols are the results for interacting bosons and ideal fermions, respectively. All the V_o-values are such that the interacting bosonic system is fermionized. This is mirrored by the overall good agreement between lines and symbols for all the curves. The plots show that for $V_o = 7E_R(\gamma = 15$, dashed-dotted line), the largest average particle occupation is $n_0 \approx 0.7$, and number fluctuations are of the order of 0.5 in the central 9 sites, while for $V_o = 12E_R(\gamma = 54$, dashed line), n_0 approaches 1 in the central 3 sites, and fluctuations at the trap center drop to a value $\Delta n_j \approx 0.1$. The sharp drop in particle fluctuations clearly signals the localization at the trap center, and is in agreement with $J < \Omega N$ for $\gamma = 54$. For $V_o = 15E_R(\gamma = 104$, dotted line), the Mott state is formed, as the mean particle number in the five central sites is one, with nearly no fluctuations. Fluctuations are larger at lattice sites far from the center, and due to the tunneling of particles to unoccupied sites.

Because of the small number of atoms that we use in the calculations, $\Omega((N-1)/2)^2/2$ and ΩN are of the same order of magnitude. It is therefore not possible to clearly distinguish the value of J for which the on-site density at the trap center approaches one from the value of J for which the Mott state is fully formed at the trap center, with reduced number fluctuations in the central N sites. Preliminary results obtained with a Quantum Monte-Carlo code, Worm Algorithm [30], confirm the existence of these two distinct parameter regions when more atoms are considered, and therefore the usefulness of both the energy scales $\Omega((N-1)/2)^2/2$ and ΩN for interacting bosons. As an example, for the parameters of the central tube of the experiment of Ref. [15], the relations $J \sim \Omega((N-1)/2)^2/2$ and $J \sim \Omega N$ are satisfied for the lattice depths $V_o/E_R \approx 8$ and 12, respectively. Accordingly, the many-body density profiles show that for $V_o/E_R = 8$ some sites at the trap center begin to have unit filling, while for $V_o/E_R = 12$ a Mott state is fully extended in all the central sites of the lattice. In all these Monte-Carlo simulations $N = 19$, $M = 101$, and the temperature is $T = 0.01 J/k_B$, with k_B the Boltzmann constant. These results will be published elsewhere.

Finally, in order to get an estimate of the dependency of our exact diagonalization results for 5 particles and 19 wells on the system size, we calculated the ground-state energy for increasing M by means of numerical Monte-Carlo simulations. By increasing the lattice size of an order of magnitude we found that the ground-state energy varies of only 2 percent. We consider this as a strong indication of the fact that the results above are not significantly affected by the limited number of sites considered.

3.5   Many-body dynamics

In this section we study the temporal dipole dynamics of an interacting bosonic system composed of 5 atoms trapped in a combined quadratic plus periodic confinement. The role of interactions on the effective damping of the dipole oscillations is studied by means of exact diagonalization of the Hamiltonian. As discussed when dealing with the ideal gas dynamics, such damping is effective because it is due to dephasing and does not have a dissipative character.

Assuming the system is initially at $T = 0$, the evolution of the center of mass is given by:

$$\langle x(t) \rangle \quad = \quad \sum_{l,k} A_{lk} e^{i\omega_{lk}t} \tag{3.41}$$

$$A_{lk} \quad \equiv \quad a \sum_j j \langle \phi_l | \hat{n}_j | \phi_k \rangle C_l^* C_k, \tag{3.42}$$

with $\hbar\omega_{lk} \equiv E_l - E_k$ and where E_l and $|\phi_l\rangle$ are eigenvalues and eigenmodes of the *BH*-Hamiltonian. The coefficients C_l are the projections of the initial displaced ground state $|\varphi(0)\rangle$ onto the eigenfunctions $\{|\phi\rangle_l\}$ of the undisplaced Hamiltonian, $C_l = \langle \phi_l | \varphi(0) \rangle$.

For the exact evolution, the ground-state $|\varphi(0)\rangle$ is calculated by shifting the center of the quadratic trap by δ lattice sites. The number of wells M is 19 for all simulations, which fixes the size of the Hilbert space to 33649. In the time propagation we only keep those eigenstates whose coefficients C_l are such that $|C_l|^2 > 10^{-3}$. The typical number of states that fulfil this requirement is about 100. The accuracy of the truncation of the Hilbert space during the time propagation has been checked by increasing the number of retained states, finding no appreciable changes in the dynamics.

We are interested in the dynamics both when a Mott insulator state is not and is present at the trap center. These two cases are discussed in Secs.3.5.1 and 3.5.2, respectively. In particular, in Sec. 3.5.1 the interaction strength U is varied, while the ratio q, specifying the ideal gas dynamics, is large and constant. For the chosen values of q and N, $J > \Omega N$ and for increasing U the system fermionizes without forming a Mott insulator at the trap center. In Sec. 3.5.2, the dynamics of systems that do exhibit a Mott insulator in the large U limit is analyzed. In this case, J and U are simultaneously varied by increasing the axial optical lattice depth.

3.5.1   Non-localized dynamics

In the absence of the optical lattice, the equations of motion for the center of mass are decoupled from those of the relative coordinates. As only the latter are affected by interactions, all modes excited during the collective oscillations have the harmonic oscillator energy spacing $\hbar\omega_T$, and therefore $\langle x(t) \rangle = \langle x(0) \rangle \cos(\omega_T t)$.

When the lattice is present, the equations of motion for the center of mass and relative coordi-

nates are coupled, and thus the many-body dynamics is interaction dependent. In this section we fix $\omega_T = 2\pi \times 100 Hz$ and $V_o = 7E_R$, and study the role of interactions in the many-atom dynamics by varying γ from 0 to 200, for constant $q = 77$. This can be experimentally realized by tuning the scattering length of the system by means of Feshbach resonances [1]. In the following, we analyze the weakly interacting, intermediate and strongly interacting regimes separately.

Weakly interacting regime: $\gamma \leq 1$

In order to study the role of interactions in the weakly interacting regime, in Fig. 3.10 the effective damping constant of dipole oscillations Γ is shown as a function of γ. The damping constant was calculated by fitting the first 10 center of mass oscillations to the ansatz $\langle x(t) \rangle = a\delta \exp\left(-\Gamma t^2\right) \cos(\omega t)$, where Γ and ω are fitting parameters. This ansatz is chosen in analogy to the non-interacting model. The effective damping Γ is in units of $\Gamma_o = \delta^2 \Omega^2/(8\hbar a_{h_o})^2$, which is the damping constant predicted by Eq. 3.30. The solid and dotted lines correspond to Γ as calculated by means of exact diagonalizations and by numerically evolving the following *Discrete Non-Linear Schrödinger Equation* (DNLSE) for the amplitudes $\{z_j\}$

$$i\hbar \frac{\partial z_j}{\partial t} = -J(z_{j+1} + z_{j-1}) + \Omega j^2 z_j + U|z_j|^2 z_j, \tag{3.43}$$

respectively. Eq.(3.43) has been obtained by replacing the field operator $\hat{a}_j$ with the c-number $z_j(t)$ in the Heisenberg equation of motion for $\hat{a}_j$. Such replacement is justified for $\gamma \ll 1$ as the many-body state is almost a product over identical single-particle wave-functions. The amplitudes $\{z_j\}$ satisfy the normalization condition $\sum_j |z_j|^2 = N$. The initial state used in the evolution of the DNLSE was found by numerically solving for the ground state of Eq. (3.43), displaced by $\delta = 2$ lattice sites.

In Fig. 3.10, the continuous and dotted lines overlap for $\gamma \leq 0.05$, and show a decrease in the damping constant with increasing interaction strength in the whole range $\gamma \leq 0.2$. For values of $\gamma > 0.05$ the mean field and exact solutions start to disagree. While the exact solution has a minimum around $\gamma \approx 0.2$,

---

[1] In an atomic gas near a Feshbach resonance, the energy of two colliding atoms is close to the energy of a bound state, i.e. a molecular state, in a closed channel that is coupled to the incoming open channel. Due to the different arrangement of the atoms in the open channel and the atoms in the molecular state, the energy difference between the bound state and the two-atom continuum threshold may be experimentally accessible by means of the Zeeman interaction of the atomic spins with a magnetic field. As a result, it is in principle possible to vary the scattering length to any value by detuning the magnetic field.
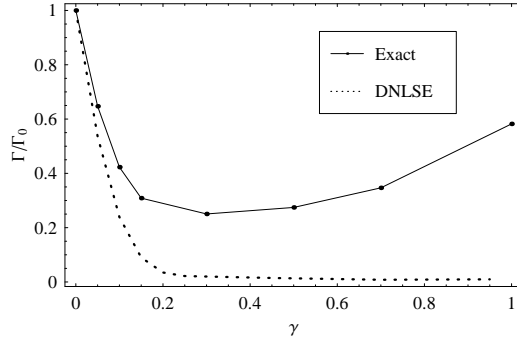
Figure 3.10: Effective damping constant of the dipole oscillations as a function of γ for a system in the weakly interacting regime. Here, $q \approx 77$, $\omega_T = 100$ Hz and $\Gamma_o = (\delta\Omega/8\hbar a_{ho})^2$.

and then grows for larger γ values, the mean field curve decreases monotonically to zero.

The fact that the mean-field solution decreases to zero for increasing interactions is explained by noting that when interaction effects become important the density profile acquires the form of an inverted parabola, or *Thomas-Fermi* profile, $|z_j^{TF}(t)|^2 \approx \Omega \left((j - \langle x(0)\rangle/a)^2 - R_{\mathrm{TF}}^2\right)/U$, $\langle x(0)\rangle = a\delta$. Substitution of the Thomas-Fermi profile in Eq. (3.43) leads to the exact cancellation of the quadratic potential, and thus, in the frame co-moving with the atomic cloud, the atoms feel an effective linear potential. The spectrum of a linear plus periodic potential is known to be equally spaced [75], and therefore no damping due to dephasing is expected.

It is important to note that the mean-field undamped oscillation occurs only in a parameter regime far from dynamical instabilities. In fact, as shown in previous theoretical and experimental studies [76, 77, 78], when the initial displacement is large enough to populate states above half of the lattice band-width, mean-field dynamical instabilities induce a chaotic dipole dynamics. In the framework of this work, this critical displacement corresponds to $\delta \approx n_c/2$. For $\delta > n_c/2$, the initial ground-state has a significant overlap with localized eigenmodes of the undisplaced system, which are therefore populated during the dipolar dynamics, causing damping. The importance of the population of these modes is enhanced by the non-linear term, which causes an abrupt suppression of the center of mass oscillations at the critical point in the mean-field solution.

While the mean-field anaysis accounts for the decrease in the damping constant, Fig. 3.10 shows
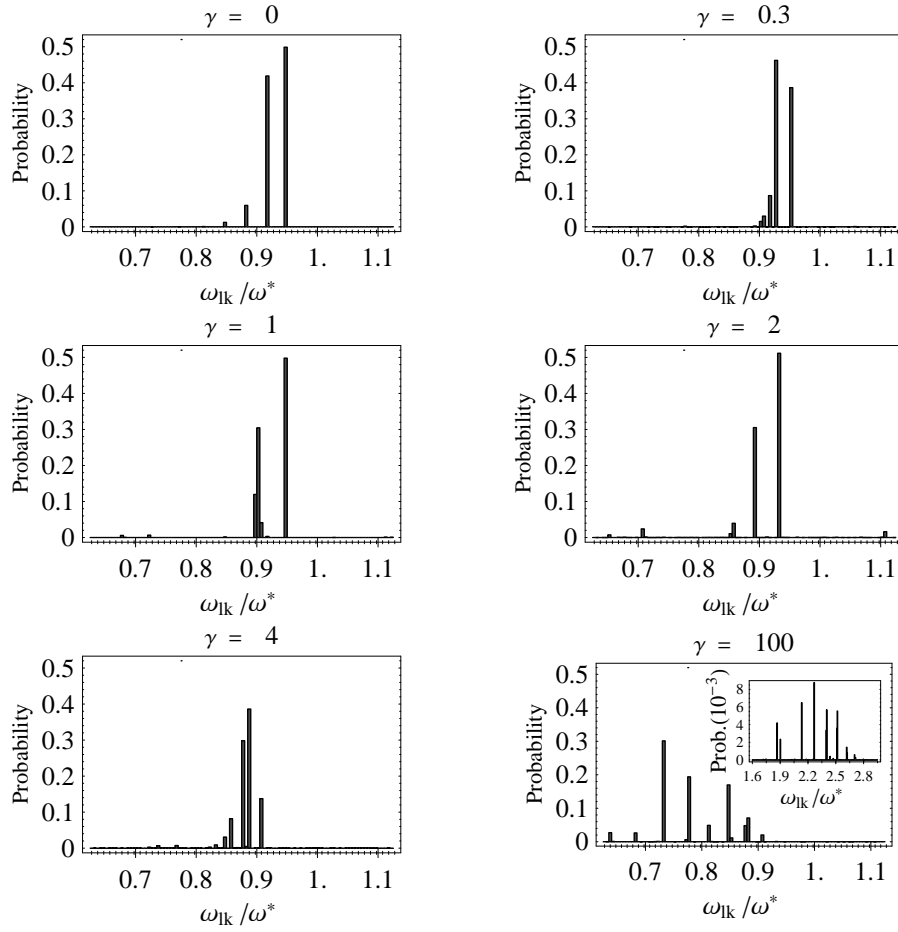
Figure 3.11: Probability distribution of frequencies for different values of γ, with $q \approx 77$ and $\omega_T = 100$ Hz. The frequencies ω_{lk} are in units of ω^*.

that it is not accurate for $\gamma \gtrsim 0.2$. This is due to the fact that the mean-field analysis completely neglects interaction-induced correlations. These correlations are responsible for the quantum depletion of the condensate, which causes some atoms to be excited to higher-energy single-particle eigenmodes which are more affected by the lattice. To show this effect in a quantitative manner, in Fig.3.11 we plot the probability distribution of the frequencies ω_{lk}, Eq. (3.41), for some values of γ. In the histograms, the height of a bar-chart centered at a given frequency ω is the occurrence probability of ω_{lk}. The probability is proportional to the normalized sum over all the weight factors $|A_{lk}|$ whose frequency lies between $\omega_{lk} - 0.0025$ and $\omega_{lk} + 0.0025$. The frequencies are in units of the effective harmonic oscillator frequency ω^* of Eq. (3.17). This approach is similar to the one used in Ref. [79], where the strength function is used to study the

collective dynamics induced by mono- and dipolar excitations.

The histogram for the case $\gamma = 0$ shows a frequency distribution with most frequencies in the interval $0.85\omega^* \leq \omega_{lk} \leq 0.96\omega^*$. In particular, two large peaks are observed in the range $0.9\omega^* \leq \omega_{lk} \leq 0.96\omega^*$. This is to be compared to the case where the lattice is not present, and a single peak at ω^* is expected. The observed frequency spread is due to the modification of the harmonic oscillator spectrum introduced by the lattice and is responsible for the observed damping in the ideal bosonic gas, as explained in detail in Sec. 3.3.1.

Figure 3.11 also shows that for $\gamma = 0.3$ the system has a narrower frequency distribution. In this case approximately 100% of the frequencies lie in the interval $0.9\omega^* \leq \omega_{lk} \leq 0.96\omega^*$. The frequency narrowing from $\gamma = 0$ to $\gamma = 0.3$ is consistent with the decrease in the damping constant shown in Fig. 3.10. For larger values of γ, $\gamma = 1$ and 2, some modes with frequency smaller than $0.7\omega^*$ and larger than $1.1\omega^*$ start to contribute to the collective dynamics. Population of such modes is related to the depletion of the condensate and signal the increased importance of quantum fluctuations in the system.

Finally, we note that for our choice of Ω, N and J, $\Omega((N-1)/2)^2/J$ is approximately 0.2, which is the value of $\gamma = U/J$ at which the mean-field and exact solutions begin to disagree. This suggests that the fulfillment of the second inequality in Eq. (6.3), $U > \Omega((N-1)/2)^2$, is related to the failure of the mean-field approach, even for $\gamma < 1$.

Intermediate Regime: $1 < \gamma < 10$

In Fig. 3.12 the numerically obtained damping constant is shown for $\gamma > 1$. In this parameter regime we find that the function $a\delta \exp(-\Gamma t^2) \cos(\omega t)$ does not provide a good fit to the center of mass evolution. Instead, we find that a better fitting ansatz is given by $a\delta \exp(-\Gamma t) \cos(\omega t)$. In the plot, the damping constant is normalized to Γ_1, which is the damping rate at $\gamma = 1$.

We observe that for $2 \leq \gamma < 5$ the damping is almost constant. This is consistent with the fact that by inspection the spectrum of excited frequencies has a similar shape and width in the entire transition region. An example of such a frequency distribution is given in Fig. 3.11 for $\gamma = 4$. The dominant peak is around $\omega_{lk} \approx 0.9\omega^*$, while multiple peaks are noticeable between $0.7\omega^* \leq \omega_{lk} \leq 0.92\omega^*$. The overall
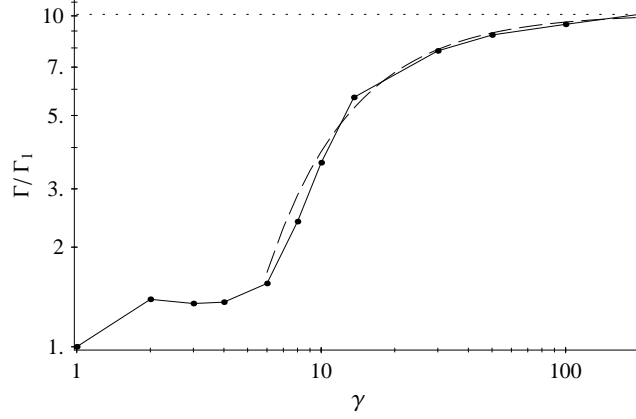
Figure 3.12: Effective damping rate of the dipole oscillations Γ as a function of γ in the intermediate and strongly correlated regimes. Here, $q \approx 77$ and $\omega_T = 100$ Hz. The damping rate has been rescaled such that $\Gamma(\gamma = 1) = 1$. The large and small dots are for interacting bosons and non-interacting fermions, respectively. The continuous line is a guide for the eye. The dashed line is the best-fit curve $\Gamma = 10.13 \exp(-16.4\gamma^{-1.25})$ to the exact damping rate for interacting bosons.

envelope of the distribution has a long tail, as opposed to the case $\gamma = 1$ where all the weight is roughly concentrated in just two frequencies.

The increased importance of the tails of the distribution for $\gamma > 1$ qualitatively accounts for the transition from an exponential decay quadratic in time towards an exponential decay which is linear in time. In fact, for $\gamma < 1$ the probability distribution of frequencies may be fitted by a Gaussian, while for $\gamma > 1$ a better fit is provided by a Lorentzian-like profile. The Fourier transforms of such distributions give precisely the observed functional form of the decay of the dipole oscillations.

Strongly interacting regime $\gamma > 10$

In Fig. 3.12 for $\gamma > 10$, the damping rate is shown to rapidly increase and approach a finite asymptotic value which is depicted in the plot by a dotted line. This asymptotic value Γ_∞ corresponds to the damping rate calculated for an ideal fermionic gas. The fermionic damping rate is constant because here J and Ω are kept constant while U increases. The tendency to approach the fermionic damping rate as γ increases is a consequence of fermionization of the bosonic wave-functions for $\gamma \gg 1$, Eq. (6.3). Numerically we find that the damping rate approaches Γ_∞ exponentially, $\Gamma(\gamma) = \Gamma_\infty \exp(-a\gamma^\alpha)$, with a best-fit exponent α of order -1. The fitting curve is shown in the plot with a dashed line.
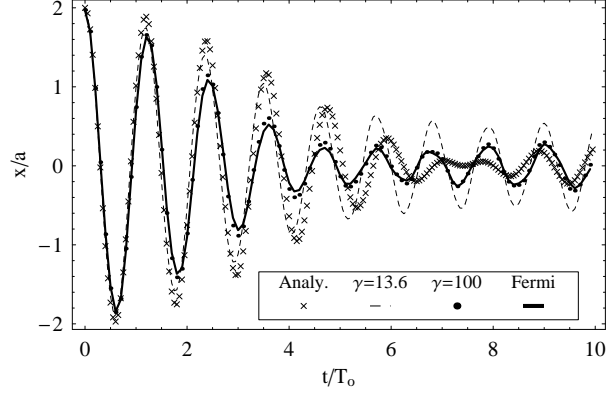
Figure 3.13: Center of mass position in lattice units as a function of time for interacting bosons, for $\gamma = 13.6$(dashed line) and $\gamma = 100$(dots). The solid line is the center of mass position for ideal fermions, while the crosses are the analytical approximation to the fermionic solution Eq.(3.33). Here, $q \approx 77$ and $\omega_T = 2\pi \times 100$ Hz and $T_o = 2\pi/\omega^*$.

The dipole dynamics of the bosonic and fermionic systems are explicitly compared in Fig. 3.13, where we plot the first 10 oscillations of the center of mass after the sudden displacement of the trap. In the figure, the dashed line and the dots are the bosonic dynamics for $\gamma = 13.6$ and 100, the solid line is the fermionic evolution, and the crosses are the analytical approximation to the fermionic evolution Eq. (3.33), respectively. Consistent with Fig. 3.12, we observe that for increasing γ the decrease of the amplitude of oscillation for the bosons resembles more and more the one for fermions. In particular, for $\gamma = 100$, the curves for the interacting bosons and ideal fermions nearly overlap. The distribution of excited frequencies for $\gamma = 100$ is shown in Fig. 3.11. The frequency distribution is broad and centered around $\omega \approx 0.75\omega^*$. Also in the inset small peaks are shown to appear in the range $1.6\omega^* \leq \omega \leq 3\omega^*$ (notice the different scale in the inset). The broad distribution is due to the population of single-particle states that are not harmonic in character. For the value of q used for the calculations no single-particle localized modes are occupied in the ground state before the trap displacement. After the displacement about 90 percent of the atoms occupy non localized single-particle modes. The phase mixing between these modes accounts for most of the observed damping. The remaining 10 percent occupy localized states and the population of these modes is responsible for the shift of the peak of the distribution to lower frequency. In fact we show below, Sec. 3.5.2, that a large population of localized states with $n \gg n_c$ yields a distribution which is peaked at $\omega \approx 0$.
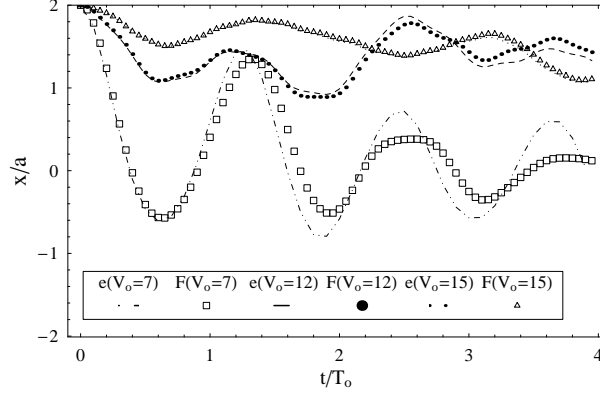
Figure 3.14: Center of mass position (in lattice sites) as a function of time calculated for different lattice depths and a fixed $\omega_T = 2\pi \times 150$ Hz. The dash-dotted, dashed and small-dotted lines are the exact solutions for interacting bosons (e in the legend) and the boxes, large-dots and triangles are the solutions for ideal fermions (F in the legend) for $V_o/E_R = 7, 12$ and 15, respectively. $T_o = 2\pi/\omega^*$.

Finally, we note that the small population of localized modes after the displacement also explains why the analytic solution Eq.(3.33) reproduces the exact fermionic evolution in Fig. 3.13 only qualitatively. In fact, Eq.(3.33) was derived under the condition $\sum_{n=n_c-1} |c_n^{(N-1)}|^2 \ll 1$, while here $n_c = 12$ and $\sum_{n=11} |c_n^{(N-1)}|^2 \approx 0.1$.

3.5.2   Localized dynamics

In analogy to recent experiments [17], in this section we study the dipole dynamics when the depth V_o of the optical lattice is varied, while the parabolic confinement is kept constant. Then, both J and U change as a function of the lattice depth, as explained in Sec. 3.4. The parabolic confinement $\omega_T = 2\pi \times 150 Hz$ has been chosen to be the same as in Sec. 3.4, so that the energy spectrum exactly matches the one discussed there, when V_o is varied.

In Fig. 3.14 lines and symbols correspond to the time evolution of the interacting bosons and ideal fermions, respectively. In particular, the dashed-dotted, dashed and small-dotted lines are for bosons, while boxes, large-dots and triangles are for fermions with $V_o/E_R = 7, 12$ and 15, respectively. For such lattice depths $\gamma = 14, 50$ and 100, respectively, and the system is fermionized, as discussed in Sec. 3.4.1. As expected, the agreement between the bosonic and fermionic solutions improves for larger γ-values, and is almost perfect for $\gamma = 100$.

Notably, for all the γ-values, no complete oscillation are observed, as the amplitudes of oscillations are strongly damped at very early times. The inhibition of the transport properties in the experiment here envisioned is a direct consequence of the large population of single-particle states which are localized in character. For the case $V_o = 7E_R$ ($\Omega N/J \approx 0.58$, $\gamma = 13.6$, $q = 134.2$ and $n_c \approx 8$) before the displacement the system is fermionized but non-localized. On the other hand, after the displacement about 20 percent of the atoms occupy localized modes of the undisplaced potential. The population of the localized modes with $n \gg n_c$ can be directly linked to the presence of low-frequency peaks ($\omega_{lk} \approx 0$) in the distribution of frequencies, Fig. 3.15. Because 80 percent of the atoms occupy non-localized modes the center of mass position can still relax to zero as shown in Fig.3.14. For the cases $V_o = 12E_R$ and $15E_R$ the Fermi energy is larger than E_{n_c}, and even before the displacement most states are localized. After the displacement has taken place, about 60 and 90 percent of the atoms occupy localized modes respectively, and the dynamics is overdamped. This is mirrored by the appearance of a large peak at $\omega_{lk} \approx 0$ in the probability distribution, Fig.3.15, and by the fact that the center of mass position does not relax to zero as shown in Fig.3.14.

3.6   Conclusions

We studied the spectrum and dipolar motion of interacting and non-interacting one-dimensional atomic gases trapped in an optical lattice plus a parabolic potential using the tight-binding approximation. We showed that the single-atom tight-binding Schrödinger equation can be exactly solved by mapping it onto the recurrence relation satisfied by the Fourier coefficients of periodic Mathieu functions. We used asymptotic expansions of such functions to fully characterize the eigenenergies and eigenmodes of the system. Our analytic approach is complementary to previous numerical and semiclassical analysis for single-atom systems. The advantage is that we can explicitly calculate the corrections to the harmonic oscillator spectrum introduced by the lattice. The knowledge of these corrections allow us also to provide analytic expressions for the modulations of the center of mass motion induced by the periodic potential when trapped ideal bosonic and fermionic gases are suddenly displaced from the trap center.

By means of numerical diagonalizations of the Bose-Hubbard Hamiltonian we studied the interact-

ing many-body bosonic problem. First, we characterized the changes in the low-energy excitation spectrum as a function of lattice depth, by comparing it with the ideal Bose and Fermi spectra. Then, we stated the necessary conditions for fermionization to occur and showed that it takes place for a large range of experimentally accessible parameters. We clarified the required conditions for the formation of a Mott insulator at the trap center and linked its appearance to the population of localized states at the Fermi level of the correspondent ideal fermionic system. We then studied the many-body dipole dynamics and showed that, in the parameter regime where the system is expected to be fermionized, the knowledge of the single-particle solutions is a powerful tool for the understanding of the strongly correlated dynamics. By studying the distribution of the frequencies pertaining the many-body modes excited during the dipole dynamics, we explicitly showed the connection between the population of single-particle localized states with the inhibition of the transport properties of the system. These spectral analysis allowed us also to gain some insight into the dynamics in the weakly-interacting regime, where an analysis beyond mean-field is required, and in the complex intermediate regime, where no mapping to single-particle solution is possible.
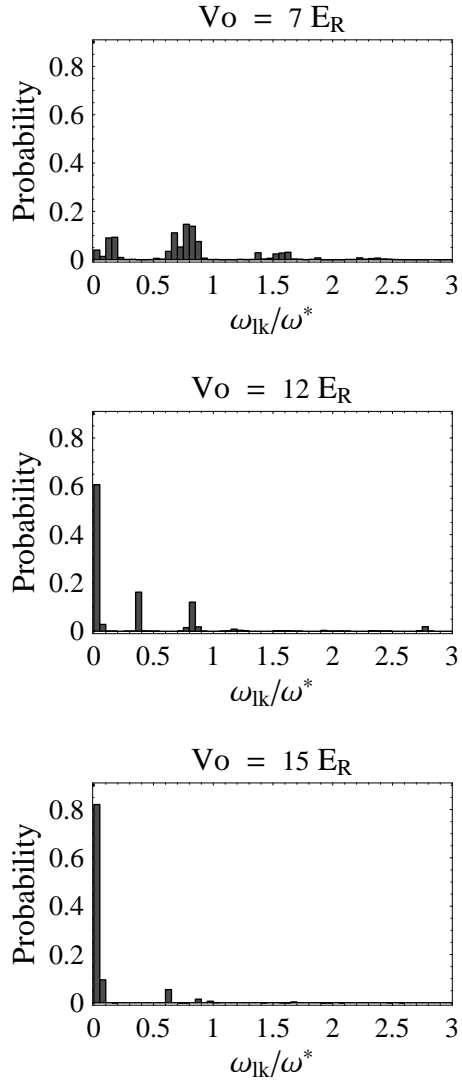
Figure 3.15: Probability distribution of frequencies for $V_o/E_R = 7, 12$ and 15 (see text). The frequencies ω_{lk} are given in units of ω^*. Because $\omega^* \propto \sqrt{J}$, ω^* decreases with increasing lattice depth.

Chapter 4

Extended fermionization of 1-D bosons in optical lattices

We present a model that generalizes the Bose-Fermi mapping for strongly correlated 1D bosons in an optical lattice, to cases in which the average number of atoms per site is larger than one. This model gives an accurate account of equilibrium properties of such systems, in parameter regimes relevant to current experiments. The application of this model to non-equilibrium phenomena is explored by a study of the dynamics of an atom cloud subject to a sudden displacement of the confining potential. Good agreement is found with results of recent experiments. The simplicity and intuitive appeal of this model make it attractive as a general tool for understanding bosonic systems in the strongly correlated regime.

4.1   Introduction

Cold bosonic atoms in optical lattices have recently been used to create quasi-one dimensional systems [14, 15, 16, 17, 18, 19]. In such experiments, arrays of one dimensional tubes are realized by first magnetically trapping a Bose-Einstein condensate (BEC) in a parabolic potential, and then imposing upon it a deep 2D optical lattice, which restricts atomic motions to 1D. These defect-free highly controllable atomic systems offer an excellent opportunity to directly study strongly correlated regimes.

For low densities or large interaction strengths, a 1D gas of ultracold bosons behaves as a gas of impenetrable particles, known as a Tonks-Girardeau (TG) gas. Ref. [47] shows there is a one to one mapping between the eigenenergies and eigenfunctions of TG bosons and the ones of non-interacting fermions, known as fermionization. Two recent experiments [15, 16] successfully reached this parameter regime. In Ref.[15] the TG regime was achieved by adding an optical lattice in the tubes' direction which increases the effective mass and therefore the ratio between interaction and kinetic energy. When the lattice is present and for large enough interactions a commensurate homogenous system not only fermionizes but also undergoes the superfluid to Mott insulator (MI) transition [12]. In the presence of a parabolic trap the MI can be realized for any number of particles [49, 50].

In the TG regime where there is at most one particle per site, single-particle solutions of the periodic plus parabolic potential have been successfully used to describe equilibrium and non-equilibrium properties of the system, both in the presence and in the absence of the MI [49, 50]. However, 1D experiments have been realized in a parameter regime where on-site particle densities are larger than one and standard fermionization is inapplicable [17, 19]. The study of these regimes beyond mean-field has relied mainly on numerical simulations, such as quantum Monte-Carlo or density matrix renormalization group techniques [27, 28, 29, 81]. Here we show that even when the on-site density is larger than one, for a wide range of conditions single-particle solutions can still describe strongly correlated regimes. We call this single-particle approach *extended fermionization* (EF). Comparison with exact Monte-Carlo simulations shows that in the appropriate parameter regimes EF can be used to accurately reproduce equilibrium properties such as the density profile, the momentum distribution, and the ground-state energy. In the final section we extend our model to treat the non-equilibrium dipole oscillations of atoms subject to a displaced potential, as has been realized in recent experiments [17, 19]. The accuracy and simplicity of the EF method suggest that it is a useful tool for understanding strongly correlated bosonic systems.

Bose-Hubbard Hamiltonian

As shown in Chapter 2, the Bose-Hubbard (*BH*) Hamiltonian describes the system's dynamics when the lattice is loaded such that only the lowest vibrational level of each lattice site is occupied and tunneling occurs only between nearest-neighbors [11]

$$H = -J \sum_{\langle i,j \rangle} \hat{a}_i^\dagger \hat{a}_j + \frac{U}{2} \sum_j \hat{n}_j(\hat{n}_j - 1) + \Omega \sum_j j^2 \hat{n}_j. \tag{4.1}$$

Here $\hat{a}_j$ is the bosonic annihilation operator of a particle at site j, $\hat{n}_j = \hat{a}_j^\dagger \hat{a}_j$, and the sum $\langle i,j \rangle$ is over nearest neighbors. In Eq.(5.1) the hopping parameter J, and the on-site interaction energy U are functions of the lattice depth V_o. Ω is proportional to the curvature of the parabolic potential.

4.2 Homogeneous system

For a homogeneous system ($\Omega = 0$) with N atoms and M sites, the spectrum is fully characterized by the ratio, $\gamma = U/J$, and the filling factor, $N/M = (n-1) + \Delta N/M$. Here n is the smallest integer larger than N/M and $\Delta N < M$. If the lattice is commensurately filled ($\Delta N = 0$), the ground state is a Mott insulator for $\gamma > \gamma_c(n-1)$, where $\gamma_c \approx 4$ [48]. For the incommensurate case, $\Delta N > 0$, if $\gamma/n \gg \gamma_c$, the population of states with more than n atoms per site is suppressed by a factor of $\approx J/U$, so the BH system may be treated as one with two states per lattice site (containing $n-1$ and n atoms respectively). In this case, it is well known [82] that the BH model maps to the XX quantum spin model. Thus, the standard Bose-Fermi mapping techniques derived for systems with $n = 1$ can be applied, if J is replaced by nJ. Here we present a generalization of standard fermionization ideas, to treat the systems that are of greatest interest in current experiments: those for which n is greater than 1 and varies across the system.

4.3 Inhomogeneous system

When the parabolic trap is present ($\Omega > 0$), the density profile of the atomic cloud is determined by an interplay of U, J, Ω and N. The system is fermionized (with at most one atom per site) if [50]

$$\gamma > \gamma_c, \quad U > \Omega((N-1)/2)^2. \tag{4.2}$$

The first inequality is the same as for a homogeneous lattice, but the second is specific to trapped systems: it suppresses multiple occupancy of single sites. In this fermionized regime, the density at the trap center increases as J decreases and, when the condition $2J \lesssim \Omega((N-1)/2)^2$ is satisfied, central trap sites begin to have unit filling [49, 50]. If the inequality

$$J < \Omega N, \tag{4.3}$$

is also satisfied, the ground state is a unit-filled Mott state in all N sites. In this case, number fluctuations occur mainly at the edge of the density distribution, due to tunneling of atoms to empty sites. Such fluctuations are proportional to ΩN, which is the trap gradient at the site $(N-1)/2$. Number fluctuations at the trap center are due to a small admixture of particle-hole excitations in the ground state for finite J [51]. By using perturbation theory, it can be shown that this admixture is proportional to $2\sqrt{2}(J/U)$.

For $\Omega((N-1)/2)^2 \gtrsim U$ it is energetically favorable for atoms to pile up at the trap center. In fact, superfluid and Mott insulator phases with different filling factors can coexist, due to the interplay between on-site interactions and the external potential [11, 28, 83]. In the trivial case $J = 0$, Fock states with a definite number of atoms in each site are eigenstates of the Hamiltonian. The density profile becomes a "cake" structure with maximal occupation n_{max} at the trap center if

$$2H^{(1/2)}_{n_{max}-1} < [(N - n_{max})\sqrt{\Omega/U}] < 2H^{(1/2)}_{n_{max}}, \tag{4.4}$$

where $H^{(1/2)}_n \equiv \sum_{i=0}^{n} \sqrt{i}$ [83]. In fact, this profile is most conveniently viewed as a "layer cake" structure of n_{max} stacked horizontal layers. The number of atoms in the n horizontal layer, N_n, can be shown to satisfy $(N_1 - N_n)(N_1 + N_n - 2) = 4U(n-1)/\Omega$ subject to $\sum_{n=1}^{n_{max}} N_n = N$. In the limiting case of $J = 0$, atoms are frozen within each layer (an ice-cream cake). Each layer can then be thought of as an independent Mott state with unit filling. For $J > 0$, atoms are no longer frozen, and it is not obvious that the layers should remain distinct. However, if the number fluctuations in adjacent horizontal layers do not overlap in space, all layers can still be thought of as independent. This situation pertains to many cases of experimental interest in the strong coupling regime, in particular when

$$\gamma > \gamma_c(n_{max} - 1), \quad \Omega N_{n_{max}-1} > J(n_{max} - 1). \tag{4.5}$$

In this case, all layers except the top can be viewed as Mott states with unit filling factor. In analogy to Eq. (4.2), the first inequality insures that within those layers, the average kinetic energy required for one atom to hop between sites is insufficient to overcome the potential energy cost; thus particle-hole excitations are suppressed by a factor of $\approx nJ/U$. The second inequality guarantees that in those layers, number fluctuations are localized at the outer edge of the layer, much like frosting. In addition, if

$$\gamma > \gamma_c n_{max}, \tag{4.6}$$

then, to a very good approximation, atoms in all layers can be treated as TG bosons with an effective hopping energy nJ. Under these conditions, single-particle solutions can be successfully used to obtain expressions for all many-body observables. We refer to this generalization of the Bose-Fermi mapping to spatially varying density distributions as *extended fermionization*. The top layer is governed by Jn_{max}, $N_{n_{max}}$, and
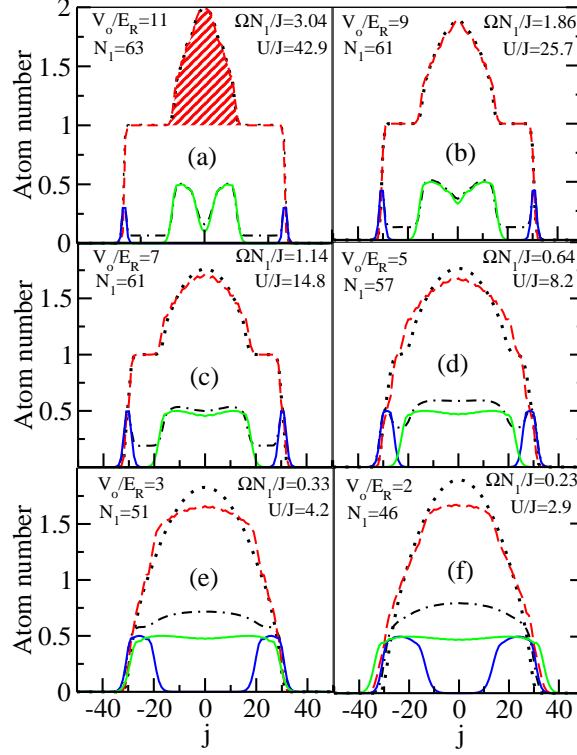
Figure 4.1: Local densities $\langle\hat{\rho}_j\rangle$ and fluctuations $\langle\Delta\hat{\rho}_j^{(n)}\rangle$ as a function of the site index j. Dotted(black) and dashed(red) lines are the numerical and analytical densities, respectively. The dashed-dotted(black) line is the numerical fluctuation, while solid-black(blue) and solid-grey(green) lines are the analytical fluctuations for the lower($n = 1$) and upper($n = 2$) layers, respectively. The shaded(red) area in panel (a) is the density in the $n = 2$ layer of the EF model.

Ω; these determine whether it is a Mott state or not.

In the following we show the success and the limitations of this approach, by applying it to a system with the same parameters as the ones used in an experiment recently performed at NIST [17].

4.4   Numerical comparisons

In the NIST experiment [17] approximately $N_T = 1.4 \times 10^5$ ^{87}Rb atoms were trapped in an array of one-dimensional tubes with $N \simeq 80$ atoms in the central tube. An additional periodic potential was added along the direction of the tubes and its depth V_o was varied for different experiments. The periodicity of the parabolic potential in the tubes' direction was such that $\Omega = 7.4 \times 10^{-4} E_R$, with E_R the photon recoil energy. Here we focus on the central tube only and consider $V_o > 2E_R$, where the tight-binding Hamiltonian Eq.(5.1) is expected to be valid. For these parameters, Eq. (4.4) yields $n_{max} = 2$.

In Fig. 4.1 we show comparisons between the density and number fluctuations for the central tube calculated by using the EF approximation and quantum Monte-Carlo numerical simulations based on the Worm algorithm [30], for lattice depths $V_o/E_R = 11(a),9(b),7(c),5(d),3(e),2(f)$. In the numerical simulations the temperature is $0.01J$. In the plots the dotted(black) and dash-dotted(black) lines correspond to the density and number fluctuations as numerically calculated by using the Monte-Carlo code, respectively. The dashed(red), the solid-black(blue) and solid-grey(green) lines correspond to the density $\langle \hat{\rho}_j \rangle$, and to the number fluctuations for the atoms in the first $\langle \Delta \hat{\rho}_j^{(1)} \rangle$ and second layer $\langle \Delta \hat{\rho}_j^{(2)} \rangle$, as calculated with the EF model respectively. In particular, the density is given by $\langle \hat{\rho}_j \rangle = \sum_{s=0}^{N_1-1} |f_j^{1\,(s)}|^2 + \sum_{s=0}^{N_2-1} |f_j^{2\,(s)}|^2$ where $\{f_j^{n=1,2\,(s)}\}$ are the sth single-particle eigenmodes of Eq.(5.1) with hopping energies nJ respectively and j is the lattice site index. The fluctuations are given by $\langle \Delta \hat{\rho}_j^{(n)} \rangle = \sqrt{\sum_{s=0}^{N_n-1} |f_j^{n\,(s)}|^2 - \left(\sum_{s=0}^{N_n-1} |f_j^{n\,(s)}|^2 \right)^2}$.

The conditions for EF to be applicable, Eqs.(4.5) and (4.6), are strictly valid for $V_o \gtrsim 5E_R$. Consistently, Fig. 4.1$(a-c)$ shows that for $V_o/E_R = 11,9,7$ the density profile and number fluctuations are very well reproduced by the model, except for the finite value of the fluctuations in the flat region of the density profile. These small fluctuations of order $2\sqrt{2}J/U$ are due to the particle-hole excitations which are neglected in the model. The model predicts that some sites at the trap center have exactly a filling factor of two when $2(2J) \lesssim \Omega((N_2-1)/2)^2$. This condition is fulfilled for $V_o = 11E_R$, and in fact a flat density distribution with two atoms per site is observed in Fig.1-(a) at the trap center, both in the analytical and numerical results. This confirms the validity of the idea of thinking of the atoms in the second layer as TG-bosons with effective hopping energy $2J$.

For $V_o = 5E_R$,γ is barely $2\gamma_c$, and $\Omega N_1 < J$ so that fluctuations at the edge of the first layer extend far enough to overlap with the ones of the second layer. We only expect EF to give qualitative predictions in this regime. For $V_o = 3,2E_R$ the conditions Eqs.(4.5) and (4.6) are not satisfied, and the model fails to reproduce the exact results. Nevertheless, we notice that the EF model predicts the formation of a Mott state in the lowest layer for $V_o \gtrsim 3E_R$ because $\gamma \approx \gamma_c$ and $\Omega(N_1-1)^2/4 > 2J$ at $3E_R$. The numerically obtained fluctuations show the appearance of a flat region at the cloud's edge for $V_o = 3E_R$. Such flat region signals the formation of a Mott state as it evolves for deeper lattices into the observed dip in the fluctuations and disappears for shallower lattices (Fig 4.1-(e)).
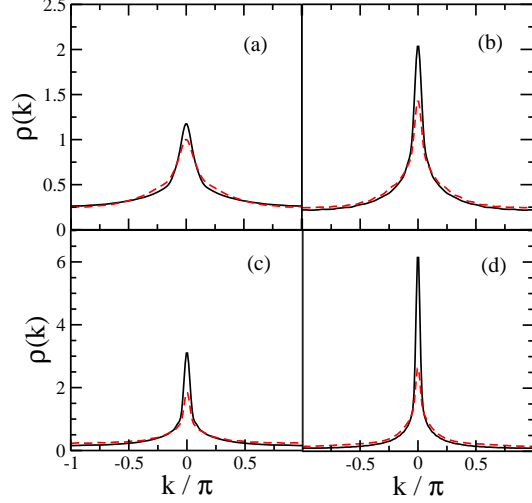
Figure 4.2: Momentum profiles $\rho(k)$ as a function of the momentum k, for lattice depths $V_o/E_R = 11(a)$, $9(b)$, $7(c)$, and $5(d)$. The solid(black) and dashed(red) lines are the exact momentum distibutions and the model momentum distributions, respectively.

In Fig.2 we compare the momentum distribution $\rho(k)$ for the many-body system, solid(black) line, with the one predicted by the EF model, dashed(red) line, for $V_o = 11(a),9(b),7(c)$, and $5(d)$. The model curves are given by $\rho(k) = \rho(k)^{(1)} + 2\rho(k)^{(2)} - N_2/M$, where $\rho(k)^{(n=1,2)}$ are the momentum distributions for N_n TG bosons with effective hopping rate nJ, calculated numerically with the Monte-Carlo code. For all curves, the height of the central peak is larger and the width at half maximum is smaller for the exact than for the model solutions. This is expected because the model neglects correlations between atoms in the first and second layers. However, the agreement is at least qualitative for all displayed lattice depths where EF applies. On the other hand the agreement for the deepest lattice in consideration is worse than the one found for the local observables $\langle \hat{\rho}_j \rangle$ and $\langle \Delta \hat{\rho}_j \rangle$, (Fig 1). This is consistent with previous observations for standard fermionization [84].

In Fig. 4.3 ground state energies are compared as a function of lattice depth. The solid(black) line is calculated numerically using the Monte-Carlo algorithm and the dashed(red) line using the EF model $E = \sum_{s=0}^{N1-1} E_1^{(s)} + \sum_{s=0}^{N2-1}(U + E_2^{(s)})$. Here, $E_{1,2}^{(s)}$ are the sth single-particle eigenenergies of systems with hopping energies J and $2J$, respectively. At $V_o = 5E_R$ the model predicts a ground-state energy which is 10% larger than the numerical solution while at $V_o = 11E_R$ the difference decreases to only 0.4%. This also confirms the validity of the EF model as the lattice deepens.

4.5 Center of mass oscillations

In the NIST experiment [17], center of mass oscillations were induced by a sudden displacement of the harmonic potential by $\delta = 8$ lattice sites. An overdamped motion was observed for lattice depths $V_o \gtrsim 3E_R$. The damping rate b was obtained by fitting to the formula $m^* \ddot{x} = -b\dot{x} - m\omega_T^2 x$, where m and m^* are the atomic and effective masses and ω_T is the magnetic trapping frequency. Previous theoretical analysis of the damping did not use real experimental parameters [50, 64, 66, 85] or were not applicable in the strongly correlated regime [67, 86]. Here we show that the EF approach reproduces the experimental results well in the overdamped regime. In Fig.4 the experimental data (black squares) are compared to the predictions of the EF model. In the model, the center of mass position of the atoms in the central tube (red dots) is given by $x(N) = a/N \left[\sum_{s=0}^{N_1-1} x_1^{(s)}(t,N) + \sum_{s=0}^{N_2-1} x_2^{(s)}(t,N) \right]$, where

$$x_n^{(s)}(t,N) = \sum_{k,l,j} j c_l^{n(s)} c_k^{n(s)} e^{-i(E_n^{(k)} - E_n^{(l)})t/\hbar} f_j^{n(k)} f_j^{n(l)}. \tag{4.7}$$

Here, N is the number of atoms in the central tube, a is the lattice spacing and the coefficients $c_k^{n(s)} = \sum_j f_j^{n(k)} f_{j-\delta}^{n}{}^{(s)}$ are the projection of the sth excited state of the displaced potential onto the kth excited eigenstate of the undisplaced potential for atoms in the $n = 1, 2$ layer, respectively. The EF model is expected to give an accurate description of the center of mass oscillations if, during the dynamics, the atoms in the first and second layer can still be treated as independent objects, *i.e.* when number fluctuations in the two layers do not overlap during the evolution. Because in the experiment the measured damping rate
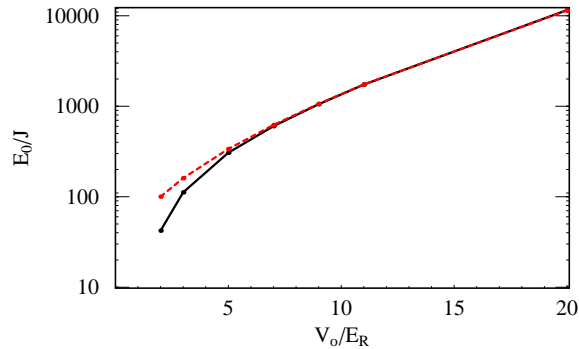
Figure 4.3: Energy as function of V_o/E_R. The solid(black) and dashed(red) lines are the numerical and analytical energies, respectively.
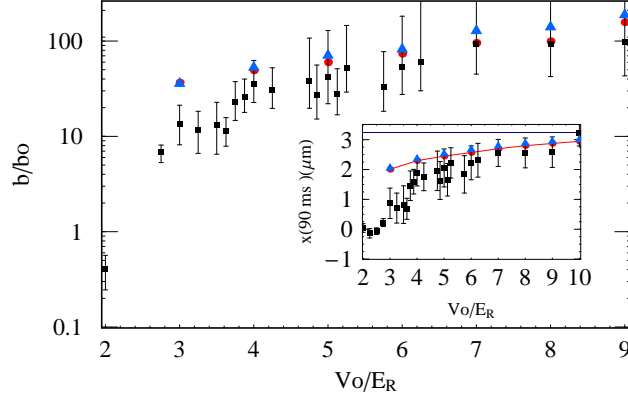
Figure 4.4: Damping rate of dipole oscillations b as a function of V_o/E_R. b is in units of $b_o = 2m\omega_T$. The squares are the NIST experimental results. The circles(red) are the model results for the central tube, and the triangles(blue) are the model results averaged over all the tubes. Inset: center of mass position after 90 ms.

was an average over all the tubes, in Fig.4 we also plot the model's prediction for the average damping rate

(blue triangles). The latter was calculated assuming that all tubes evolve independently and therefore that

$x(t) = \left[\sum_{\mathcal{N}=1}^{N} \mathcal{N} P(\mathcal{N}) x(\mathcal{N}, t)\right] / \sum_{\mathcal{N}=1}^{N} P(\mathcal{N}) \mathcal{N}$ is the average center of mass position. Here, $P(\mathcal{N})$ is

the probability of having a tube with $\mathcal{N}$ atoms. Assuming an initial Thomas-Fermi distribution of the 3D

system, $P(\mathcal{N}) \approx 2/3(N^2\mathcal{N})^{-(1/3)}$ [15].

When there is at most one atom per site, atoms in the Mott state have been shown to be responsible

for the overdamped dynamics [50, 85]. Here, the two-layer model predicts that a Mott state is created in the

lowest layer for $V_o \gtrsim 3E_R$, Fig.1, and therefore atoms in this layer are almost frozen. However, atoms in

the second layer are not necessarily localized, and their dynamics can be underdamped. Because there are

always more atoms in the lowest layer than in the upper one, the overall dynamics is overdamped, and this

explains the large damping observed in the experiment for $V_o \gtrsim 3E_R$. This is also in agreement with the

qualitative explanation of the damping given in Ref.[19].

Strictly speaking, the fluctuations in the two layers do not overlap during the dynamics only for

$V_o > 7E_R$, thus we expect the model to be valid for the deepest lattice depths only. Nevertheless, Fig.4

shows that the theoretical calculations are within the experimental error bars already for $V_o \gtrsim 4$. Figure 4

also shows that the damping rates for the central tube and the average are very similar, and this is because

tubes with about $N = 80$ atoms have the largest weight. The average shows a larger damping because it

takes into account contributions from tubes that do not have extra atoms in the second layer. In the inset we also compare the experimental center of mass position of the atomic cloud after $90ms$ with the model solutions. The agreement between experiment and theory is consistent with the one found for the damping rate.

4.6   Summary

We have developed a simple model that generalizes the Bose-Fermi mapping to regimes where the filling factor is larger than one. The model is relevant for 1D trapped gases where the co-existence of Mott-insulating regions with different occupation numbers is permitted. We presented the necessary conditions for the model to be valid and showed the uselfuness and limitations of the method by comparing its predictions for some physical observables with numerical Monte-Carlo simulations. Very good agreement between the model and the numerical solutions was found in the parameter regime where the model is valid. Finally we used the EF model to study the overdamped dynamics of the center of mass after a sudden displacement of the trapping potential, and found good agreement with recent experiments. In particular, the overdamped motion was linked to the presence of a Mott state in the lowest atomic layer.

Chapter 5

Bragg Spectroscopy of ultracold atoms loaded in an optical lattice

We study Bragg spectroscopy of ultra-cold atoms in one-dimensional optical lattices as a method for probing the excitation spectrum in the Mott insulator phase, in particular the one particle-hole excitation band. Within the framework of perturbation theory we obtain an analytical expression for the dynamic structure factor $S(q,\omega)$ and use it to calculate the imparted energy which has shown to be a relevant observable in recent experiments. We test the accuracy of our approximations by comparing them with numerically exact solutions of the Bose-Hubbard model in restricted cases and establish the limits of validity of our linear response analysis. Finally we show that when the system is deep in the Mott insulator regime, its response to the Bragg perturbation is temperature dependent. We suggest that this dependence might be used as a tool to probe temperatures of the order of the Mott gap.

5.1   Introduction

Recently, there has been a lot of experimental progress studying cold atoms confined in optical lattices. The defect free nature of the lattice potential, the long coherence times of the constituent atoms, and the experimental control of the lattice parameters [87, 88] make this a unique system for precisely studying many-body physics. In particular, the experimental observation of the superfluid to Mott insulator quantum phase transition [13] has stimulated much interest in this area of research.

Perhaps one of the most important potential applications of the Mott insulator transition is to use it as a means to initialize a quantum computer register[89, 90, 91, 92]. In this case, it is important to have tools for thoroughly characterizing the experimentally obtained Mott insulator states. The usual procedure for entering the Mott insulator regime is to begin with a magnetically trapped BEC (with almost all the atoms in the condensate), and then slowly load it into an optical lattice by increasing the lattice depth. One key piece of evidence for the quantum phase transition is the loss of global phase coherence of the matter wavefunction when the lattice depth increases beyond a critical value [13]. However, the loss of

coherence could arise from many other sources, such as the decoherence induced by quantum or thermal depletion of the condensate during the loading process [74] and therefore decoherence is not a sufficient signature that the system is in the Mott insulator state. For this reason, in the experiments by Greiner *et al.*[13], complementary evidence for the Mott insulator transition was provided by applying a potential gradient to the lattice to show the presence of a gap in the excitation spectrum. In this chapter we show that Bragg spectroscopy, done by applying additional laser beams independent from the lattice beams, is an experimental technique with the potential to thoroughly characterize the Mott phase. In addition to determining the energy gap, we show that Bragg spectroscopy provides detailed information about the excitation spectrum, information unavailable using other techniques. Moreover, in contrast to applying a potential across the lattice, Bragg spectroscopy is not susceptible to effects like Bloch oscillations and Zener tunneling. Furthermore, we show that different from the superfluid regime, the system's response to Bragg perturbation in the Mott regime is sensitive to finite temperature. This property might be used as a tool to probe temperatures of order of the Mott gap.

Our analysis is based on a perturbative treatment, which we show to be applicable in the strong Mott regime that has been reached in current experiments [15]. Although our approach is applicable only in the range of validity of first order perturbation theory, it has the advantage of properly including one-particle-hole correlations. Such correlations have dominant influence on the spectrum of the system and are not accounted for in mean-field treatments [35].

The organization of this Chapter is the following. In Sec. 5.2 we introduce the basic formalism that describes Bragg spectroscopy in an optical lattice and use a linear response approach to calculate the energy imparted to the system. In Sec. 5.3 we derive the zero temperature response to the Bragg spectroscopy of a translationally invariant lattice deep in the Mott regime and in Sec. 5.4 we discuss the conditions required for our linear response analysis to be valid. In Sec. 5.5 we extend the zero temperature analysis to finite temperature and finally in Sec. 5.6 we conclude.

5.2 Formalism

The typical Bragg spectroscopic procedure is to gently scatter atoms in an ultra-cold gas system with a moving potential of the form $V_0 \cos(qx - \omega t)$. This type of experiment was first demonstrated by the NIST and MIT groups [31, 32]. In contrast to earlier experiments that used momentum as the response observable, here we choose to examine the imparted energy. In trapped systems this allows long excitation duration that facilitates more precise spectral resolution. Energy-spectroscopy is not so well developed as momentum spectroscopy but recent experiments have demonstrated the use of this technique [19]. The Bragg potential is formed by the ac-Stark shift arising from a pair of interfering light fields (e.g. see [93]). In this chapter we will always assume that the Bragg potential is *generated independently* of and is much weaker than the lattice potential. We therefore treat the scattering process with linear response theory. Using an independent set of beams to generate the Bragg potential also provides considerable flexibility in the range of q and ω values that can be obtained.

In this work we consider one-dimensional bosons loaded in an optical lattice. Effective 1D systems have been realized in recent experiments by loading a Bose-Einstein condensate into a three-dimensional optical lattice, which is very deep in two directions. The dynamics is then restricted to the third, or axial, direction only. In this work we study the response of the system to Bragg perturbation in the axial direction, assuming that the dynamics in the transverse directions is frozen. We consider a one-dimensional optical lattice which is sufficiently deep that the tight binding approximation is valid and assume that we can restrict the dynamics of the atoms to the lowest vibrational band. This applies when changing the lattice potential does not induce band excitations. This condition is fulfilled when the frequency, ω, of the Bragg perturbation is less than the gap between the first and second bands, and when the momentum transfer q is contained within the first Brillioun zone. A detailed analysis of the validity of this first-band approximation to study Bragg scattering of a dilute weakly-interacting gas in an optical lattice is found in [94] where the authors used a mean field approach combined with Bogoliubov analysis. In the single-band approximation and in absence of external potentials, the system is described by the Bose-Hubbard Hamiltonian (BHH)

$$\hat{H} \quad = \quad -J\sum_{\langle n,l \rangle} \hat{a}_n^\dagger \hat{a}_l + \frac{U}{2}\sum_n \hat{a}_n^\dagger \hat{a}_n^\dagger \hat{a}_n \hat{a}_n. \tag{5.1}$$

Here $\hat{a}_n$ is the annihilation operator at site n which obeys the canonical commutation relations for bosons, J is the hopping matrix element between nearest neighbors, and U is the on-site repulsion energy. The sum $\langle n,l \rangle$ is taken over nearest neighbors. We use N for the total number of atoms and M for the total number of wells. In the tight binding approximation the Hamiltonian describing the Bragg perturbation reads

$$\hat{H}_B = \frac{1}{2}V_0(\hat{\rho}_q^\dagger e^{-i\omega t} + \hat{\rho}_q e^{i\omega t}), \tag{5.2}$$

where the density fluctuation operator $\hat{\rho}_q^\dagger$ is defined as $\hat{\rho}_q^\dagger = \sum_{n,m=0}^{M-1} I_q^{n-m} \hat{a}_m^\dagger \hat{a}_n e^{iqmd}$, where $I_q^n = \int dx e^{iqx} \phi_0^*(x)\phi_0(x-dn)$ is a geometrical factor that involves integration over Wannier functions $\phi_0(x)$, and d is the lattice constant. For deep lattices $I_q^n \propto \delta_{n,0}$ [94].

To analyze the Bragg spectrum of the system we study the energy transfer, which can be measured by time-of-flight techniques[19]. Under linear response theory, the energy transfer is related to the so called *dynamic structure factor*, $S(q,\omega)$, which is given by

$$S(q,\omega) \quad = \quad \frac{1}{\mathcal{Z}}\sum_{ij} e^{-\beta E_i} f_q(\omega_{ij}), \tag{5.3}$$

where $f_q(\omega_{ij}) \equiv |\langle i| \hat{\rho}_q |j\rangle|^2 \delta(\omega - \omega_{ij})$, $|i\rangle$ and E_i are eigenstates and eigenenergies of the unperturbed Hamiltonian (5.1), $e^{-\beta E_i}$ is the usual Boltzmann factor with $\beta = 1/k_B T$ where k_B is Boltzmann's constant and T the temperature, $\mathcal{Z}$ is the canonical partition function, and $\hbar\omega_{ij} = E_j - E_i$. Because of the factor $f_q(\omega_{ij})$, the system's response shows peaks whenever the frequency of perturbation matches the energy difference between two eigenstates of the BHH. The peak height is proportional to the the transition probability between the two eigenstates, $|\langle i| \hat{\rho}_q |j\rangle|^2$.

The total energy transfer after applying the Bragg perturbation can be shown to be given by [95]:

$$\delta E \quad = \quad \frac{V_0^2}{2\hbar}\int_0^{T_p} dt \int_{-\infty}^\infty d\omega' \omega' \chi(q,\omega')\frac{\sin((\omega-\omega')t)}{(\omega-\omega')}, \tag{5.4}$$

where T_p is the duration of the perturbation and $\chi(q,\omega) = S(q,\omega) - S(-q,-\omega)$. Here we derive analytic expressions for the dynamic structure factor assuming we are deep in the Mott insulator regime, where treating the hopping term in the Hamiltonian as a perturbation is justified.

5.3 Zero temperature response

In this work we assume a commensurately filled lattice with no external confinement, filling factor $N/M = g$ and periodic boundary conditions. The unperturbed Hamiltonian includes only the on-site interaction term, which is diagonal in a number Fock-state basis. To zeroth order the ground state $|\Phi_0^{(0)}\rangle$ is the Fock state with g atoms in every lattice site. The lowest lying excitations correspond to the one-particle-hole (1-ph) states $|\Psi_{mn}\rangle$ with $g + 1$ particles at site m, $g - 1$ particles at site n, and exactly g particles in every other site. There are $M(M - 1)$ 1-ph excitations and, because of the translational symmetry, they are degenerate at zeroth order with excitation energy U. To zeroth order the dynamic structure factor vanishes. At first order the ground state wave-function is $|\Phi_0^{(1)}\rangle = |\Phi_0^{(0)}\rangle + J/U\sqrt{2Mg(g + 1)}|S\rangle$, where $|S\rangle \equiv \sum_{n=1}^{M}(|\Psi_{nn+1}\rangle + |\Psi_{nn-1}\rangle)/\sqrt{2M}$ is the normalized translationally invariant state of adjacent particle-hole excitations. In order for perturbation theory to be valid, the parameter $Jg\sqrt{M}/U$ has to be small [92]. This could be a significant restriction for systems with a large number of filled sites but can be perfectly realized in experiments such as Ref.[15] where the system has only 20 occupied sites in the central tube. To find first order corrections to the $M(M-1)$ low lying excited states we must diagonalize the kinetic energy Hamiltonian within the 1-ph subspace. If we expand the eigenstates as a linear combinations of 1-ph excitations $|\Phi_i^{(1)}\rangle = \sum_{n,m\neq n} c_{nm}^i |\Psi_{nm}\rangle$ the necessary and sufficient conditions that the coefficients c_{nm}^i have to fulfill are

$$(g + 1)(c_{n+1m}^i + c_{n-1m}^i) + g(c_{nm+1}^i + c_{nm-1}^i) = \widetilde{E}_i c_{nm}^i, \tag{5.5}$$

with $E_i^{(1)} = U - J\widetilde{E}_i$. Besides Eq. (5.5), the amplitudes c_{nm}^i have to satisfy periodic boundary conditions $c_{n+Mm}^i = c_{nm+M}^i = c_{nm}^i$ and the constraint $c_{nn}^i = 0$ (which prevents particle and hole excitations occurring at the same site). Eq. (5.5) is analogous to the tight binding Schrödinger equation of a two dimensional square lattice in the xy-plane. The x direction is associated with the position of the extra particle and the y direction with the position of the hole. The different weights $g+1$ and g can be understood in the 2D-lattice model as different effective masses in the two directions and the constraint $c_{nn}^i = 0$ as a hard wall along the $x = y$ line. The solutions are not straightforward due to the fact that the effective mass difference breaks the lattice symmetry around the $x = y$ axis and makes the hard wall constraint hard to fulfill. However, in the limiting case of high filling factor, $g \gg 1$ the solutions of Eq. (5.5) (including the

constraints) are

$$E_{rR}^{(1)} = U - 2J(2g+1)\cos\left(\frac{\pi r}{M}\right)\cos\left(\frac{\pi R}{M}\right),$$ (5.6)

$$c_{nm}^{r,R\neq 0} = \begin{cases} \frac{2}{M}\sin(\frac{\pi r}{M}|n-m|)\sin(\frac{\pi R'}{M}(n+m)+\alpha_{rR}), \\[2mm] \frac{2}{M}\sin(\frac{\pi r}{M}(n-m))\sin(\frac{\pi R''}{M}(n+m)+\beta_{rR}), \end{cases}$$ (5.7)

$$c_{nm}^{r,0} = \begin{cases} \frac{\sqrt{2}}{M}\sin\left(\frac{\pi r}{M}|n-m|\right), & r \quad \text{odd} \\[2mm] \frac{\sqrt{2}}{M}\sin\left(\frac{\pi r}{M}(n-m)\right), & r \quad \text{even} \end{cases}$$ (5.8)

Where we used $i = (r, R)$, with $r = 1, \ldots M-1$ and $R = 0, \ldots M-1$. The notation R' restricts the values of R to the ones where $R + r$ is an odd number and R'' to the values where $R + r$ is even. The constants $\alpha_{rR} = \pi(r - R + 1)/4$ and $\beta_{rR} = \pi(r + R - 1 + M)/4$ guarantee the orthogonality of the eigenmodes.

Using Eqs. (5.6) and (5.8) we get an expression for the zero temperature dynamic structure factor given by

$$S_0(q, \omega) = \frac{J^2}{U^2}g(g+1)\sum_{r,R}\delta\left(\omega - E_{rR}^{(1)}/\hbar\right)|\sum_{m=1}^{M}e^{iqdm}H_m^{rR}|^2$$

$$= 32\frac{J^2}{U^2}g(g+1)\sin^2\left(\frac{qd}{2}\right)\sum_r{}'\sin^2\left(\frac{\pi r}{M}\right)\delta(\omega - \frac{E_{r\tilde{q}}^{(1)}}{\hbar}).$$ (5.9)

Where $H_m^{rR} = c_{m\,m+1}^{rR} + c_{m\,m-1}^{rR} - c_{m+1\,m}^{rR} - c_{m-1\,m}^{rR}$, $qd = 2\pi\tilde{q}/M$, and $\tilde{q}$ an integer between 0 and $M - 1$. The prime in the sum imposes the constraint $\tilde{q} + r$ is even. It is important to emphasize that only the states with $R = 0$ have a dispersion relation which agrees to first order in J to the mean-field solution found in Ref. [35]. However, for these states $H_m^{r0} = 0$.

In Fig. 5.1 we compare the energy transfer as a function of the Bragg frequency calculated from Eq. (5.9) to results obtained by the exact diagonalization of the BHH for four values of Bragg momenta q. In contrast to the superfluid regime [94], where Bragg spectroscopy excites only the quasiparticle state with quasimomentum q, in the Mott regime we observe $M - 1$ peaks pertaining to the two dimensional character of the 1-ph dispersion relation. The Bragg momentum q fixes one quantum number R but the other can take $M - 1$ different values. In the analytic solution due to the constraint in Eq. (5.9), $\tilde{q} + r$ even, only $(M - 1)/2$ of the possible $M - 1$ peaks are present. The constraint is a consequence of the extra symmetry introduced in the high filling factor approximation where similar "effective masses" are assumed.
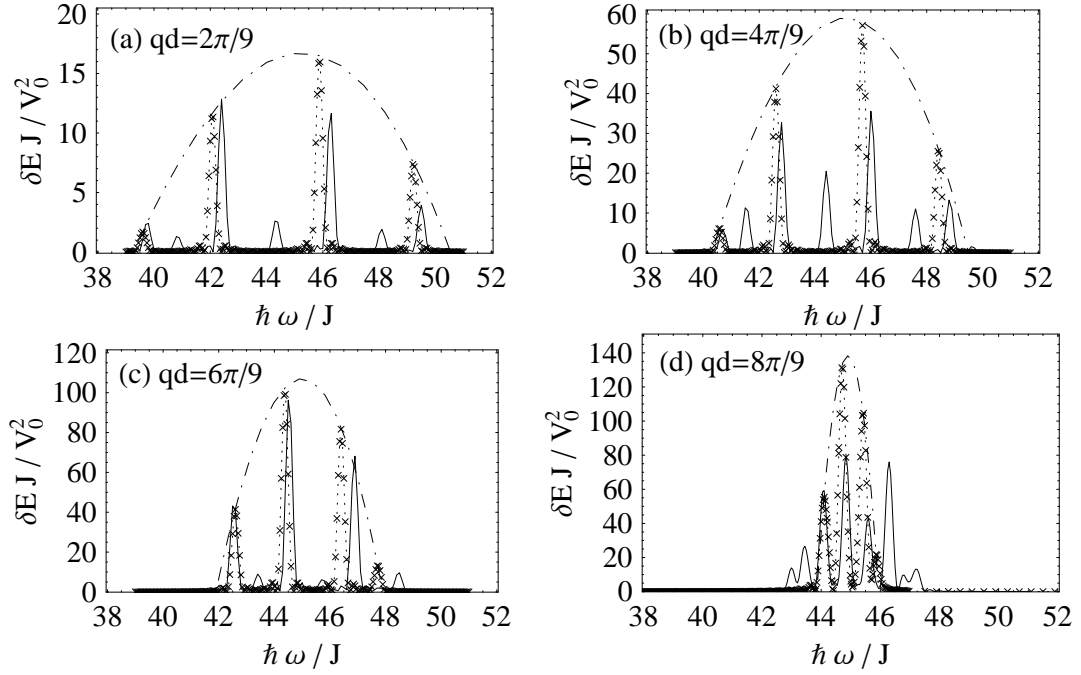
Figure 5.1: Energy transfer for a homogeneous system at zero temperature. Solid line exact solution. crosses perturbative solution (envelope: dashed line). Other parameters: $M = N = 9$, $J\tau/\hbar = 20$, $U/J = 45$.

In the analytic solution, Bragg peaks have an overall envelope of the form of an inverted parabola centered at the gap energy U, with a maximum height proportional to $\sin^2(qd/2)$ and extended over an interval with an approximated width of $4J(2g+1)\cos(qd/2)$. The $\cos(qd/2)$ dependence of the width and $\sin^2(qd/2)$ dependence of the height indicate that as q approaches π/d the energy transfer is highly peaked around U. This behavior is observed in Fig. 5.1, where the overall width decreases as q approaches π/d, while the peak height increases. In spite of the fact that the analytic solution uses the high filling factor approximation, the dependence on q of the width and peak height of the envelope is in agreement with the $g = 1$ exact energy response as shown in Fig. 5.1.

We found no structure around $\hbar\omega = 2U$ in the exact numerical results. This is consistent with the fact that the parameters used in this chapter lie within the regime of validity of first-order perturbation theory.

For the form of energy spectroscopy we consider here, there is no fundamental limit to Bragg pulsed

durations in contrast to momentum-spectroscopy [1]. However, practical considerations will likely inhibit the resolution of the individual excitation peaks in current experiments (see discussion below). In this case the envelope shown in Fig. 5.1 will provide a more realistic depiction of the experimentally observable spectrum.

5.4   Validity conditions

The treatment we present here is based on linear response. In this section we indicate its strict validity conditions in terms of the Bragg strength V_0 which is the relevant experimental parameter.

After the Bragg perturbation is applied, the many-body state is no longer in the BHH ground state, $|0\rangle$. The transition probability to an excited state $|i\rangle$, $|c_i(t)|^2$, according to first order perturbation theory is given by

$$|c_i(t)|^2 \;=\; V_0^2 |\langle i|\hat{\rho}_q^\dagger|0\rangle|^2 \frac{\sin^2((E_i/\hbar - \omega)t/2)}{\hbar^2(E_i/\hbar - \omega)^2}, \tag{5.10}$$

where the eigenenergies E_i of the states are measured with respect to the ground state energy. The validity of linear response requires the total excited state population at the conclusion of the Bragg perturbation to be small compared to unity:

$$\sum_{i\neq 0} |c_i(T_p)|^2 \ll 1. \tag{5.11}$$

Deep in the Mott regime the response of the system is dominated by the M excited states $|\Phi_i^{(1)}\rangle$. Because all these states have energies $E_i^{(1)}$ approximately given by U, the maximum transfer energy possible is of order U. The validity of linear response constrains the total imparted energy to be much less than U and the heating rate $\delta E/\delta t = U \sum_{i\neq 0} |c_i(t)|^2/t$ due to the Bragg perturbation to be much less than U/T_p.

It was previously shown that the M excited states $|\Phi_i^{(1)}\rangle$, have an energy spread given by $4J(2g + 1)\cos(qd/2)$ (Eq. (5.6)), and matrix elements given by: $|\langle \Phi_i^{(1)}|\hat{\rho}_q^\dagger|\Phi_0^{(1)}\rangle| \propto J\sin(qd/2)\sqrt{32g(g+1)}/U$, (Eq. (5.9)). The average separation between two consecutive states is of order $\Delta E \sim 4J(2g+1)\cos(qd/2)/M$. Individually resolving the different lines will require one to apply the Bragg pulse for a time of order

---

[1]Momentum spectroscopy requires that the pulse length does not exceed a quarter of the period of the magnetic trap used to experimentally confine the atoms[**?**]

$T_p^{(s)} \gtrsim Mh/(4J(2g+1)\cos(qd/2))$. The validity of linear response, Eq. (5.11), therefore requires that

$$V_0 \ll \frac{U}{M} \cot\left(\frac{qd}{2}\right).$$

(5.12)

For the parameters of Ref.[15], where ^{87}Rb atoms are trapped in a lattice of depth $18.5E_R$, the tunneling time h/J is about $0.1s$. The number of occupied wells is $M \sim 20$, with a filling factor $g \sim 1$. Resolving a single peak would require a Bragg pulse of duration $T_p^{(s)} \sim 0.2s$. With these conditions linear response is valid if $V_0 \ll 0.015 \cot(qd/2)E_R$. The acceptable heating rate is much less than $1.8E_R/s$.

If the duration of the applied perturbation is $T_p \leq T_p^{(s)}$, excited states will not be individually discernible. Near resonance ($\hbar\omega \approx U$), for pulse durations smaller than the inverse bandwidth: $T_p < T_p^{(e)}$, $T_p^{(e)} = h/(4J(2g+1)\cos(qd/2))$, all states will be resonantly excited. If $T_p \sim T_p^{(e)}$ the validity of linear response requires

$$V_0 \ll \frac{U}{\sqrt{M}} \cot\left(\frac{qd}{2}\right).$$

(5.13)

where the factor of $\sqrt{M}$, accounts for the contribution from all M excited states. For the parameters given above this inequality implies $V_0 \ll 0.07 \cot(qd/2)E_R$. Here, the acceptable heating rate is much less than $36E_R/s$.

We note that in the superfluid regime the uncorrelated nature of the system allows for a less stringent validity condition to hold: it is only required the amount of excited atoms to be small compared to the condensate population.

5.5   Finite temperature case

It is well known in the literature (see for example [95]) that in the superfluid regime, Bragg spectroscopy is not an appropriate tool for probing the temperature of the system. The reason is that even though $S(q,\omega)$ is temperature dependent, experimental observables such as the energy transfer depend on $\chi(q,\omega)$ which is very weakly temperature dependent. This is not the case deep in the Mott insulator regime. In a translationally invariant lattice all the 1-ph excitations have an energy separation of order U from the ground state and a splitting between them of order J. If the temperature is $k_BT \lesssim U/3$, it is still valid to restrict the Hilbert
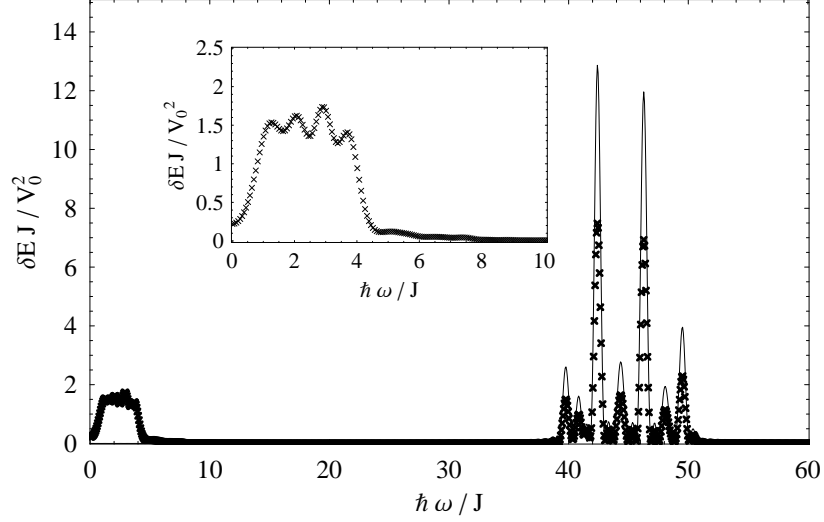
Figure 5.2: Energy transfer for a system at finite temperature. Solid line $k_B T/U = 0.007$, crosses $k_B T/U = 0.21$. The other parameters are the same as those in Fig.5.1

space to the one spanned by the 1-ph excitations. In this regime $\chi(q, \omega)$ (see Eq. (5.4)) can be written as:

$$\chi(q, \omega) = \frac{(1 - e^{-\beta U})}{\mathcal{Z}} \chi(q, \omega)|_{T=0} + \frac{1}{\mathcal{Z}} \chi^{ph}(q, \omega_{ij}) \tag{5.14}$$

$$\chi^{ph}(q, \omega_{ij}) \equiv \sum_{i,j>i} (e^{-\beta E_i^{(1)}} - e^{-\beta E_j^{(1)}})(f_q(\omega_{ij}) - f_{-q}(-\omega_{ij})) \tag{5.15}$$

where the sum runs over the states in the one particle-hole band, and $\mathcal{Z} \approx 1 + M(M + 1)e^{-\beta U}$. The

first term in Eq.(5.14), proportional to $\chi_q(\omega)|_{T=0}$, causes a thermal reduction of the zero temperature

response. The second term, which scales like $e^{-\beta U}\beta J/\mathcal{Z}$ [2], makes the system sensitive to low energy

Bragg perturbations at frequencies resonant with the energy difference between two 1-ph excitations. The

factor $e^{-\beta U}$ suppresses the observability of these thermal effects for $k_B T < U/5$.

In Fig. 5.2 we plot the energy transfer as a function of the Bragg frequency, as calculated from

exact diagonalization of the BHH for two different temperatures. The figure shows that for temperatures

$k_B T/U \gtrsim 1/5$ the height of the zero temperature peaks around U decreases, while low frequency peaks

appear. The presence of these low-frequency peaks is therefore a signature of finite temperature. In partic-

ular, if peaks around U are observed in absence of low frequency response, the temperature is lower than

$U/(5k_B)$. While this analysis does not provide a precise determination of the temperature, it is still useful

---

[2]Notice that due to the the zeroth order degeneracy of the $1 - ph$ subspace, $|\langle i| \hat{\rho}_q |j\rangle|^2 \sim 1$.

because it shows that Bragg spectroscopy is sensitive to temperatures of order of the interaction energy. Current experimental techniques do not provide any information on the scale of U. In fact, in current experiments temperature measurements rely on the analysis of atomic interference patterns after a certain time of flight following the release of atoms, and the measurement precision is of the order of the energy spacing to the second lattice band, which is typically one order of magnitude larger than U.

5.6   Final Remarks

In recent experiments [19], Bragg spectroscopy was performed using a setup where the Bragg momentum equals the lattice momentum and response was observed. Our present analysis, in agreement with previous ones ([35],[94]), predicts no response for $q = 2\pi/d$. Using similar perturbative techniques as the ones described here, we extended our calculation to inhomogeneous systems with a strong harmonic magnetic confinement. We also found no scattering for $q = 2\pi/d$ in these systems. The fact that neither the inhomogeneity nor the finite size of the system are responsible for the observed signal suggests that nonlinear effects are the most plausible explanation for the experimental results.

In summary, we have shown that Bragg spectroscopy can be a suitable experimental tool for characterizing the Mott insulator phase. By measuring the transfer energy at different Bragg momenta we proved it is possible to get information about the excitation spectrum: Bragg peaks are centered around the characteristic Mott excitation gap and are contained in an interval whose width is proportional to the 1-ph excitation band width. Their average height is maximized when the Bragg momentum approaches π/d. Finally looking at the low frequency response we showed that Bragg spectroscopy is sensitive to temperatures of order of the Mott gap.

Chapter 6

Finite temperature effects in the Mott insulator state.

We study the effects of finite temperature on ultracold atoms confined in an optical lattice plus a parabolic potential in the Mott insulator state, and we propose a novel method to estimate the system's temperature. The measurement we propose is based on molecular photo-association of atomic pairs, and is sensitive to finite temperature population of high energy states as well as zero-temperature mixing of high energy basis states into the ground state. Therefore, the measurement may be used both to determine temperature and to characterize the ground state of the system [15]. The temperature measurement is largely insensitive to the total number of atoms and may therefore be suited to calibrate experimental setups. Additional information on the total number of atoms can be extracted at sufficiently low temperatures.

6.1   Introduction

Great progress has been achieved in the coherent control and manipulation of ultracold atoms and molecules. In a series of recent experiments, several groups demonstrated the loading of an atomic Bose-Einstein condensate into the lowest vibrational level of single wells of an optical lattice [13, 19, 88]. In a remarkable experiment, M. Greiner *et al.*, [13], demonstrated a reversible quantum phase transition between a superfluid and an insulator state for bosonic atoms induced by varying the intensity of the trapping laser beams and therefore the depth of single potential wells. In a very recent experiment, the same group demonstrated an effective one dimensional superfluid/insulator transition, with on-site peak density equal to one [15] in an array of quasi one dimensional tubes. Several proposals suggest this system has potentially fundamental applications in the field of quantum computation, as the realized array of atoms in the insulating regime can be used to create an ideal register for qubits [21, 36, 51, 92, 96]. One of these proposals suggests a scheme which is robust at moderate finite temperatures, and is therefore potentially viable for practical implementations [51] .

Despite the achieved extreme system control, so far no *in-situ* techniques have been developed to

determine the temperature of an atomic ensemble loaded into the lattice. From the point of view of quantum computation, finite temperature can introduce errors in the register, that is empty or multiply occupied sites, and therefore a decrease in overall gate fidelities that must be corrected for only at the cost of overheads in computational resources and gate times. Current schemes for temperature measurements rely on the analysis of atomic interference patterns after a certain time of flight following the release of atoms from external confinements, in absence of the lattice. These schemes are highly unsatisfactory, as they require the destruction of the sample, provide no information on temperature changes due to loading of the lattice, do not work *in-situ*, and the measurement precision is on the order of the level spacing to the second lattice band, while the relevant energy scale in the lattice is the onsite interaction energy. The latter is typically at least one order of magnitude smaller than the lattice level spacing [11].

In this Chapter we analyze the effects of finite temperature on the Mott insulator state in presence of an external quadratic potential, and propose a method for estimating this temperature. In typical experiments, the quadratic potential is provided by a magnetic potential and is used to collect atoms at the center of the trap. The scheme requires the engineering of magnetic and optical potentials in such a way that multiple particle occupancy of single wells is suppressed and a certain number of sites at the center of the lattice has unitary filling [15, 92]. Under these conditions, multiple site occupancy is related to residual mixing of high energy basis states into the ground state at zero temperature [97, 98], and finite temperature population of high energy eigenstates. Below we show that molecular photo-association and statistics of ionization of atomic pairs can provide information on the creation of a zero temperature Mott state, while simultaneously they may be used to estimate the temperature of atoms in the trap for energies of the order of the onsite interaction energy. While we focus our attention on bosons in one dimensional lattices, results can be readily extended to higher dimensions.

6.2 The Mott insulator state

The Bose-Hubbard Hamiltonian describes the system's dynamics when the lattice is loaded such that only the lowest vibrational level of each lattice site is occupied [11]

$$H_{BH} = \sum_j \left[\epsilon(j) n_j - J(a_j^\dagger a_{j+1} + a_{j+1}^\dagger a_j) + \frac{U}{2} n_j(n_j - 1) \right]. \tag{6.1}$$

Here a_j is the bosonic annihilation operator of a particle at site j and $n_j = a_j^\dagger a_j$. The site-dependent $\epsilon(j)$ models an external magnetic quadratic potential, while J and U are the tunneling and on-site interaction energies respectively. For deep lattices with potential energy $V(x) = V\cos^2(kx)$, the tunneling energy is approximated by $J = 4/(\sqrt{\pi})E_R(V/E_R)^{3/4}e^{-2\sqrt{V/E_R}}$, where $E_R = (\hbar k)^2/2m$ is the recoil energy, k the light wave vector, and m the atomic mass. The on-site interaction energy is due to ground state collisions between atoms each in the motional state $\phi(\mathbf{x})$ and is given by $U = \frac{4\pi a_s \hbar^2}{m} \int d\mathbf{x} |\phi(\mathbf{x})|^4$, with a_s the s-wave scattering length and $\phi(\mathbf{x})$ a Wannier state. J and U are assumed to be site independent [11].

For a homogeneous lattice ($\epsilon(j) = 0, \forall j$) of M sites at zero temperature T, an insulating state, the *Mott state*, occurs only if the number of particles N equals M and the interaction energy dominates over the tunneling energy. If $\sqrt{N}J/U \ll 1$ the ground state has approximately energy $E_g = -4NJ^2/U$ and is given by

$$|\Psi_g\rangle = \alpha(|T\rangle + 2\sqrt{N}J/U|S\rangle), \tag{6.2}$$

where the normalization constant is $\alpha = (1 + 4N(J/U)^2)^{-1/2}$. The Fock state $|T\rangle = \Pi_{j=1}^N a_j^\dagger |0\rangle$ has one particle per site and zero energy, and the symmetrized state $|S\rangle = 1/\sqrt{2N}\sum_{j=1}^N (a_j^\dagger a_{j+1} + a_{j+1}^\dagger a_j)|T\rangle$ has energy U. Indeed, in the homogeneous system all Fock states with an empty site and an atomic pair in another site are degenerate with energy U. The latter is roughly the lowest excitation energy for the many-body system in the homogenous commensurately filled case [12].

The probability of creating exactly $N = M$ particles in an experiment is negligible. An insulator state can be recovered if an external quadratic potential is present. Then, $\epsilon(j) = \Omega j^2$ where $\Omega = m/2(\pi/k)^2\omega_T^2$ is a characteristic energy scale for a trap of frequency ω_T. At $T = 0$, a Mott state with average occupation one in the center of the trap can be realized for $\sqrt{N}J/U \ll 1$ if

$$N < M, U > \epsilon((N-1)/2), \Omega N > J. \tag{6.3}$$

The last two inequalities insure that multiple particle occupancy and tunneling of holes from the borders to the center of the lattice are suppressed, respectively [92]. The first inequality in Eq. 6.3 simply states the number of wells be larger than the number of atoms. As a consequence, there are $M!/((M - N)!N!)$ Fock states with maximal on-site occupation one, at variance with the single state of the case $N = M$. In presence of the trap these states are not degenerate, spanning an energy range which may be larger than U. We redefine as $|T\rangle = \Pi_{j=-(N-1)/2}^{(N-1)/2} a_j^\dagger |0\rangle$ the lowest energy state and set its energy to zero [99]. The state $|T\rangle$ is the ground state of the system to zeroth order in J, while the true ground state has coherences due to tunneling of a hole in either one of sites $\pm(N - 1)/2$ and mixing of Fock states $|S_{n,m}\rangle = a_n^\dagger a_m |T\rangle/\sqrt{2}$ with an atomic pair and a hole at sites n and m respectively, with $n, m < |(N - 1)/2|$, in analogy to the homogeneous case. States $|S_{n,m}\rangle$ are not degenerate, due to the trap presence. States $|S_{n,m}\rangle$ with $m = n \pm 1$ dominate the mixing into the ground state, and for $\Omega \ll U$ the amplitude of mixing approaches the homogeneous system's one $\sqrt{2}\alpha J/U$.

In general, the $|T\rangle$-state is coupled *via* the BH-Hamiltonian to $|S_{n,m}\rangle$-states with a matrix element of order $(J/U)^{|n-m|}$, which is negligible for $|n - m|$ large enough in the insulating regime. On the other hand, a temperature of the order of the energy difference between $|T\rangle$ and $|S_{n,m}\rangle$-states allows for population of the latters. In particular, the lowest energy Fock state $|S_{n,m}\rangle$ has two particles in the central site of the lattice and a hole at site $|(N - 1)/2|$. Its energy is $\Delta = U - \epsilon((N - 1)/2)$.

We propose to utilize a measurement scheme which is selectively sensitive to the presence of atomic pairs in the lattice and to determine the temperature through statistics of positive detection of atomic pairs. While in principle any measurements sensitive to atomic pairs may be used, we propose to collect statistics of atomic pairs through resonant photo-association of two atoms in a single well to a molecular excited state, followed by ionization of the formed molecules and detection of the emitted ions, as the latter can be performed with high efficiency. The molecular excited state should be chosen to be far from atomic dissociation, meaning that the atomic probability of spontaneous emission is not enhanced by the photo-associative laser. We show that in the appropriate parameter regime the density distribution of atomic pairs, which is proportional to the experimental probability of pair detection, has a Gaussian profile as a function of the position in the lattice. The width of the profile solely depends on the temperature and on the known trap

geometry. Moreover, the height of the distribution peak at low temperatures provides direct information on the energy Δ and therefore on the number of particles N.

6.3   Effective single-particle spectrum

Neglecting for a moment mixing of $|S_{n,m}\rangle$-states in low lying modes, a Gaussian profile for the density distribution of an atomic pair as a function of the position in the lattice at finite temperature T can be expected for the following argument. Given a lattice with M wells, $N = M + 1$ particles and $U \gg J$, the ground state has roughly one particle per site and an extra particle at the center of the trap, forming an atomic pair. For weak enough quadratic traps, $\Omega \ll J$, tunneling of the extra particle is not suppressed over a certain number of lattice sites at the center of the trap where the external potential is essentially flat, meaning that the atomic pair acts approximately as a conventional harmonic oscillator with *effective* mass $m_* = 1/(4J)$ and trapping frequency $\omega_* = 2\sqrt{2\Omega J}$. Here lattice constant π/k and $\hbar = h/2\pi$ have been set to unity, where h is Planck constant. The tight binding spectrum is therefore approximated by an harmonic oscillator spectrum whose level spacing is ω_* with an error of order $O(\Omega/J)$. If $T > \omega_*/k_B$, it can be shown that the quantum density distribution $P(j)$ for the atomic pair, which is proportional to the probability for pair detection at site j, becomes equivalent to the classical distribution which is proportional to

$$P(j) \propto e^{-\beta m_* \omega_*^2 j^2 /2} = e^{-\beta \Omega j^2} \tag{6.4}$$

where $\beta = 1/(k_B T)$, and k_B is Boltzmann constant. The distribution $P(j)$ as a function of lattice site j, Eq. 6.4, is therefore a Gaussian whose width is $x_0 = \sqrt{1/(2\beta\Omega)}$.

Harmonic oscillator states actually approximate the incomplete basis set defined on the central N sites of the lattice in the energy range $\Delta \lesssim E \ll 3U - 2\epsilon((N-1)/2)$, where $3U - 2\epsilon((N-1)/2)$ is a characteristic energy for population of states with two extra particles in one of the the central $N - 2$ sites. Apart of a normalization factor, we therefore expect that the density distribution as a function of the position j in the lattice has the same Gaussian profile as in Eq. 6.4 with an exponential suppression due to

the energy shift Δ

$$P(j) \propto e^{-\beta\Delta}e^{-\beta\Omega j^2}. \tag{6.5}$$

The width x_0 of the density distribution can be therefore directly related to the temperature of the sample, while the height of the peak is an indication of Δ, and therefore of the number of particles N. We expect the width to be an accurate measure of temperature for $k_B T \lesssim \Delta$. In fact, while for a temperature of order Δ states are populated with more than one pair in the central sites, the various pairs approximately behave like non-overlapping harmonic oscillators, meaning that the probability of finding two extra particles in the same site is strongly suppressed. In the language of Chapters 3 and 4, these extra particles are fermionized. Therefore, the density distribution at a single site should still approximately maintain a Gaussian profile of width x_0. On the other hand, the height of the Gaussian depends on the normalization. We expect Eq. 6.5 to well approximate the value of the density peak for $k_B T \ll \Delta$, where the overall normalization is approximately one.

6.4   Numerical simulations

We perform numerical simulations of the density distribution of atomic pairs in the lattice as a function of temperature for some realistic experimental parameters. We employ a quantum Monte-Carlo code based on the continuous-time Worm algorithm [30]. A sample of $N = 101$ atoms of ^{87}Rb is trapped in a lattice with wavelength $\lambda = 785$ nm and parallel and transverse confinements $V_\parallel = 15E_R$ and $V_\perp = 40.5E_R$ respectively. Using $a_s = 5.6$ nm, the interaction energy in frequency units is $U/h = 3.340$ kHz and $U/J = 120$. The external magnetic trapping frequency is $\omega_T \approx 2\pi \times 40$ Hz and therefore the number of atoms N fixes $\epsilon(N-1)/2 \approx 0.8U$, $\Delta \approx 24J$. We have chosen these parameters because they are experimentally feasible and satisfy Eq. 6.3, so that at zero temperature a Mott state is formed with one particle occupying each one of the central N sites of the lattice. In particular, zero temperature mixing of basis states with an empty site in one of the central N sites of the lattice is suppressed, the largest amplitude of mixing corresponding to the outer most trapped particle tunneling to the adjacent empty site. Calculations have been performed for $M \gg N$, so that atoms never reach the border of the lattice.
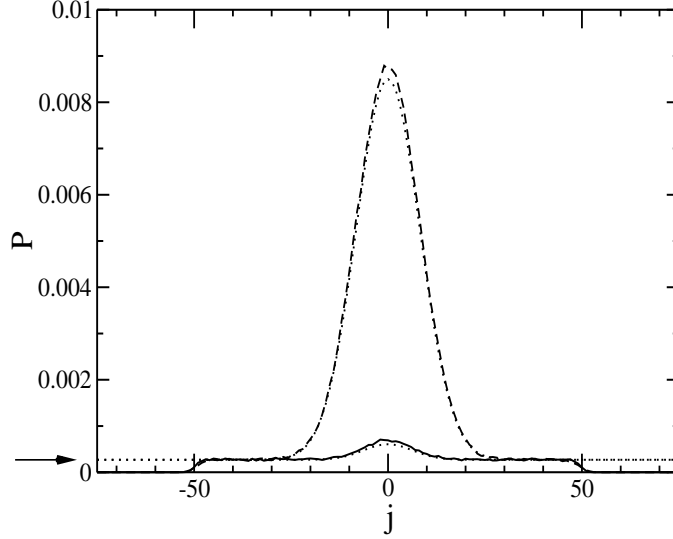
Figure 6.1: Density distribution of atomic pairs P as a function of lattice index j. Continuous and dashed lines are numerical results for $T = 3J/k_B$ and $T = 5J/k_B$ respectively. Dotted lines are analytical curves for the same temperatures. The arrow indicates the zero-temperature mixing of $|S_{n,n\pm1}\rangle$-states. Here $N = 101, U/J = 120, \Omega/J = 0.0374226$, and $\Delta/J = 24$.

In Fig. 6.1 the atomic pair density distribution P is plotted as a function of site index j for $Tk_B/J = 3$ and 5. Continuous and dashed lines are numerical results, while dotted lines are analytical curves. For $Tk_B/J = 3$, lower curves, the numerical solution shows essentially a flat density distribution throughout the central N sites, with a shallow gaussian peak at the center. The flat distribution corresponds to the zero temperature residual mixing of $|S_{n,n\pm1}\rangle$-states into the ground state, characteristics of the Mott state. As $\Omega \ll U$, corrections to the density distribution due to the external trapping potential are not distinguishable on the scale of the graph, and the on-site density matches the homogeneous system's value $2 \times 2(J/U)^2 \approx 0.000278$. The factor of two in front of last expression is due to the fact that the extra atom can tunnel from the left or right. The latter constant has been added to the analytic curves, and is indicated by an arrow in Fig. 6.1. Finite atomic pair density due to zero-temperature mixing of $|S_{n,n\pm1}\rangle$-states is a direct signature of the creation of a Mott state. For sufficiently low temperatures, selective probe of the density distribution in lattice sites j with $j \gg x_0$ can give direct *in situ* evidence of the formation of the Mott plateau in the center of the trap, while the shallow peak around $j = 0$ measures finite temperature population of $|S_{n,m}\rangle$-states.

For $Tk_B/J = 5$ the Gaussian peak is more evident on the scale of the graph. We observe that
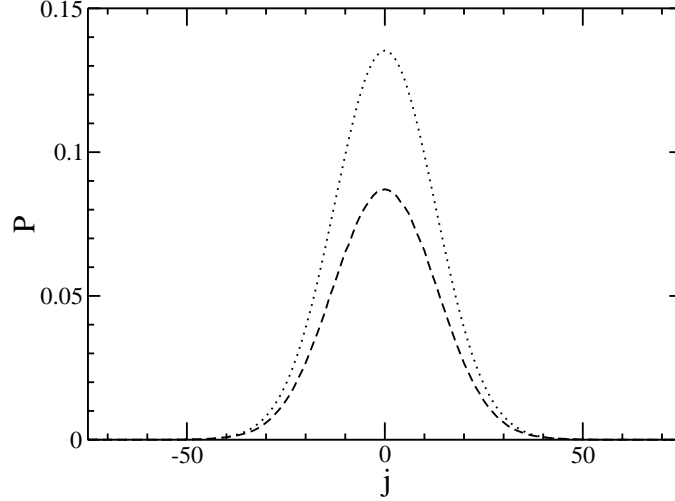
Figure 6.2: Density distribution of atomic pairs P as a function of lattice index j, for $T = 12J/k_B$. Dashed and dotted lines are numerical and analytical results respectively. Here $N = 101$, $U/J = 120$, $\Omega/J = 0.0374226$, and $\Delta/J = 24$.

numerical and analytical curves nearly overlap. In particular, the widths of the Gaussians perfectly match, while the height of the peak is slightly underestimated by the analytic curve. This is due to the fact that $U - \epsilon((N-1)/2)$ is only approximately Δ for the chosen parameters, and the difference is amplified by the exponential function. Moreover, the Monte-Carlo code fixes the chemical potential, meaning N is actually an average value in the numerics. A larger disagreement in the peak height is observable for $k_B T/J = 12$ in Fig. 6.2, where the analytic curve largely overestimates the exact result. This is expected, as for higher temperatures the normalization constant differs more and more from one, therefore suppressing the peak height in the exact solution.

In Fig. 6.3 the width x_0 is plotted against the temperature, up to $T = \Delta/k_B$. Circles are numerical results, while the continuous line is the analytic solution $\sqrt{k_B T/(2\Omega)}$. The plot shows a good agreement between numerics and analytical results for $k_B T \lesssim \Delta/4$. Deviation for higher temperatures is due to population of states with a large number of atomic pairs.

Provided inequalities in Eq. 6.3 are satisfied for each experiment given the uncertainties on the number of atoms, accurate calibration of average system's temperatures may be performed by accumulating statistics of pair detection on successive experiments with the same trapping potentials, as x_0 is insensitive
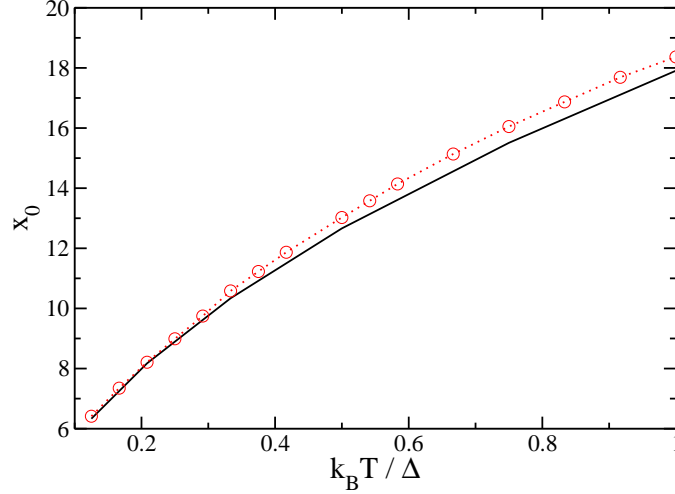
Figure 6.3: Width x_0 of the density distribution of atomic pairs as a function of $k_B T/\Delta$. The width x_0 is in units of the lattice constant. Circles(red) are numerical values, while the continuous line is the analytic curve $(k_B T/2\Omega)^{1/2}$. Here $N = 101$, $U/J = 120$, $\Omega/J = 0.0374226$, and $\Delta/J = 24$.

to N. Information on temperature in a single experiment may be extracted by taking ratios $P(j)/P(0)$ of molecular photoassociation probabilities on different lattice locations.

In typical experimental setups it is not possible to focus a photoassociative laser onto a single site. In fact, the intensity of the photoassociative laser has a Gaussian profile whose width is typically on the order of the light's wavelength, meaning the laser intensity may not be negligible on few lattice sites, depending on the ratio between the wavelength of the photoassociative laser and the lattice spacing. The collected stastistics of atomic pair detection should then be appropriately averaged over a few lattice sites.

6.5   Summary

In summary, we have studied the effects of temperature on the Mott insulator state, and proposed a method to estimate the temperature of ultracold bosons trapped in deep lattices. The proposed method is largely insensitive to total particle numbers, possibly making it a viable tool for the calibration of experimental setups. While we focused on one dimensional systems, the above treatment can be readily generalized to higher dimensions.

Chapter 7

Scalable register initialization for quantum computing in an optical lattice

The Mott insulator state created by loading an atomic Bose-Einstein condensate (BEC) into an optical lattice may be used as a means to prepare a register of atomic qubits in a quantum computer. Such architecture requires a lattice commensurately filled with atoms, which corresponds to the insulator state only in the limit of zero inter-well tunneling. We show that a lattice with spatial inhomogeneity created by a quadratic magnetic trapping potential can be used to isolate a subspace in the center which is impervious to hole-hoping. Components of the wavefunction with more than one atom in any well can be projected out by selective measurement on a molecular photo-associative transition. Maintaining the molecular coupling induces a quantum Zeno effect that can sustain a commensurately filled register for the duration of a quantum computation.

7.1   Introduction

In the past decade, tremendous progress has been made creating and manipulating macroscopic quantum states of atoms in Bose-Einstein condensates [100]. Concurrently, experiments have achieved precise control of a small number ($<$ 10) of interacting atoms and demonstrated entangling operations between them [101]. A potential application that marries atomic control on the large and small scale is the implementation of quantum computation with neutral atoms. Building a scalable quantum computer requires the initialization of a many body system to a simple fiducial state with well characterized qubits [24]. Ultimately, this must be done by either allowing the system to naturally cool to its ground state, or performing a suitable projective measurement of the system.

Several years ago the loading of an optical lattice from an atomic BEC was proposed [11]. If one begins with a superfluid-like BEC and adiabatically turns on a lattice potential, the system experiences a phase transition to the Mott insulator (MI) state. This many body state is characterized by the same number of atoms in each lattice well and is the ground state when the intra-well interaction energy is much greater

than the inter-well tunneling [12]. Recent experiments [13] have demonstrated the Mott insulator phase transition in a magnetically confined optical lattice, with an average filling factor of two atoms per well. In this chapter we demonstrate that the many body ground state of atoms in an optical lattice contains intrinsic number fluctuations that make it an imperfect register. We show how this can be corrected in two steps, first by introducing an inhomogeneity to the lattice using a quadratic trapping potential and second by selective measurement of atomic pairs. This strategy allows the MI transition to become a robust mechanism for register initialization.

Homogeneous system

A key advantage of loading an optical lattice from a BEC is the availability of an initially high phase space density which can be frozen to the MI state with atoms occupying every lattice site. When the lattice is loaded such that only the lowest vibrational state of each lattice well is occupied, the system is well described by the Bose-Hubbard Hamiltonian:

$$H_{BH} = \sum_j \epsilon(j) n_j - J(a_j^\dagger a_{j+1} + a_{j+1}^\dagger a_j) + \frac{U}{2} n_j(n_j - 1) \tag{7.1}$$

Here a_j are the bosonic annihilation operators and $n_j = a_j^\dagger a_j$ the number operators for an atom in the lowest vibrational state of lattice well j. The energy offset at each lattice site is $\epsilon(j)$ which models a continuously varying external potential. The energies J and U are the tunneling and on-site interaction energies respectively. In the tight-binding model, the nearest neighbor tunneling energy J is defined as one fourth the band width of the lowest occupied band. For tunneling through a potential barrier given by $V(x) = V \cos^2(kx)$, the tunneling rate is closely approximated by [57] $J/\hbar = 4/(\sqrt{\pi}\hbar) E_R (V/E_R)^{3/4} e^{-2\sqrt{V/E_R}}$, where the recoil energy is $E_R = (\hbar k)^2/2m$ (m=atomic mass). The on-site interaction is a result of the ground state collisions described by the s-wave scattering length a_s between two atoms each in the motional state $\phi(\mathbf{x})$ and is given by $U = \frac{4\pi a_s \hbar^2}{m} \int d\mathbf{x} |\phi(\mathbf{x})|^4$.

For the homogeneous system ($\epsilon(j) = 0 \ \forall j$) of fixed extent, the behavior of the system is uniquely described by the ratio U/J which decreases exponentially with the trap depth V. While our results are applicable to higher dimensions, henceforth we assume a three dimensional lattice with tight transverse confinement and tunneling dynamics along one dimension only. For the homogeneous system, only com-

mensurate fillings give rise to a MI transition. For the homogeneous lattice with M lattice sites, which is filled with a number of atoms whose variance is $\Delta N \gg M$, the ground state of the system has a probability of approximately $1/M$ of being commensurately filled. Therefore this is not a robust mechanism for initializing a quantum computer. However, one should note that an adiabatic transfer mechanism between two sublevels of each atom may be used to fix nonuniform filling [36]. A caveat is that even with unit filling, the MI state still carries small but non-zero number fluctuations which provide a small residual coherence across the system that scales as the number of trapped atoms [97, 98]. Applying first order perturbation theory in H_{BH}, the ground state for N atoms in M wells in one dimension with $N = M$ is approximately

$$|\Psi_g\rangle = \alpha(|T\rangle + 2\sqrt{N}J/U|S\rangle), \tag{7.2}$$

where the normalization constant is $\alpha = (1 + 4N(J/U)^2)^{-1/2}$. Here the unit filled target state is $|T\rangle = \prod_{j=1}^{N} a_j^\dagger |0\rangle$ and the symmetrized state, assuming periodic boundary conditions ($j + M \equiv j$), is $|S\rangle = 1/\sqrt{4N} \sum_{j=1}^{N} (a_{j+1}^\dagger a_j + a_j^\dagger a_{j+1})|T\rangle$. The energy of the ground state is approximately $E_g = -4NJ^2/U$.

7.1.1 The protocol

We propose to use an inhomogeneous lattice with open boundaries created by a weak quadratic magnetic trap that acts to collect atoms near the center of the trap and leaves empty wells (holes) at the edges. For our analysis we assume a one dimensional optical lattice, with $N < M$ [102], in the presence of a weak magnetic trap with oscillation frequency ω_T. The characteristic trap energy scale $\Omega = m/2(\pi/k)^2\omega_T^2$ is defined so that $\epsilon(j) = \Omega j^2$. We stipulate that the on site interaction energy be larger than the trapping energy of the most externally trapped atom, or $U > \epsilon((N-1)/2)$, in order to inhibit multiple atom occupation in any well. The register is defined by a physical subspace $\mathcal{R}$ comprising a number of wells $K < N$ in the center region of the trap. The barrier space flanking $\mathcal{R}$ will act to suppress percolation of holes from the edges to the center. The estimated probability for holes in $\mathcal{R}$ due to tunneling through the barrier is $p_h \approx \prod_{j=(K-1)/2}^{(N+1)/2} (J/\Omega(2j+1))^2 = (J/2\Omega)^{N-K+4}(\Gamma[K/2]/\Gamma[N/2+1])^2$, which is negligible provided the barrier region is sufficiently large and $J/K\Omega < 1$.

When expanded in the Fock state basis, the ground state of the register has amplitude in those states with holes neighboring atomic pairs, analogous to the homogeneous case. We describe a protocol

which projects out these components by a null result from selective measurement of atomic pairs within any lattice site. This measurement detects population on an excited molecular state and can be made with high efficiency. Once the unit filled state is reached with high confidence, continuing the measurement will maintain this state.

The measurement will map the register from the ground state $|\Psi_g\rangle$ to the unit filled target state which is not an eigenstate of H_{BH}. To describe the dynamics in the register during the measurement, it is convenient to use the following incomplete basis over $\mathcal{R}$:

$$|T\rangle = \prod_{j=-(K-1)/2}^{(K-1)/2} a_j^\dagger |0\rangle, |S_j^+\rangle = \frac{a_j^\dagger a_{j+1}}{\sqrt{2}} |T\rangle, |S_j^-\rangle = \frac{a_{j+1}^\dagger a_j}{\sqrt{2}} |T\rangle. \tag{7.3}$$

For each j the states $|S_j^\pm\rangle$ are distinguished by the two energetically distinct orientations of an atomic pair and its neighboring hole with energies, $E(S_j^\pm) = U(1 \mp \frac{\Omega}{U}(2j-1))$. The target state $|T\rangle$ defines the zero of energy. The $|T\rangle$ and the $|S_j^\pm\rangle$ states are coupled to first order in H_{BH} and they span the reduced state in $\mathcal{R}$ of the ground state of the total system.

In the limit of large K, the dynamics of the register is restricted to the basis of Eq. 7.3. This argument is understood by comparison to the dynamics in the homogeneous system. In the latter, the state with the largest coupling from the target state is the symmetrized $|S\rangle$ with coupling matrix element $\langle T|H_{BH}|S\rangle = -2\sqrt{K}J$. The state $|S\rangle$ itself couples to a symmetrized state $|S'\rangle$ of all Fock states with a one site separation between the atomic pair and the hole: $|S'\rangle = 1/\sqrt{4K} \sum_j (a_j^\dagger a_{j+2} + a_{j+2}^\dagger a_j)|T\rangle$. The coupling between these states is $\langle S'|H_{BH}|S\rangle = -3J$. The dynamics on time scales $t < 1/J$ are therefore constrained to the subspace $\{|T\rangle, |S\rangle\}$ when $K \gg 1$. In the inhomogeneous case, the degeneracy is absent between states with neighboring pairs and holes, $\{|S_j^\pm\rangle\}$ and states where pairs and holes are separated. Hence, the coupling to states outside the restricted subspace can only be smaller than in the homogeneous case.

7.1.2   The measurement

For the measurement, we choose a catalysis laser that is on resonance from the ground state of two atoms in a single well to a bound state ν of a dipole-dipole coupled molecular $S + P$ state. The bound state is chosen such that the catalysis laser is far off resonance from other bound states and repulsive
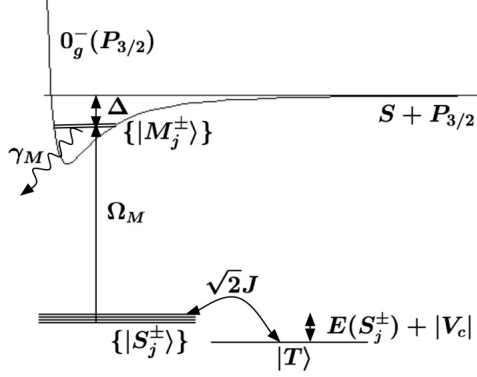
Figure 7.1: Schematic of the relevant couplings in the problem. The unit filled state $|T\rangle$ describing a target quantum register and the states $|S_j^\pm\rangle$ having one doubly occupied lattice site and a neighboring hole are coupled to first order in H_{BH}. A catalysis laser resonantly couples the ground states $|S_j^\pm\rangle$ to the excited states $|M_j^\pm\rangle$ describing a bound molecule at the doubly occupied site. The bound states quickly decay and give the possibility of monitoring population in the "faulty" register states $|S_j^\pm\rangle$.

potentials, see Fig.7.1. For our many body system, we adopt the set of many body states $\{|M_j^\pm\rangle = (1/\sqrt{2})b^\dagger_{j+(1\mp1)/2}a^2_{j+(1\mp1)/2}|S_j^\pm\rangle\}$, where $b^\dagger$ is the creation operator for a molecule in the bound state ν. These states describe $K-2$ atoms trapped in the lattice and a single molecule at site $j+(1\mp1)/2$, with dipole-dipole coupling energy $\langle M_j^\pm|H_{dd}|M_j^\pm\rangle = \hbar\omega_\nu$. The free atomic Hamiltonian for K atoms is $H_A = \sum_j \hbar\omega_{eg}|e_j\rangle\langle e_j|$ where $|e_j\rangle(|g_j\rangle)$ denotes the excited(ground) state for an atom at site j. The "bare" energy Hamiltonian H_0 including coupling in the restricted basis of H_{BH} is then:

$$
\begin{aligned}
H_0 &= H_A + H_{dd} + H_{BH} \\
&= \hbar\omega_{eg}\sum_j|e_j\rangle\langle e_j| + \sum_{j,\pm}E(S_j^\pm)|S_j^\pm\rangle\langle S_j^\pm| \\
&\quad +(\hbar\omega_\nu + E(S_j^\pm) - U)|M_j^\pm\rangle\langle M_j^\pm| - \sqrt{2}J\sum_{j,\pm}(|S_j^\pm\rangle\langle T| + |T\rangle\langle S_j^\pm|),
\end{aligned}
\tag{7.4}
$$

Under the atom laser interaction, H_{AL}, the ground and excited state of each atom is coupled as is each many body state $|M_j^\pm\rangle$ and its corresponding ground state $|S_j^\pm\rangle$. In the rotating wave approximation, the interaction is:

$$
H_{AL} = \frac{\hbar\Omega_A}{2}\sum_j(e^{-i\omega_L t}|e_j\rangle\langle g_j| + h.c.) + \frac{\hbar\Omega_M}{2}\sum_{j,\pm}(e^{-i\omega_L t}|M_j^\pm\rangle\langle S_j^\pm| + h.c.),
\tag{7.5}
$$

where $\Omega_{A(M)}$ are the atomic (molecular) Rabi frequencies, related by $\Omega_M = \sqrt{F_\nu}\Omega_A$, and F_ν is the Franck-Condon factor equaling the spatial overlap between the relative coördinate wavefunction describing

two ground electronic state atoms trapped in a single lattice well and the molecular bound state ν. For bound states of interest, such as the long range bound states of the $0_g^-\,(P_{3/2})$ potential [103], the catalysis detuning from *atomic* resonance, $\Delta = \omega_L - \omega_{eg}$, is several thousands linewidths meaning the atomic saturation is low $s_A = (\Omega_A^2/2\Delta^2) \ll 1$. In this case, the excited atomic states can be adiabatically eliminated and each atom in a singly occupied well experiences a light shift equal to $V_c = \Delta s_A/2$. There are K singly occupied wells in the $|T\rangle$ state and the total single atom light shift is therefore equal to KV_c. The $|S_j^\pm\rangle$ states have $K - 2$ singly occupied wells giving a corresponding light shift of $(K - 2)V_c$. The differential *single atom* light shift between these states is then $2|V_c|$. The total Hamiltonian $H_0 + H_{AL}$ in the rotating frame is,

$$
\begin{aligned}
H_I \;=\; & \sum_{j,\pm}((2|V_c| + E(S_j^\pm))|S_j^\pm\rangle\langle S_j^\pm|) + (2|V_c| + E(S_j^\pm) - U)|M_j^\pm\rangle\langle M_j^\pm| \\
& -\sqrt{2}J(|S_j^\pm\rangle\langle T| + |T\rangle\langle S_j^\pm|) + \tfrac{\hbar\Omega_M}{2}(|M_j^\pm\rangle\langle S_j^\pm| + |S_j^\pm\rangle\langle M_j^\pm|)).
\end{aligned}
\tag{7.6}
$$

Any population in the bound molecular states will decay at a rate $\gamma_M \approx 2\Gamma$, where Γ is the single atom decay rate. For molecular photo-association by red detuned light, the decay products are typically ground state molecular species or "hot" atoms meaning the atoms escape the trapped ground states described by Eq. 7.3. We therefore model the system according to a trace non-preserving master equation:

$$
\dot{\rho} = -i[H_I, \rho]/\hbar - \gamma_M/2 \sum_{j,\pm}(|M_j^\pm\rangle\langle M_j^\pm|\rho + \rho|M_j^\pm\rangle\langle M_j^\pm|).
\tag{7.7}
$$

We have ignored spontaneous emission due to decay from the single atom excited states at a rate $s_A\Gamma \ll \Gamma$ per atom. For time scales $1/\gamma_M \ll t \ll \hbar/(U + 2|V_c|)$, the excited state coherences can be solved for. To second order in $U/\hbar\gamma_M, 2|V_c|/\hbar\gamma_M$ they are

$$
\begin{aligned}
\rho_{M_j^\pm,T}(t) \;&=\; -i\frac{\Omega_M\gamma_M/4}{[(2|V_c|+E(S_j^\pm)-U)/\hbar]^2+(\gamma_M/2)^2}\rho_{S_j^\pm,T}(t) \\
\rho_{M_j^\pm,M_j^\pm}(t) \;&=\; \frac{\Omega_M^2/4}{(U/\hbar)^2+(\gamma_M/2)^2}\rho_{S_j^\pm,S_j^\pm}(t) \\
\rho_{M_j^\pm,S_j^\pm}(t) \;&=\; -i\frac{\Omega_M\gamma/4}{(U/\hbar)^2+(\gamma_M/2)^2}\rho_{S_j^\pm,S_j^\pm}(t).
\end{aligned}
\tag{7.8}
$$

Inserting these expressions back into the equations for the dynamics in the ground state we have

$$
\begin{aligned}
\dot{\rho}_{S_j^\pm,T} \;&=\; -i(E(S_j^\pm) + 2|V_c|)\rho_{S_j^\pm,T}/\hbar + i\sqrt{2}J(\rho_{T,T} - \rho_{S_j^\pm,S_j^\pm})/\hbar \\
& \quad -\frac{\Omega_M^2\gamma_M/8}{[(2|V_c|+E(S_j^\pm)-U)/\hbar]^2+(\gamma_M/2)^2}\rho_{S_j^\pm,T} \\
\dot{\rho}_{T,T} \;&=\; i\sqrt{2}J\sum_{j,\pm}(\rho_{S_j^\pm,T} - \rho_{T,S_j^\pm})/\hbar \\
\dot{\rho}_{S_j^\pm,S_j^\pm} \;&=\; -i\sqrt{2}J(\rho_{S_j^\pm,T} - \rho_{T,S_j^\pm})/\hbar - \frac{\Omega_M^2\gamma_M/4}{(U/\hbar)^2+(\gamma_M/2)^2}\rho_{S_j^\pm,S_j^\pm}.
\end{aligned}
\tag{7.9}
$$

These equations describe the Bose-Hubbard coupled states with a decay in population of each state with an atomic pair at a rate $2\kappa = \Omega_M^2 \gamma_M / (4((U/\hbar)^2 + (\gamma_M/2)^2)$, and decay of coherences between each of these states and state $|T\rangle$ at a rate κ.

This type of evolution characterized by measurement induced phase damping was studied extensively by Gagen and Milburn [104]. We now show that our system can satisfy the conditions for this effect and in particular can be driven to the $|T\rangle$ state by monitoring the environment for a signature of decay from the molecular bound state.

For the inhomogeneous system, the state $|T\rangle$ couples to $2K$ distinguishable states $|S_j^{\pm}\rangle$. However, we can define an effective Rabi frequency between the state $|T\rangle$ and the subspace spanned by $\{|S_J^{\pm}\rangle\}$. This frequency is close to the coupling matrix element between the state $|T\rangle$ and the state $|S\rangle$ in the homogeneous system, namely $2\sqrt{K}J$. The coherences between the two subspaces decay at a rate κ, and the population in the subspace $\{|S_j^{\pm}\rangle\}$ decays at a rate 2κ. The "good" measurement regime as derived in [104] is then:

$$\Omega_M/\gamma_M \ll 1 < \hbar\kappa/2\sqrt{K}J. \tag{7.10}$$

The left side inequality ensures that the excited states $|M_j^{\pm}\rangle$ are weakly populated (equivalent to the condition for adiabatic elimination of these states). The right side inequality ensures that measurement is sufficiently strong to damp coherences on the time scale that they develop due to tunneling.

The limiting quantity that determines the decay rate of the weakly saturated molecular states and hence the measurement strength is the Franck-Condon factor F_ν. It is calculated for bound-bound transitions using the reflection approximation of Julienne [105] where we solve for the ground state relative coördinate wavefunction for two atoms in a lattice well using a pseudo potential appropriate for ^{87}Rb. We choose to couple to the $\nu = 17$ bound state of the $0_g^-(P_{3/2})$ potential which is at an energy $\Delta = -6.85 \times 10^4 \Gamma$ from dissociation. For a lattice with wavelength 785 nm and transverse and parallel confinements $V^{\perp} = 38.5 E_R$, $V^{||} = 22 E_R$, the result is $F_\nu \approx 5 \times 10^{-7}$. Given this confinement, the on-site interaction using $a_s = 5.6$ nm is $U/h = 3.574$kHz. Choosing an experimentally reasonable atomic Rabi frequency $\Omega_A = 25\Gamma$, where $\Gamma = 2\pi \times 6.065$MHz, we find $\kappa \approx 0.13 U/h$. Here the atomic scattering due to the catalysis laser is $s_A \Gamma \approx 6.7 \times 10^{-8} \Gamma$ per atom and the off resonant light shift is $|V_c| = 3.87U$.

By way of example we define a one dimensional register $\mathcal{R}$ with 501 atoms that resides inside a
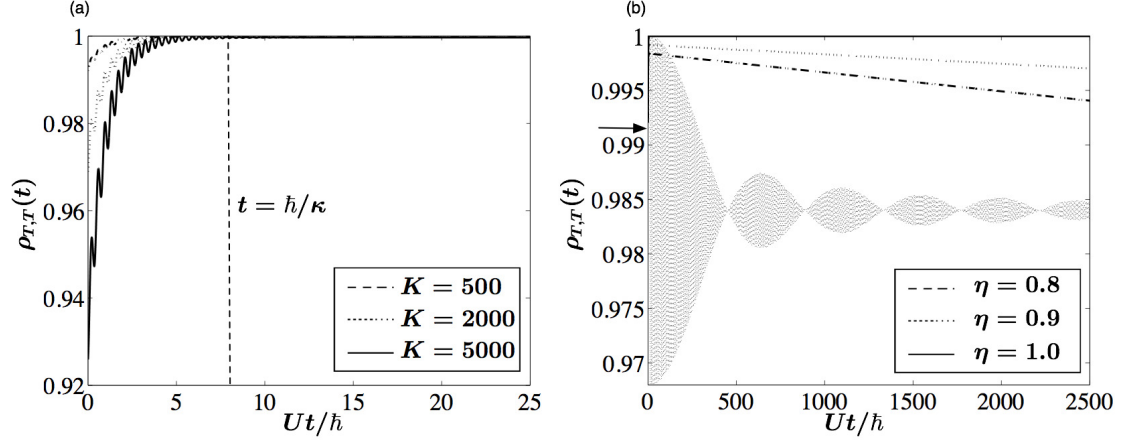
Figure 7.2: Population in the unit filled register state $|T\rangle_{\mathcal{R}}$ during continuous measurement of the register beginning in the Bose-Hubbard ground state $|\Psi_g\rangle$. The plots show dynamics appropriate to tunneling in one dimension with $U/J = 500$. (a) Quantum trajectories corresponding to a null measurement result for three different register sizes K. The time scale to saturate the target state is independent of the number of qubits: $t_{sat} \approx 1/\kappa$. (b) Long time dynamics for $K = 501$, $N = 551$ and finite detector efficiencies η. The population in $|T\rangle_{\mathcal{R}}$ for $\eta = 1$ is indistinguishable from one. Also shown is the oscillatory dynamics at fundamental frequency $U/\hbar$ described by Eq. 7.13 if the measurement is turned off after the target state is reached. The arrow indicates $\rho_{T,T}(0)$.

lattice filled with $N = 551$ atoms. An external magnetic trapping frequency of $\omega_T = 2\pi \times 8\text{Hz}$ ensures that the last occupied well has an energy $\epsilon((N-1)/2) = 0.9U$. We note that the probability for tunneling of holes from the edges is negligible as $J/(K\Omega) = 0.34$. In practice it is not important to know the exact number of atoms in the lattice as long as the trap strength is chosen such that, given the uncertainty in the number of atoms, the constraint $\epsilon((N-1)/2) < U$ is always satisfied. These parameters fix the ratio $U/J = 500$ and the measurement strength is therefore $\hbar\kappa/2\sqrt{K}J \approx 1.5$.

When the environment is monitored, for instance by looking for photon scattering from the bound molecular state, the evolution of ground states can be modeled using quantum trajectories. For our simulation, the ground state wavefunction $|\psi(t)\rangle = c_T(t)|T\rangle + \sum_{j,\pm} c_{S_j^\pm}(t)|S_j^\pm\rangle$ is updated according to the non-Hermitian Hamiltonian $H = H_I - i\hbar\gamma_M/2 \sum_{j,\pm} |M_j^\pm\rangle\langle M_j^\pm|$. A quantum trajectory corresponding to a null measurement result converges to the target state $|T\rangle$ and freezes the state there as demonstrated in Fig. 7.2 (for a similar effect with ions see [106]). The preparation time scale is $t_{prep} = 1/\kappa$. The success or failure of the preparation is conclusive with failure probability $p_{fail} = 1 - \rho_{T,T}(0)$.

Real experiments will be constrained to finite detector efficiencies η. For $\eta = 0$, corresponding to

103

nonselective measurement, the system dynamics evolve according to Eq. 7.9. If we represent the dynamics of the system as a pseudo two state system $|T\rangle$ and $|S\rangle$, with an average energy splitting $U + 2|V_c|$, the equations of motion for the pseudo Bloch vector are:

$$
\begin{aligned}
\dot{u} &= (U + 2|V_c|)v/\hbar - \kappa u \\
\dot{v} &= -\kappa v - (U + 2|V_c|)u/\hbar - \sqrt{2K}Jw \\
\dot{w} &= -\kappa(x + w) + 4\sqrt{2K}Jv/\hbar \\
\dot{x} &= -\kappa(x + w),
\end{aligned}
\tag{7.11}
$$

where $u = \mathrm{Re}[\rho_{S,T}]$, $v = \mathrm{Im}[\rho_{S,T}]$, $w = \rho_{S,S} - \rho_{T,T}$, and the decreasing norm is $x = \mathrm{Tr}[\rho]$. After a period $1/2|V_c|$, the coherences approach steady state, and the target state population, assuming $\rho_{T,T}(0) \approx 1$ and $\hbar\kappa/2\sqrt{K}J > 1$, is

$$
\rho_{T,T}^{ns}(t) = \rho_{T,T}(0)\exp[-(8KJ^2\kappa t)/((U + 2|V_c|)^2 + (\hbar\kappa)^2)].
\tag{7.12}
$$

As shown in Fig. 7.2, if the initial state is close to the target state then the decay time is long compared to $\hbar/U$. For our parameters, the decay of population from the target state is predominately suppressed due to the single atom light shift V_c which shifts the coupled states $\{|T\rangle, |S_j^{\pm}\rangle\}$ out of resonance. This shift is dependent on the molecular state coupled to (through the detuning) and is therefore system dependent. However, in the strong measurement limit $\hbar\kappa/2\sqrt{K}J \to \infty$, the system dynamics are frozen by virtue of the continuous quantum Zeno effect. In the case of finite detector efficiencies, we can express the approximate fidelity to be in the target state. Assuming a null measurement result, for times $t > t_{prep}, \hbar/2|V_c|$, it is: $F(\eta, t) = \rho_{T,T}(t) = \eta + (1 - \eta)\rho_{T,T}^{ns}(t)$. In practice, high detection efficiencies may be obtained by applying a second photo ionizing laser on resonance with the molecular bound state and monitoring the emission of ions.

It is necessary to keep the measurement on during a computation to maintain high fidelity in the unit filled state. If instead, the catalysis field is turned off after the target state is reached, the system will freely evolve according to H_{BH}. For $\Omega/U \ll 1$ and for times $t < \hbar/J$ the fidelity can be calculated using the restricted basis set:

$$
F(t) = 1 - 8(J/U)^2(K - \cos(Ut/\hbar)(1 + \sin(\Omega(K-1)t/\hbar)/\sin(\Omega t/\hbar))).
\tag{7.13}
$$

This solution compares well with exact numerical simulations. Note that the time averaged deviation from perfect fidelity is $1 - \langle F(t) \rangle = 8K(J/U)^2$; which is twice as bad as the deviation if the system were left in the ground state $|\Psi_g\rangle$. This result shows that other *dissipative* techniques for initializing a register in a lattice such as Raman side-band cooling [107], and phase space compression [108], if not corrected, will suffer from the same loss of fidelity as described by Eq. 7.13.

7.1.3 Measurement at finite temperature

Up to now we have been focusing on dynamics of pure states of the many body system. In the remainder of this Section we show that the protocol for register initialization may be made robust against the effects of moderate finite temperatures. In fact, the selective measurement is an entropy decreasing map, because it damps amplitude in multiple occupied wells, and it can therefore be effective even for mixed states at finite temperature. We hereby assume a thermal distribution of the eigenstates of the BH-Hamiltonian. The overall effect of finite temperature is to increase the weight of reduced Fock states other than the target state and therefore to decrease the fidelity. For a temperature $T_d k_B \approx \left(U - \epsilon_{(N-1)/2}\right)$ states are populated which have more than one particle in one or more sites in the register. k_B is the Boltzmann constant. The projective measurement is effective on these states and the primary consequence of their presence is to reduce the initial fidelity of the system. We can identify another temperature, $T_h k_B \approx \left(\epsilon_{(N+1)/2} - \epsilon_{((K-1)/2)}\right)$ corresponding to the energy of the Fock state with a hole at site $(K-1)/2$. For $T \sim T_h$ there is appreciable population in eigenstates which have holes in the register. The measurement is insensitive to population of states with holes in the register, and the probability that the measurement does not project the system into the target state, given a null measurement result, is then at least $1/e$ when the temperature is greater than T_h. As a low initial fidelity can cause quantum jumps during the meaurement, large population of states with multiple occupancy in the central sites should also be avoided. This leads to the rough estimate $T_{max} \approx min\{T_d, T_h\}$.

The exponential growth of the Hilbert space with particle number makes the computation laborious. We have obtained numerical results for a model system consisting of 11 sites and 9 particles by exact diagonalization of H_{BH} in a Hilbert space of dimension 92378. The fidelity is shown in Fig. 7.3. The
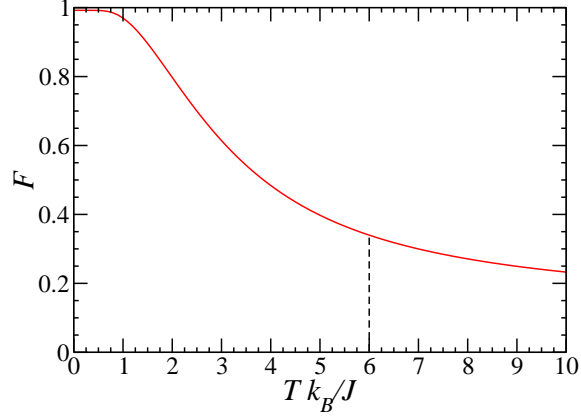
Figure 7.3: Equilibrium fidelity to be in the unit filled register state $|T\rangle_{\mathcal{R}}$ as a function of temperature in presence of the trap for $M = 11$, $N = 9$, $K = 5$. The relevant energies are $U/J = 60$ and $\Omega/J = 3.375$. Here $T_d \approx 6.0 J/k_B$ and $T_h \approx 70 J/k_B$. The dashed line indicates the scaled energy $T_d k_B/J$ where $F(T_{max}) \approx 0.33988$. The fidelity at $T = 0$ is $F(T = 0) \approx 0.99208$.

coupling ratio is chosen to be $U/J = 60$ and the register is defined by the central 5 sites. In order to suppress tunneling of holes into the register, the ratio Ω/J has been chosen to be very large, $\Omega/J \approx 3.375$. This does not correspond to a typical experimental situation, as it implies that the number of sites in the register for which $\epsilon(j) < U$ is small (9, in this case). The fidelity drops to values lower than $F < 1/e$ at $T_d \approx 6.0 J/k_B = min\{T_d, T_h\}$, see caption of Fig. 7.3. For different setups T_d and T_h can assume approximately the same value. In the experimentally relevant setup discussed in relation to the measurements, where $N = 551$ and $K = 501$, $T_d \approx 50 J/k_B$, and $T_h \approx 80 J/k_B$.

7.1.4 Conclusions

In summary, we have shown that efforts to prepare a register of atomic qubits in an optical lattice suffer from errors inherent in the underlying many body dynamics. We have introduced a protocol that addresses this issue to make the MI transition a robust mechanism for initialization. While the discussion has focused on one dimensional dynamics, the method is also applicable to higher dimensions, which is the relevant regime for scalability. Numerical studies on small sized systems indicate that this protocol can be made robust even at finite temperature which is appropriate to real experimental implementations.

Chapter 8

Conclusions

A comprehensive theoretical study of the properties of atoms confined in realistic periodic and quadratic potentials was presented, with the goal of supporting ongoing experimental efforts in the field of atomic physics. The following summarizes the main results presented in this thesis:

- We solved exactly the problem of a particle in the periodic plus parabolic potentials in the tight-binding limit. The existence of both harmonic-oscillator-like modes extended around the center of the parabolic potential and of modes which are localized far from the trap center was shown. Localization of the modes occurs for energies larger than the lattice band-width, and is linked to the appearance of lattice-induced non-classical turning points for the atoms.

- We studied the interacting bosonic problem in the case where the onsite particle density is smaller than or equal to one by means of numerical diagonalizations of the Bose-Hubbard Hamiltonian. We explored the applicability of fermionization techniques when the parabolic trap is present and used these techniques to explain microscopically the formation of a Mott insulator state with one atom per site at the center of the parabolic potential.

- We explored the dynamical properties of bosons in periodic potentials, by studying the dipole oscillations of an atomic cloud subject to a sudden displacement of the parabolic potential. In the non-interacting system, damping of the center of mass motion was observed due to the dephasing of single-particle states which are not fully harmonic in character. In the strongly interacting system, a strong inhibition of the transport properties was observed for deep enough lattices. We explained this suppression of the oscillations by means of fermionization techniques with the population of localized single-particle states in the corresponding fermionic system during the dynamics. In particular, the dynamics was shown to be completely overdamped when a unit filled Mott insulator was formed at the trap center.

- We introduced a simple model that generalizes the Bose-Fermi mapping to cases where the onsite density is larger than one and varies spatially across the lattice. We showed the model's accuracy in reproducing the equilibrium properties of confined strongly interacting bosons by comparing its predictions with exact quantum Monte-Carlo results. We applied the model to study the decay of the center of mass oscillations of an atomic cloud after a sudden displacement of the parabolic potential, finding good quantitative agreement with recent experiments. The model provides an intuitive insight into the physical mechanisms responsible for the decay of the oscillations.

- We studied Bragg spectroscopy as a means for probing the excitation spectrum and for estimating the system's temperature in the Mott insulator phase for homogeneous lattices. We delimited the regime of validity of linear response theory, finding that the correlated nature of the Mott state may make reaching this regime experimentally challenging. Contrary to the superfluid case, we showed that Bragg spectroscopy in the Mott regime is sensitive to temperature. This sensitivity may be used to provide information on the system's temperature at energies of the order of the interaction energy, which are out of reach for current experimental techniques based on the analysis of time-of-flight images of expanding clouds after the release of atoms from all trapping potentials.

- We analyzed the effects of temperature on the Mott insulator state in the presence of the quadratic potential and suggested an experiment to estimate the system's temperature at energies of the order of the interaction energy. In particular, we introduced a simple model for describing the dependence upon lattice position of the finite-temperature atomic-pair density distribution. This dependence is then utilized to infer the system's temperature, by devising a position-dependent measurement of the atomic pair density.

- We devised a protocol for using the Mott state with one atom per site as a robust register for quantum computation. We showed that errors in the register initialization such as population of states with empty or doubly-occupied sites can be eliminated by a proper choice of the parabolic confining potential, which inhibits the presence of unoccupied sites in the register, and by selective measurement on a molecular photo-associative transition. The latter projects out components of the many-body

wavefunction with more than one atom per well. This proposal was shown to be robust against the effects of moderate finite temperatures.

The results above, although significant, are a fraction of the total amount of theoretical work produced in the last few years, as a result of the interest generated by the tremendous progress achieved in the coherent manipulation of ultracold atoms. Yet, many areas of research remain to be explored. As concerns single-component bosons, a detailed study of the spectrum of confined atoms in two and three dimensions in the strongly correlated regime will be certainly a subject of future research, in analogy to the one dimensional case. The hope is to gain further insight into the physics of quantum phase transitions, by studying both theoretically and experimentally the defect free, highly controllable systems offered by bosons in optical lattices.

More generally, atomic gases offer an alternative approach to traditional theoretical tools for the study of strongly correlated regimes, through the design of quantum simulators, where a microscopic Hamiltonian is implemented in a quantum gas and its phase diagram is studied experimentally by controlling the strength of the interaction terms. The simulation of Hamiltonians with atoms in optical lattices is particularly attractive for fermionic systems, where the presence of the well known sign problem largely reduces the utility of numerical Monte-Carlo methods, which are to date the most succesful tools for exploring strongly correlated regimes. In this respect, it will be of crucial importance to develop schemes for the read-out of the results of the quantum simulations. Spectroscopic techniques like the Bragg spectroscopy presented in this thesis are likely to play an important role in extracting useful information out of the simulations' results.

BIBLIOGRAPHY

[1] O. Frisch, Z. Phys. **86**, 42 (1933); T. Haensch and A.L. Schawlow, Opt. Commun. **13**, 68 (1975).

[2] P.L. Gould, G.A. Ruff, and D.E. Pritchard, Phys. Rev. Lett. **56**, 827 (1986).

[3] D. Meschede, H. Walther, and G. Mueller, Phys. Rev. Lett. **54**, 551 (1985); G. Rempe, H. Walther, and N. Klein, Phys. Rev. Lett. **58**, 353 (1987).

[4] C.I. Westbrook, R.N. Watts, C.E. Tanner, S.L. Rolston, W.D. Phillips, and P.D. Lett, and P.L. Gould, Phys. Rev. Lett. **65**, 33 (1990); P. Verkerk, B. Lounis, C. Salomon, C. Cohen Tannoudji, J. Courtois, and G. Grynberg, Phys. Rev. Lett. **68**, 3861 (1992); P.S. Jessen, C. Gerz, P.D. Lett, W.D. Phillips, S.L. Rolston, R.J.C. Spreeuw, and C.I. Westbrook, Phys. Rev. Lett. 69, 49 (1992); A. Hemmerich and T. W. Haensch, Phys. Rev. Lett. **70**, 410 (1993).

[5] M. Kasevich and S. Chu, Phys. Rev. Lett. **69**, 1741 (1992).

[6] B.P. Anderson and M.A. Kasevich, Science **282**, 1686 (1998).

[7] J.V. Porto, S. Rolston, B. Laburthe Tolra, C.J. Williams, and W.D. Phillips, Phil. Trans. R. Soc. Lond. A **361**, 1417 (2003).

[8] A. Einstein, Sitzber. Kgl. Preuss. Akad. Wiss., 261 (1924).

[9] F. London, Nature **141**, 643 (1938).

[10] M.H. Anderson, J.R. Ensher, M.R. Matthews, C.E. Wieman, and E.A. Cornell, Science **269**, 198 (1995); K. B. Davis, M.-O. Mewes, M.R. Andrews, N.J. van Druten, D.S. Durfee, D.M. Kurn, and W. Ketterle, Phys. Rev. Lett. **75**, 3969 (1995).

[11] D. Jaksch, C. Bruder, J. I. Cirac, C. W. Gardiner, and P. Zoller, Phys. Rev. Lett. **81**, 3108 (1998).

[12] M.P.A. Fisher, P.B.M. Weichman, G. Grinstein, and D.S. Fisher, Phys. Rev. B **40**, 546 (1989).

[13] M. Greiner, O. Mandel, T. Esslinger, T.W. Hänsch, and I. Bloch, Nature **415**, 39 (2002).

[14] B. Laburthe Tolra, K. M. O'Hara, J. H. Huckans, W. D. Phillips, S. L. Rolston, and J.V. Porto, Phys. Rev. Lett. **92**, 190401 (2004).

[15] B. Paredes, A. Widera, V. Murg, O. Mandel, S. Fölling, I. Cirac, G. V. Shlyapnikov, T. W. Hänsch, and I. Bloch, Nature **429**, 277 (2004).

[16] T. Kinoshita, T. Wenger and D. S. Weiss, Science **305**, 1125 (2004).

[17] C. D. Fertig, K. M. O'Hara, J. H. Huckans, S. L. Rolston, W. D. Phillips, and J. V. Porto, Phys. Rev. Lett. **94**, 120403 (2005).

[18] H. Moritz, T. Stöferle, M. Köhl, and T. Esslinger, Phys. Rev. Lett. **91**, 250402 (2003).

[19] T. Stöferle, H. Moritz, C. Schori, M. Köhl, T. Esslinger, Phys.Rev. Lett. **92**, 130403 (2004).

[20] L. Pezzè, L. Pitaevskii, A. Smerzi, S. Stringari, G. Modugno, E. de Mirandes, F. Ferlaino, H. Ott, G. Roati, and M. Inguscio, Phys. Rev. Lett. **93**, 120401 (2004).

[21] D. Jaksch, H.-J. Briegel, J. I. Cirac, C. W. Gardiner, and

P. Zoller, Phys. Rev. Lett. **82**, 1975 (1999).

[22] G.K. Brennen, C.M. Caves, P.S. Jessen, and I.H. Deutsch, Phys. Rev.

Lett. **82**, 1060 (1999).

[23] D. Jaksch, J.I. Cirac, P. Zoller, S.L. Rolston, R. Cote, and M.D. Lukin,

Phys. Rev. Lett. **85**, 2208 (2000).

[24] D.P. DiVincenzo, Fortschr. Phys. **48**, 771 (2000).

[25] O. Mandel, M. Greiner, A. Widera, T. Rom, T.W. Haensch, and I. Bloch, Nature **425**, 937 (2003).

[26] S. Das Sarma, A. Kobayashi, and R. E. Prange, Phys. Rev. Lett. **56**, 1280 (1986); V.W. Scarola and S. Das Sarma, cond-mat/0506415 (2005).

[27] V. A. Kashurnikov, N.V. Prokof'ev, and B.V. Svistunov, Phys. Rev. A **66**, 031601 (2002).

[28] G.G. Batrouni, V. Rousseau, R.T. Scalettar, M. Rigol, A. Muramatsu, P.J.H. Denteneer, and M. Troyer, Phys. Rev. Lett. **89**, 117203 (2002).

[29] C. Kollath, U. Schollwoeck, J. von Delft, and W. Zwerger, Phys. Rev. A **69** 031601 (2004).

[30] N.V. Prokof'ev, B.V. Svistunov, and I.S. Tupitsyn, Phys. Lett. A **238**, 253 (1998); JETP **87**, 310 (1998).

[31] M. Kozuma, L. Deng, E.W. Hagley, J. Wen, R. Lutwak, K. Helmerson, S.L. Rolston, and W.D. Phillips, Phys. Rev. Lett. **82**, 871 (1998).

[32] D.M. Stamper-Kurn, A.P. Chikkatur, A. Gorlitz, S. Inouye, S. Gupta, D.E. Pritchard, and W. Ketterle, Phys. Rev. Lett. **83**, 2876 (1999).

[33] G. Grynberg and C. Robiliard, Phys. Rep. **355**, 335 (2001).

[34] A.M. Rey, P.B. Blakie, G. Pupillo, C.J. Williams, and C.W. Clark, cond-mat/0407075 (2004), accepted for publication in Phys. Rev. A.

[35] D. van Oosten, D.B.M. Dickerscheid, B. Farid, P. van der Straten, and H. T. C. Stoof, Phys. Rev. A **71**, 021601(R) (2005).

[36] P. Rabl, A.J. Daley, P.O. Fedichev, J.I. Cirac, and P. Zoller, Phys. Rev. Lett. **91**, 110403 (2003).

[37] P.B. Blakie and C.W. Clark, J. Phys. B: At. Mol. Opt. Phys. **37**, 1391 (2004).

[38] D. Jaksch and P. Zoller, Ann. Phys. **315**, 52 (2005).

[39] L. Pitaevskii and S. Stringari, J. Low Temp. Phys. **85**, 377 (1991).

[40] N. Laflorencie, S. Capponi, and E.S. Sørensen, Eur. Phys. J. B **24**, 77 (2001).

[41] E. H. Lieb and W. Liniger, Phys. Rev. **130**, 1605 (1963).

[42] K. Huang, *Statistical mechanics II* (John Wiley and Sons, Inc., New York); K. Huang and C.N. Yang, Phys. Rev. **105**, 767 (1957); K. Huang, C.N. Yang, and J.M. Luttinger, Phys. Rev. **105**, 776 (1957).

[43] M.E. Fisher, M.N. Barber, and D. Jasnow, Phys. Rev. A **8**, 1111 (1973).

[44] R. Roth and K. Burnett, Phys. Rev. A **67**, 031602(R) (2003).

[45] A.J. Leggett, Rev. Mod. Phys. **73**, 307-356 (2001).

[46] M. Aizenman, E.H. Lieb, R. Seiringer, J.P. Solovej, and J. Yngvason, Phys. Rev. A **70**, 023612 (2004); E.H. Lieb, R. Seiringer, and Jakob Yngvason, Commun. Math. Phys. **244**, 347 (2004).

[47] M. Girardeau, J. Math. Phys. **1**, 516 (1960).

[48] J. K. Freericks and H. Monien, Phys. Rev. B **53**, 2691 (1996).

[49] M. Rigol and A. Muramatsu, Phys. Rev. A **70**, 043627 (2004).

[50] A.M. Rey, G. Pupillo, C.W. Clark, and C.J. Williams, cond-mat/0503477 (2005).

[51] G. Pupillo, A.M. Rey, G.K. Brennen, C.J. Williams, and C.W. Clark, J. Mod. Opt. **51**, 2395 (2004).

[52] H. Ott, E. de Mirandes, F. Ferlaino, G. Roati, V. Türck, G. Modugno, and M. Inguscio, Phys. Rev. Lett. **93**, 120407 (2004).

[53] V. Ruuska and P. Törmä, New J. of Phys. **6**, 59 (2004).

[54] A. Polkovnikov, S. Sachdev, and S. M. Girvin, Phys. Rev. A **66**, 053607 (2002).

[55] C. Hooley and J. Quintanilla, Phys. Rev. Lett. **93**, 080404 (2004).

[56] I. Abramowitz and I. A. Stegun, *Handbook of Mathematical Functions*, National Bureau of Standards (1964).

[57] J. Meixner and F.W. Schäfke, *Mathieusche funktionen und sphäroidfunktionen*, Springer-Verlag (1954); N.W. McLachlan, *Theory and Application of Mathieu Functions*, Dover (1964).

[58] M. Aunola , J. Math. Phys. **44**, 1913 (2003).

[59] N. W. Ashcroft and N. D. Mermin, *Solid State Physics*, W. B. Saunders Company (1976).

[60] J. M. Ziman, *Principles of the Theory of Solids*, Cambridge University Press (1964).

[61] D. Jaksch, PhD-Thesis, University of Innsbruck (1999).

[62] F. S. Cataliotti, S. Burger, C. Fort, P. Maddaloni, F. Minardi, A. Trombettoni, A. Smerzi, and M. Inguscio, Science **293**, 843 (2001).

[63] O. Morsch, J. H. Müller, M. Cristiani, D. Ciampini, and E. Arimondo, Phys. Rev. Lett. **87**, 140402 (2001).

[64] A. Polkovnikov and D.-W.Wang, Phys. Rev. Lett. **93**, 070401 (2004).

[65] A. Polkovnikov, E. Altman, E. Demler, B. Halperin and M.D. Lukin, cond-mat/0412497 (2004).

[66] E. Altman, A. Polkovnikov, E. Demler, B. Halperin, and M. D. Lukin, cond-mat/0411047 (2004).

[67] J. Gea-Banacloche, A. M. Rey, G. Pupillo, C.J. Williams, and C.W. Clark, cond-mat/0410677 (2004).

[68] W. Kohn, Phys. Rev. **123**, 1242 (1961); J. F. Dobson, Phys. Rev. Lett. **73**, 2244 (1994).

[69] S.L. Cornish, N.R. Claussen, J.L. Roberts, E.A. Cornell, and C.E. Wieman, Phys. Rev. Lett. **85**, 1795 (2000).

[70] E.A. Donley, N.R. Claussen, S.L. Cornish, J.L. Roberts, E.A. Cornell, and C.E. Wieman, Nature **412**, 295 (2001).

[71] A.M. Rey, PhD Thesis, University of Maryland at College Park (2004).

[72] M. Olshanii and V. Dunjko, Phys. Rev. Lett. **91**, 090401 (2003).

[73] G. G. Batrouni, R. T. Scalettar, and G. T. Zimanyi, Phys. Rev. Lett. **65**, 1765 (1990).

[74] A.M. Rey, K. Burnett, R. Roth, M. Edwards, C.J. Williams, and C.W. Clark, J. Phys. B: At. Mol. Opt. Phys, **36** , 825 (2003).

[75] H. Fukuyama, R.A. Bari, and H.C. Fogedby, Phys. Rev. B **8**, 5579 (1973); G. Wannier, Phys. Rev. **17**, 432 (1960).

[76] B. Wu, R. B. Diener, and Q. Niu, Phys. Rev. A **65**, 025601 (2002), and references therein.

[77] S. Burger, F. S. Cataliotti, C. Fort, F. Minardi, M. Inguscio, M. L. Chiofalo, and M. P. Tosi, Phys. Rev. Lett. **86**, 4447 (2001).

[78] A. Smerzi, A. Trombettoni, P. G. Kevrekidis, and A. R. Bishop, Phys. Rev. Lett. **89**, 170402 (2002).

[79] E. Lundh, Phys. Rev. A **70**, 061602 (2004).

[80] M. Rigol, V. Rousseau, R. T. Scalettar and R. R. P. Singh, cond-mat/0503302.

[81] A.J. Daley, C. Kollath, U. Schollwoeck, and G. Vidal, J. Stat. Mech.: Theor. Exp., P04005 (2004).

[82] S. Sachdev, *Quantum Phase Transitions*, Cambridge University Press (1999).

[83] B. DeMarco, C. Lannert, S. Vishveshwara, and T.-C. Wei, cond-mat/0501718 (2005).

[84] L. Pollet, S.M.A. Rombouts, and P.J.H. Denteneer, Phys. Rev. Lett. **93**, 210401 (2004).

[85] M. Rigol, V. Rousseau, R.T. Scalettar, and R.R.P. Singh, cond-mat/0503302 (2005).

[86] J. Ruostekoski and L. Isella, cond-mat/0504026 (2005).

[87] J.H. Denschlag, J.E. Simsarian, H. Haeffner, C. McKenzie, A. Browaeys, D. Cho, K. Helmerson, S.L. Rolston, and W.D. Phillips, J. Phys. B **35**, 3095 (2002).

[88] S. Peil, J.V. Porto, B. Laburthe Tolra, J.M. Obrecht, B.E. King, M. Subbotin, S.L. Rolston, and W.D. Phillips, Phys. Rev. A **67**, 051603(R) (2003).

[89] I. Deutsch and P.S. Jessen, Phys. Rev. A **57**, 1972 (1998).

[90] T. Calarco, H.-J. Briegel, D. Jaksch, J.I. Cirac, and P. Zoller, J. Mod. Opt. **47**, 2137 (2000).

[91] D. Jaksch and P. Zoller, New J. Phys. **5**, 56 (2003).

[92] G.K. Brennen, G. Pupillo, A.M. Rey, C.W. Clark, and C.J. Williams, J. Phys. B **38**, 1687 (2005).

[93] P.B. Blakie, R.J. Ballagh, and C. W. Gardiner, Phys. Rev. A **65**, 033602 (2002).

[94] C. Menotti, M. Krämer, L. Pitaevskii, and S. Stringari, Phys. Rev. A **67**, 053609 (2003).

[95] A. Brunello, F. Dalfovo, L. Pitaevskii, S. Stringari, and F. Zambelli, Phys. Rev. A **64**, 063614 (2001).

[96] L. Viverit, C. Menotti, T. Calarco, and A. Smerzi, Phys. Rev. Lett. **93**, 110401 (2004).

[97] D.C. Roberts and K. Burnett, Phys. Rev. Lett. **90**, 150401 (2003).

[98] G. Pupillo, E. Tiesinga, and C. J. Williams, Phys. Rev. A **68**, 063604 (2003).

[99] For convenience we choose N odd and fix the site index $j = 0$ at the minimum of the magnetic trap

[100] M. R. Andrews, C.G. Townsend, H.-J. Miesner, D.S. Durfee, D.M. Kurn, and W. Ketterle, Science **275**, 637 (1997)..

[101] C.A. Sackett, D. Kielpinski, B.E. King, C. Langer, V. Meyer, C.J. Myatt, M. Rowe, Q.A. Turchette, W.M. Itano, D.J. Wineland, and C. Monroe, Nature **404** 256 (2000).

[102] For convenience we choose N odd and fix the site index $j = 0$ at the minimum of the magnetic trap.

[103] A. Fioretti, C. Amiot, C.M. Dion, O. Dulieu, M. Mazzoni, G. Smirne, and C. Gabbanini, Eur. Phys. J. D **15**, 189 (2001).

[104] M.J. Gagen and G.J. Milburn, Phys. Rev. A **47**, 1467 (1993).

[105] P.S. Julienne, J. Res. Natl. Inst. Stand. Technol. **101**, 487 (1996).

[106] A. Beige, D. Braun, B. Tregenna, and P.L. Knight, Phys. Rev. Lett. **85**, 1762 (2000).

[107] S.E. Hamann, D.L. Haycock, G. Klose, P.H. Pax, I.H. Deutsch, and P.S. Jessen, Phys. Rev. Lett. **80**, 4149 (1998).

[108] D.J. Han, M.T. DePue, and D.S. Weiss, Phys. Rev. A **63**, 023405 (2001).